POLITECNICO DI TORINO

Master's Degree in Aerospace Engineering

Full Authority Digital Engine and Propeller Control: effect assessment of turboprop compressor modification on the control system

Supervisors	Candidate
Ph.D. Pangcheng David CEN CHENG	**Bartolomeo ALFIERI**
Eng. Davide BARBANERA	

31 MARCH 2026

Abstract

The master's thesis work presented in this paper was carried out at the offices and with the resources of AvioAero in Rivalta (TO) and presents the results of an analysis on the effectiveness of the Full Authority Digital Engine and Propeller Control (FADEPC) on a turboprop engine, following a structural re-design that involved the low-pressure compressor and which became necessary during development. In particular, it was intended to demonstrate that, despite the modification, the control system would maintain the functionality of the engine within its functional limits, ensuring its performance and safe operating conditions.

The analysis includes the verification that this modification will impact the engine-system in accordance with the project team's expectations, i.e. that it respects the already agreed limits on controllability and that it does not affect engine performance except within the expected and accepted engine-to-engine variability, i.e. the expected small differences in performance between one prototype and another.

The results of the analysis confirmed that the effect of the re-design remains limited in the order of engine-to-engine variability, fixed in the $\pm 1.5\%$ percentage variation band.

The subsequent parametric analysis focused on the effect of the expected inertia variation and showed that, up to an increase of more than 2% - all other structural and functional characteristics being equal - the change does not have an appreciable impact on the control system.

All analyses were performed with computing tools. Ground and altitude maneuvers were simulated, representative of the operating conditions that the engine system will experience during typical missions within the planned flight envelope, from which parameters of interest were extrapolated to investigate the responses of the control system. The results were obtained with a company's proprietary software, developed in an NPSS (Numerical Propulsion System Simulation) environment; then processed with a MATLAB script developed *ad hoc* by the author and finally reorganized on an Excel spreadsheet.

All the results presented in this work are part of the risk mitigation activity (*derisking*), i.e. a design criterion that prescribes to carry out a set of analyses downstream of each significant change to the architecture of the engine-system: the aim is to demonstrate that the modified system continues to meet the design requirements, as well as to identify in advance all the risks related to its functionality and safety and possibly activate corrective measures, in preparation for the next testing phase.

Table of Contents

List of Tables

List of Figures

Chapter 1

Introduction

1.1 What we knew

This paper contains the master's thesis work carried out by the author as part of his work activity in the corporate context of AvioAero – GE Aerospace, at the plants of *Rivalta (TO), Bari, Prague* and *Hradec Králové (CZ)*.

The work focuses on the analysis of a turboprop engine in an advanced state of design, integration and testing, which has undergone a hardware redesign of its `LPC` (Low Pressure Compressor) component. The redesign required thickening the rotor blades of some stages: this consequently caused a new distribution of the rotating masses and therefore an increase in the overall rotational inertia of the *gas generator*, the group composed of compressor-turbine assembly. Since the hardware modification was not scheduled in the life-cycle of the engine, the decision to pursue this path was long and meticulously considered, as an intervention of this magnitude could have meant significant delays in the delivery of the final product to the customer. This paper will not deal with the mechanical-structural design process of the engine, but rather a subsequent step that directly involved the Controls team. Therefore, following the validation of the hardware modification by the Mechanics, Vibrodynamics and Performance teams, the question to be resolved was whether this intervention would have modified the intrinsic characteristics of the turboprop so much that its operating points would change as well as the dynamic response to the automatic control system, consisting of the software developed by the Controls team and installed on the electronic control unit, the `FADEPC`. If the engine had behaved too far from the design points, this would have caused a re-working of the control logic, which could not be immediately assessed in advance in terms of costs and working hours. The decision of the Controls team was to start a *de-risking* activity, performing a set of tests and numerical simulations, in order to assess the real impact of the re-design in a safe and controlled manner, identifying

in advance any critical issues and risks on the functionality of the engine and its ability to operate at the level of the declared performance and in safe conditions.

1.1.1 Overview

This thesis deals in detail with this *derisking* analysis: in Chapter 2 we offer an overview of the state-of-art on the architecture of a classic turboprop, its development and implementation process as an aeronautical product and its synergy with the control system, the FADEPC (Full Authority Digital Engine and Propeller Control), specifying which parameters are physically correlated with its rotational inertia and which are therefore eligible for evaluation metrics for the analysis; in Chapter 3 the set of theoretical and numerical tools used for the analysis is examined in detail; in Chapter 4 the comparison analysis between the nominal version of the engine and the modified version (**Ruggedized**) is addressed, referring to graphical representations of the study metrics; Chapter 5 extends the analysis to hypothetical scenarios in which the increase in inertia is greater than the nominal, with a view to developing the engine for other applications that may require further hardware modifications; finally, in Chapter 6 there is a brief account of the results of both analyses.

De-Risking

The term de-risking indicates a set of strategies designed to systematically reduce exposure to uncertain events that can compromise the achievement of the objectives of a project or organization, without necessarily eliminating the risk completely, but lowering its probability and impact within acceptable thresholds. In engineering and industrial design, this translates into methodological, technical and organizational choices that *shift* the risk from the late and expensive phases of the life-cycle (final prototyping, production, operation, etc.) to earlier phases, where the effects of errors are less expensive.

De-risking, in a broad managerial/engineering sense, is a proactive and iterative process that includes identifying, analyzing, prioritizing, and reducing exposure to key risks with respect to technical, economic, time, and security objectives. [1]
In industrial design, de-risking is typically integrated into the design process through risk management practices *by design*:

- early identification of risks: systematic analysis of failure modes, interfaces, regulatory and security constraints, supply chain, costs, and times from the early stages of conceptual design
- analysis and prioritization: assessment of the probability and impact of each risk and prioritization, focusing de-risking efforts on risks with high severity

and high uncertainty [2]

- countermeasure planning: definition of strategies such as reduction, relocation, sharing, controlled acceptance [3]
- continuous iteration: de-risking is not a one-time activity, but is updated as the design is refined, test data is acquired, and constraints and context change; a PDCA (Plan–Do–Check–Act) cycle is applied [4]

Some typical methods by which de-risking is implemented in industrial design are: [2]

- FMEA/FMECA analyses
- availability/reliability analyses
- incremental prototyping and early testing
- numerical simulation and modeling
- redundancy and robust design
- project risk management

Chapter 2

Technical Context

2.1 Where we are

Automatic control systems are nowadays widely integrated into modern technology and play a fundamental role in ensuring the correct functioning and efficiency of a vast set of systems. The integration of automatic control systems into everyday technologies mainly brings benefits in terms of efficiency, safety, quality, and comfort perceived by the end user. [5]
Common examples can be found in everyday applications: thermostats and home air conditioning [6], automated lighting [7], home appliances [8], automotive cruise control systems [6], where control algorithms continuously adjust key variables in response to external disturbances or user input. These systems operate by capturing real-time data via sensors, processing it according to predefined control laws, and triggering appropriate responses to maintain the desired operating conditions. This closed-loop approach allows for improved performance, increased safety, and less reliance on human intervention.

The first widely recognized automatic feedback control system on an industrial machine is James Watt's flyball governor applied to his steam engines between 1769 and 1788, with the first documented practical realization in 1788–1789. He adapted the centrifugal regulator to automatically control the speed of the steam engine by varying the steam intake as a function of the speed deviation, thus introducing a clear mechanical negative feedback loop [9]

The same fundamental principles can be applied, with the appropriate scaling, to aeronautical propulsion systems, where automatic control becomes essential to manage the behavior of the engine throughout the operating envelope.

2.1.1 Turboprop architecture

A classic turboprop consists of a gas-turbine core mechanically coupled to a gearbox that drives a propeller at (often) constant pitch; most of the power is extracted on the shaft, while the thrust from the jet is secondary.
A turboprop typically includes: air intake, compressor, combustion chamber, turbine (usually in several sections), gearbox assembly, propeller, and exhaust nozzle.
The core (air intake–compressor–combustor–turbines that drive the compressor) constitutes the gas generator, while the power train (power turbine + gearbox + propeller) converts the torque developed at the shaft into propulsive thrust [10]

Components

- **Intake** - It conveys the inlet air flow, reducing total pressure losses and distortions, ensuring stable conditions for the compressor even in the presence of angles of attack or crosswind

- **Compressor** - Increases air pressure: it can be axial, centrifugal, or combined axial-centrifugal, increasing the temperature and density of the fluid

- **Diffuser and Combustor** - The diffuser slows down the flow out of the compressor, the chamber mixes compressed air and fuel, achieves stable combustion, and distributes the heat load between the primary, intermediate, and dilution zones

- **Gas generator turbine** - It expands the flue gases by taking sufficient work to drag the compressor and accessories (pumps, generators, etc.)

- **Power turbine** - In free-turbine architectures, it exploits the residual energy of the gases to provide torque to the shaft that feeds the gearbox and the propeller, kinematically decoupled from the gas generator

- **Reduction gearbox** - Converts the turbine's high rotational speed (tens of thousands of rpm) into the low speed required by the propeller (typically 1,900–2,200 rpm), via planetary stages and auxiliary gears

- **Propeller** - Generates aerodynamic thrust by converting shaft power; pitch control maintains rated speed, optimising propulsive efficiency and limiting peripheral blade speeds

- **Exhaust nozzle** - Conveys exhaust gases; in a turboprop, its contribution to the total thrust is modest compared to that of the propeller [11]

Control systems and auxiliaries

- Propeller Control Unit (PCU): steers pitch and beta/reverse modes, including main governor, overspeed, and often fuel-topping to limit torque in overspeed conditions
- Fuel system: doses the fuel flow to the gas generator according to the FADEC/PCU commands in compliance with temperature, speed, and transient constraints
- Accessory gearbox: draws power from the gas generator to operate oil pumps, fuel pumps, electric generator, and other on-board services [12]

Figure 2.1 shows a classic turboprop architecture with direct-flow, i.e., the air intake flows in the same direction as the aircraft moves forward. A reverse flow turboprop instead features airflow that enters from the rear side of the gas generator, makes a 180° turn, and proceeds forward before entering the combustion chamber, making the engine more compact than direct-flow designs. [13]

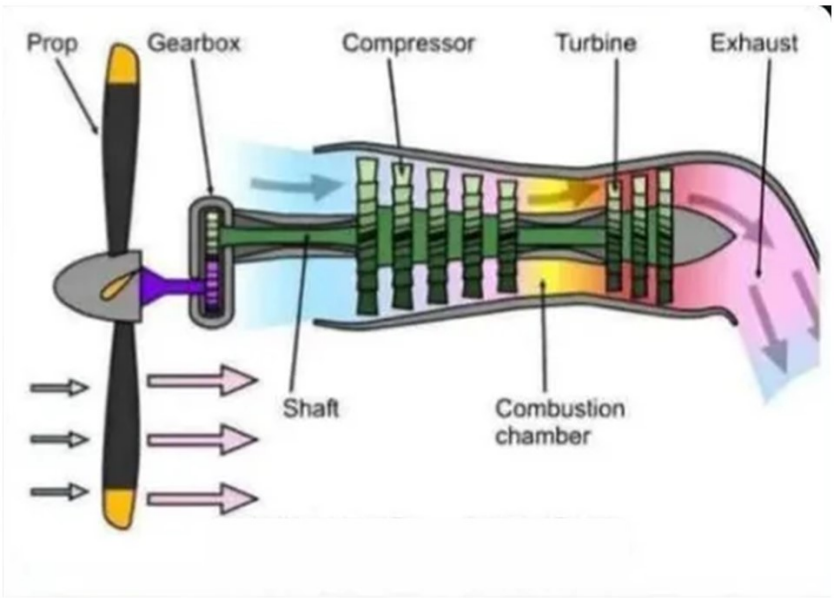

Figure 2.1: Classic turboprop architecture [14].

2.1.2 FADEC

A *FADEC* (Full Authority Digital Engine Control, sometimes referred to as *FADEPC* when the control is also emphasized on the propeller system) is a

digital control system that manages all the operating parameters of the aircraft engine with total (full) authority, without manual override modes. [15]

The FADEC consists of a digital computer (EEC - Electronic Engine Control / ECU - Engine Control Unit) and a set of sensors and actuators dedicated to the engine, which implement control and protection laws in software form.
The system samples dozens of quantities (temperatures, pressures, revolutions, throttle position, ambient conditions) many times per second and processes commands for fuel metering, stator vane, bleed, ignition, etc., ensuring efficiency and compliance with limits at every point of the flight envelope. [15]

Architecturally, the FADEC is typically mounted on or near the engine, with point-to-point interfaces to sensors (temperatures, rotational speed, variable vane position, oil and fuel pressures) and actuators (fuel system, valves, electro-hydraulic actuators). [16] The FADEC closes the control loops inside the engine (e.g., on speed control, turbine temperature or compression ratio control) and acts as a supervisor that coordinates start, shutdown, thrust limitation, health monitoring, and diagnostic functions. [15]

From the pilot's point of view, the main command is the power lever/throttle; systems with FADEC are often said about single-lever power control: the pilot only sets the power/thrust request and the FADEC automatically calculates all the internal parameters (fuel, propeller pitch, mixture, etc.). [17] The pilot inputs are acquired as electrical signals and interpreted by the FADEC as torque, thrust, or rpm set-point, with logics that include automatic protections (e.g., over-temperature, over-speed, surge/stall prevention), also against any improper pilot maneuvers. [15]

The FADEC acquires environmental parameters such as outside air temperature and pressure and, based on altitude and density, recalculates the optimal thrust set-points, compression ratios, and margins with respect to mechanical and thermal limits. [15] The system is integrated into the avionics system via digital buses for data exchange with the Flight Management System, allowing functions such as autothrust, fuel optimization, engine fault management, and maintenance data logging. [18]

The FADEC is normally with redundant channels (twin-lane or dual-channel), in which each channel is able to control the entire motor, with lane management and fault detection & isolation logics to maintain control even in the presence of sensor, actuator or software failures. Hardware and software are developed according to aeronautical standards (DO-178C, DO-254, DO-160), given the safety-critical nature: a true FADEC does not provide for manual bypasses, so a total failure implies the loss of the engine, mitigated by the redundancy and multi-engine philosophy of the aircraft. [18]

The first fully electronic FADEC without backup hydromechanical components was operationally introduced on the `Pratt & Whitney F100-PW-200` engine, mounted on the `F-16 Fighting Falcon` fighter, with its first certified flight in 1978 and entered service in 1981. [19]

2.1.3 Inertia correlated parameters

In the control model of a turboprop, the rotational inertia of the core does not appear as a measured state, but is intrinsically contained in all parameters that describe the speed dynamics of the shaft(s) and their coupling with the fuel/propeller control. [20]

The inertia of the core explicitly enters the equation of motion of the shaft(s) as the moment of inertia J or constant of inertia H. From the point of view of the control system, this J is incorporated into: [21]

- core speed time constant τ in reduced gas turbine models, often in the form

  $$\tau_N \dot{N} = f(W_f, N, p_3, T_4, ...)$$

  , with W_f fuel flow, $\dot{N}$ e N rotational acceleration and speed of the shaft, p_3 discharge compressor pressure, T_4 gas temperature from the combustor exit [22]

- equivalent inertia and damping parameters in multi-mass torsional models (core, power turbine, gearbox, propeller) [23]

- inertia constant of the generator/turbine in power generation applications (H parameter in frequency models), conceptually identical for a turboprop coupled to a mechanical load [21]

In summary, any model parameter that multiplies $\dot{N}$ or that determines the rise/settle time of the core velocity is directly related to rotational inertia [20]

The control does not measure J, but some dynamic quantities are strongly correlated with core inertia or equivalent drive train inertia:

- shaft rotation speed (NG/core speed, NP/power turbine speed, Nprop/propeller rotation): the slope $\dot{N} = \frac{dN}{dt}$ (t=time) with respect to a known fuel or load step is inversely proportional to the equivalent inertia [20]

- power shaft torque allows to identify an equivalent inertia value, and is used in torsional models with two-three masses to calibrate the governor

- frequency and amplitude of torsional oscillations (torsional vibrations, rpm oscillations in the drive train): the proper modes and their damping depend on the J of the various rotors, the shaft stiffness and the gearbox (multi-mass models) [23]

Identification quantities used to estimate inertia

From an experimental and control system point of view, the inertia of the core is quantified through:

- responses to load or fuel flow steps: input signal (step in W_f or applied torque) and N response, plus any torque measurements, allow J to be estimated by fitting first/second order models
- start-up and shutdown transients: the slope of acceleration during start-up (at known torque of the starter) and deceleration slope at fuel off provides a direct estimate of the moment of inertia of the core [21]
- vibrational and modal measurements of the rotor system: identification of torsional and flexural modes allows tracing the moments of inertia of the various subsystems, which then enter the advanced control models [24]

Chapter 3

Methods and Tools

3.1 How we did it: test cases, control parameters, and maneuvers

In this chapter, the method, parameters, and tools of comparative and parametric analysis between engine versions are presented. Please note that, in accordance with the company's confidentiality constraints, in the development of this chapter, data and technical details will be presented exclusively for dissemination purposes, therefore, in a non-dimensional form: whenever necessary, they will be used in a normalized form using reference values not numerically declared.

More than 340 cases have been numerically simulated, to study each version of the engine, with and without hardware modifications (hereinafter defined as **Ruggedized** and **noRuggedized**): they consist of elementary maneuvers, frequent during typical engine missions, performed in various external conditions of altitude, relative air speed and temperature. The simulated maneuvers were chosen to highlight the engine functions and the critical issues faced by the control system during characteristic transients. External conditions fall within and on the edges of the engine envelopes, in accordance with its certified operating limits. The parameters used to analyze the engine response under the effect of pilot commands, ambient conditions, and FADEC control are some of the typical quantities of a turboprop with a classic architecture.

3.1.1 Engine Operating Envelope: steady, Start and Take Off

For an aeroengine, the operating envelope represents the set of stationary operating points that simultaneously respect the aerodynamic, mechanical, and thermal constraints of the engine, within which it can work without incurring stalling,

overheating, or other risky phenomena [25]. It is often represented as *altitude vs Mach* for the entire engine (altitude range and number of Mach in which thrust is available and limits are respected) or as a compressor/turbine map, in which the whole set of constraints (stall surge line, choke, temperature limits, maximum revolutions, etc.) generates an allowed area in the space COMPRESSION RATIO – FLOW RATE – ROTATION SPEED [26].

In modeling and simulation, the envelope is used to establish the area in which the model is valid and stable, for example by extending the operation below sub-idle, or up to the maximum certified regime. In engine controls it is used to design and calibrate the FADEC: the envelope is translated into limiters (max rpm, max temperature, max fuel, etc.) as for each thrust request, the control searches for an allowed operating point on the map and limits the commands if there is a risk of exceeding the envelope [26]. In the definition of performance maps, the operating envelope is systematically *covered* with a grid of speed and load points, on which consumption, efficiencies, and emissions are measured or estimated. [26]

The flight envelope also depends on the engine envelope: in certain combinations of altitude and speed, the engine cannot deliver the necessary thrust or cannot be started, and this restricts the overall operational envelope of the aircraft. [27]

Steady Operating Envelope

An altitude–CAS envelope is the diagram that shows, in the altitude–speed plane (expressed as Calibrated Air Speed[1]), the set of flight conditions allowed for a certain aircraft (or for a certain configuration), i.e., its operating range in terms of height and indicated/corrected speed. [27]

On the horizontal axis, the CAS range is entered, and on the vertical axis, the altitude (barometric or pressure). [28] The various limit curves are drawn on the plane: minimum CAS at each altitude (stall limit), structural maximum speed limit, any engine limits (area where there is no more power for level flight), regulatory or system limits (pressurization, ice, etc.).
The set of points inside these curves is the operational envelope in terms of altitude and CAS, similar to a classic flight envelope expressed in *Mach–altitude* or *V–n*. [27]

[1]Calibrated Air Speed (CAS) is the relative air speed indicated by the aircraft's sensors and then corrected for errors in instrument calibration and positioning; it is useful because it provides a more faithful measurement of the dynamic pressure acting on the probe, therefore of the aerodynamic performance (lift, stall margin, maneuverability) regardless of altitude, temperature and wind

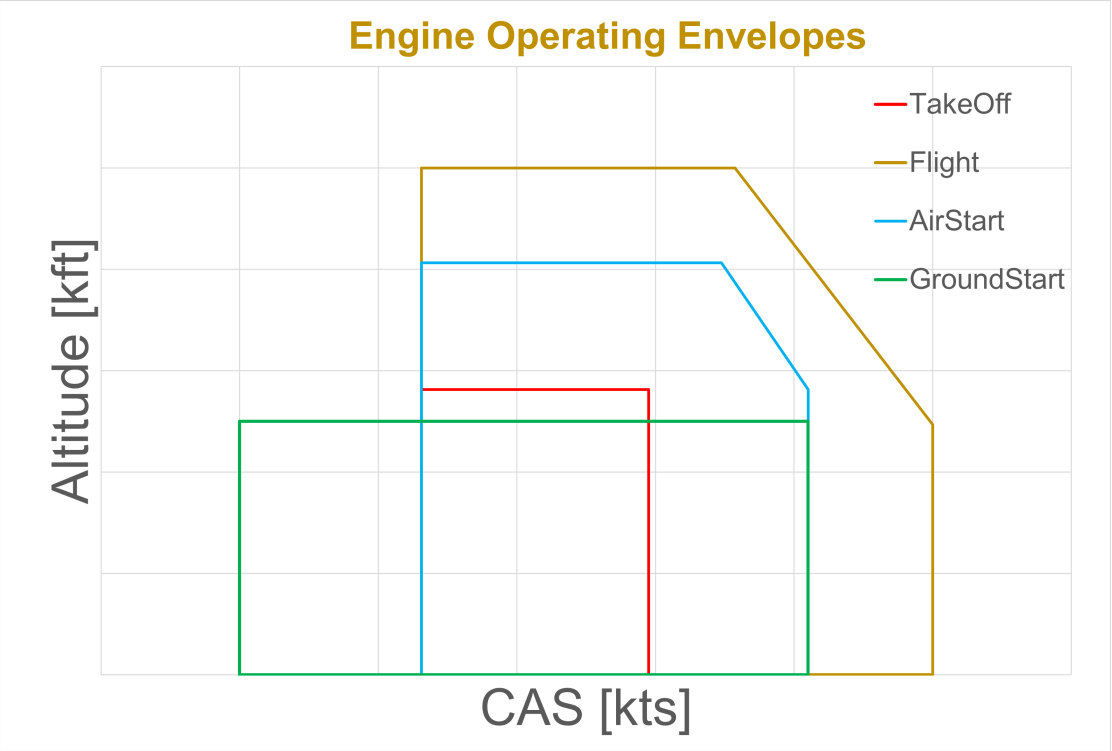

Figure 3.1: Engine Operating Envelopes [alt-CAS]

Start & TakeOff Operating Envelopes

Figure 3.1 shows how the *start* and *takeoff* simplified envelopes are narrower, because in these phases the engine operates in transient and thermally critical conditions, with smaller safety margins than the *steady* conditions for which the base envelope is defined. To avoid thermal damage, compressor stability problems, and exceeding certified limits (ITT, NG, torque, vibration), additional or stricter limits are imposed on time, power, and operating conditions [29]. Moreover, during start-up, the flow is still weak and the internal cooling is limited, so ITT can rise rapidly and as consequence there are specific limits to prevent **hot start** and **hung start** [30]; during take-off the engine is almost maximum thrust and the thermal margin is the most critical of the entire mission profile so the maneuver is limited in time and environmental conditions. [31] Figure 3.2 shows more clearly the various envelope shapes correlated to the maneuvers exploited for the Rugged analysis and detailed in Chapter 4.

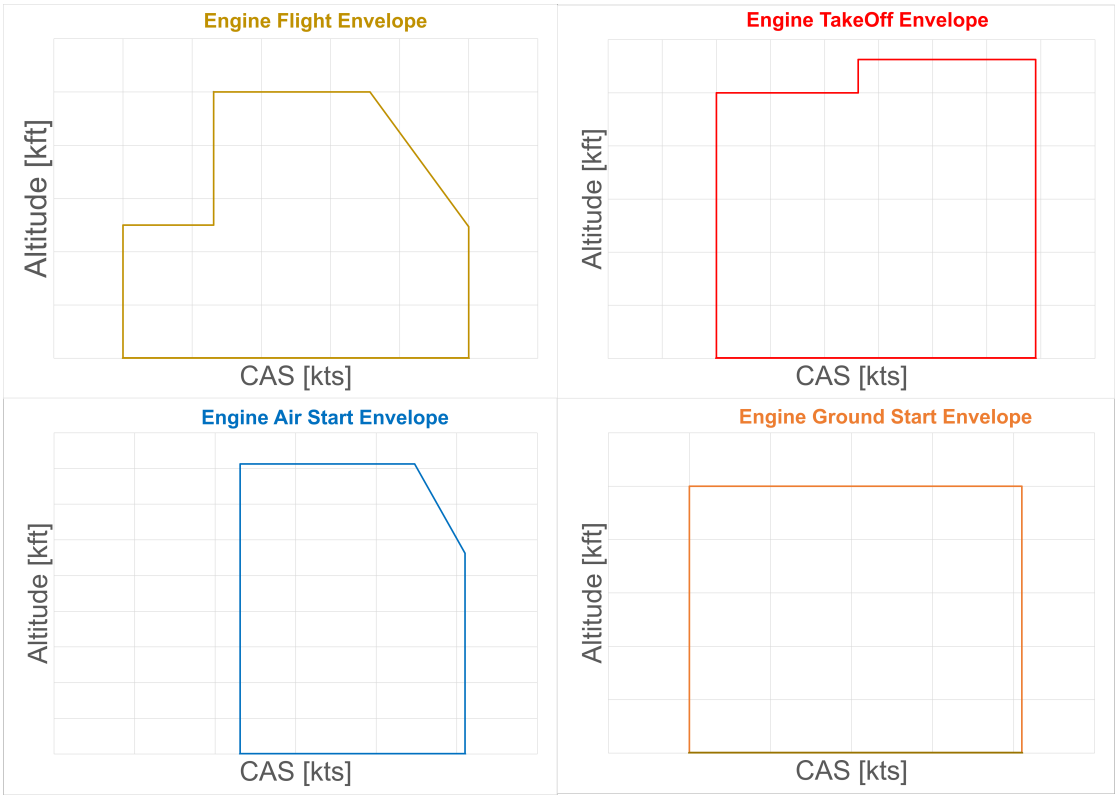

Figure 3.2: Engine Flight Envelopes [alt-CAS]

3.1.2 Test points

The *ISA (International Standard Atmosphere, or ICAO Standard Atmosphere)* model is a stationary atmospheric model that specifies the temperature, pressure, density, and viscosity of dry air as a function of altitude, assuming ideal air, absence of humidity, wind, and turbulence. The ISA model is used to calibrate aircraft instruments, define aircraft performance, and standardize aerodynamic calculations. The atmosphere is modeled into layers with linear or zero temperature gradient, hence imposing hydrostatic equilibrium

$$\frac{dp}{dh} = -\rho g$$

and ideal gas equation

$$p = nRT$$

the laws of variation of pressure and density are derived with altitude [32].
In the above mentioned formulas: p = pressure, h = altitude, ρ = air density, g = acceleration of gravity, R = universal gas constant, T = temperature.

EHD (Extremely Hot Day) and *ECD (Extremely Cold Day)* are extreme environmental conditions used in aeronautical performance analyses for gas turbines, defined with respect to ISA as significant thermal deviations:

- EHD: $T = T_{ISA} + 35° \div 40°C$, $\frac{\rho}{\rho_{ISA}} < 0.8$ for hot air has low density
- ECD: $T = T_{ISA} - 30° \div 40°C$, $\frac{\rho}{\rho_{ISA}} > 1.2$ for cold air has high density [33]

These deviations alter the ISA parameters $\delta = \frac{p}{p_{SL}}$, $\theta = \frac{T}{T_{SL}}$, $\sigma = \frac{\rho}{\rho_{SL}}$[2], without changing layers, but require off-design corrections for cycle matching and component maps:

- EHD: it reduces air mass flow, net power, compressor efficiency [33]
- ECD: it increases air mass flow and specific power, but reduces surge margin [34]

By cross-referencing these atmospheric conditions with the altitude and velocity ranges of each operating envelope, sets of test points were derived, evenly distributed over the entire internal area, and on the upper and lower altitude edges[3] and the minimum and maximum CAS margins, to be representative of the behavior of the engine system. These cross-conditions then served to generate the input test cases described in Section 3.2.1 for the Rugged and Parametric analyses, which are discussed in the following chapters. The following figures show these distributions with respect to the envelopes presented in Figure 3.2.

3.1.3 Control parameters

As explained in Chapter 2, some parameters of a turbomachinery are indirectly influenced by the rotational inertia of the gas generator and can be used as metrics of the robustness of the control system.

Below is a list of the acronyms used and their meanings

PLA: Power Lever Angle, is the throttle, expressed in *angular degrees* of actuation; it is the main command with which the pilot transmits the power

[2] δ, θ and σ are respectively pressure, temperature and density dimensionless normalized ratios with respect to their own reference value at SL (sea level): are used in aeronautical fields to define not standard atmospheric conditions and to scale those data from ideal ISA to real environment [32]

[3] It is relevant to notice that the upper and lower limits of altitude are not always covered by test points since in some cases the certified envelope is wider than some current real constraints, such as the current physical altitudes of the highest and lowest airports in the world [35]: consequently, they have not been taken into account in subsequent analyses

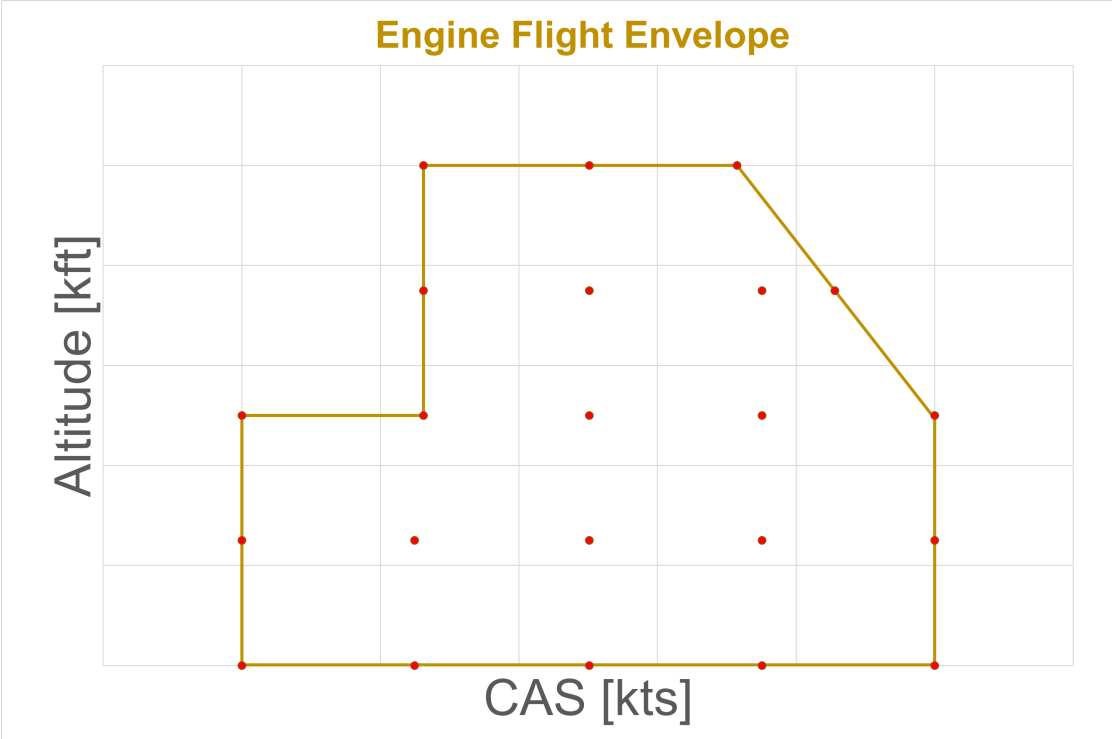

Figure 3.3: Flight Operating Envelope with Test Points

requests to the FADEC, which is then interpreted and converted - taking into account the ambient conditions and the punctual operating status of the engine - into references for the rotational speed of the generator gas, the fuel flow in the combustor, the actuation of any accessory valves, the torque control at the propeller shaft and the propeller pitch.

NG: number of revolutions of the gas generator, expressed in *rpm* (revolutions per minute) or more conveniently as a percentage of the maximum operating value; since the compressor and the turbine are mounted on the same shaft, this value represents their common speed.

ITT: Internal (or Intermediate) Turbine Temperature, the temperature measured between the turbine stages, in $°C$ or F (more rarely in K); it is the main safety control parameter in a turbomachinery because it is related to the thermo-mechanical stress to which the moving parts of the turbine are subjected.

Nprop: number of revolutions of the propeller, expressed in *rpm* (revolutions per minute); since the design choice of the turboprop under investigation was to maintain the rotational speed fixed, varying only the pitch of the propeller to obtain the different power/torque speeds, this parameter has a limited variability

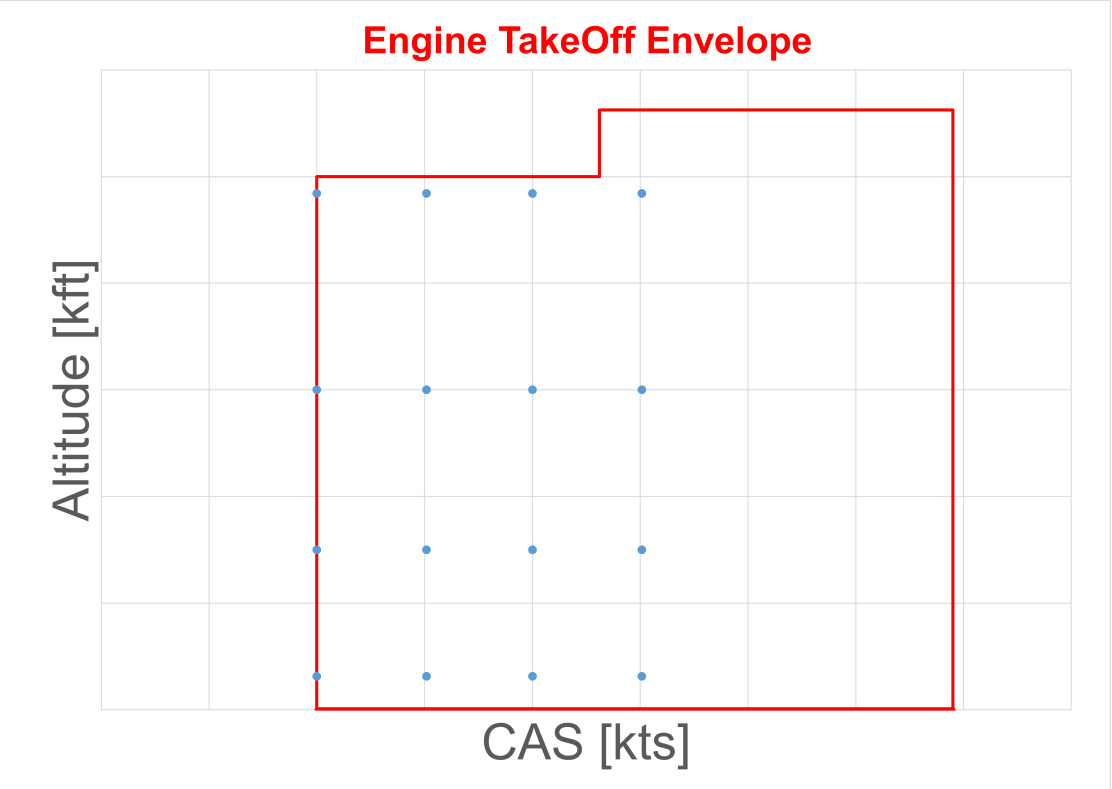

Figure 3.4: Take Off Operating Envelope with Test Points

at IDLE[4], cruising power and maximum power, obviously excluding transients.

PWR: share of the mechanical power supplied by the gas generator to the propeller, to be converted into propulsive thrust. It is given by the product of the torque developed at the propeller shaft, multiplied by its angular velocity. It is expressed in *lbs*ft* (pounds force per foot) as per the Anglo-Saxon metric system.

To correlate these parameters to the control system, the maximum value (to evaluate performance and safety) reached at the critical points of each maneuver and the settling times to the reference value (to monitor the controllability by the FADEC) required by the pilot command will be analyzed, between the Ruggedized version and the noRuggedized version, in each flight condition assigned by the test points: if the difference falls within a fixed band of variability accepted by the

[4]IDLE indicates the minimum self-sustaining speed of a turbomachine, i.e., the minimum rotational speed that allows the engine to sustain combustion and remain on and running without external energy aid

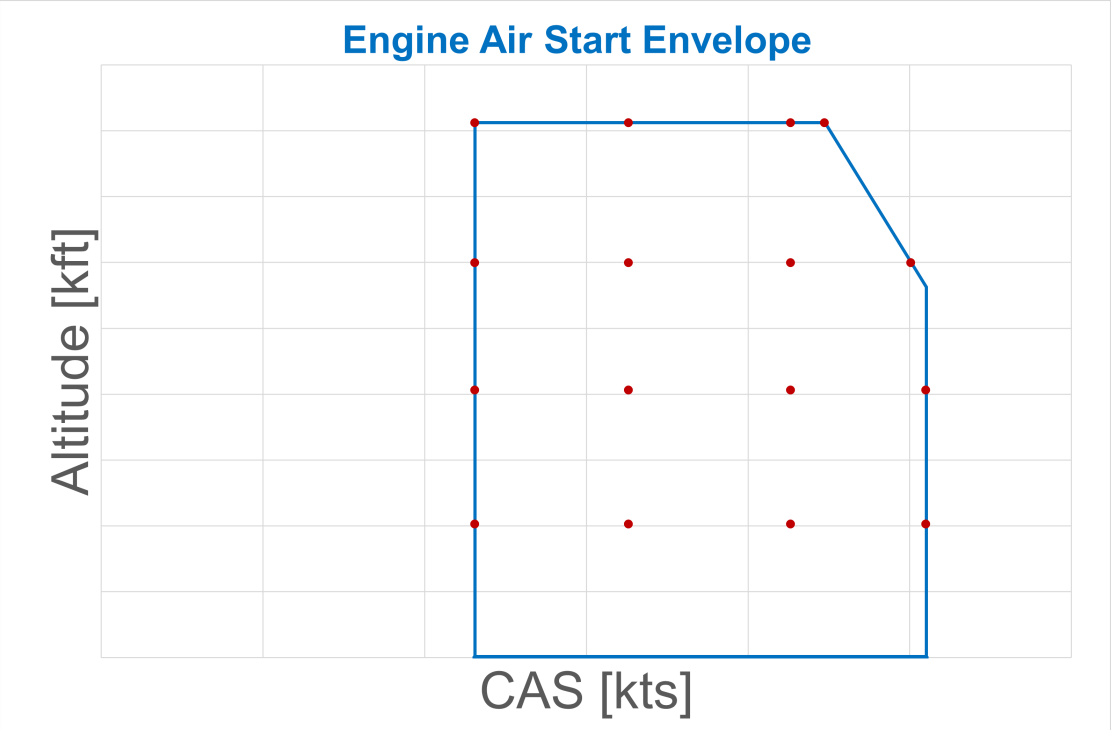

Figure 3.5: Air Start Operating Envelope with Test Points

project[5], the noRuggedized version can be considered acceptable and safe to test with subsequent methods (e.g., in a test cell).

3.1.4 Maneuvers

The maneuvers used to test the response and performance of the Ruggedized version are listed and elaborated below, with an overview of their peculiar phases, pilot commands, critical issues faced by the engine and the highlights of the control exercised by the FADEC.
Some observations

- Take Off & Climb - The maneuver begins with the engine already running, to save computational resources and simulation time already used for the Ground Start maneuver; it is the maneuver with the fewest test cases because since it is a particularly complex maneuver, which includes strong variations

[5]The so-called *engine-to-engine* variability is the small difference in performance and responses observed between the engine specimens produced at the time of analysis, caused by the construction tolerances of the various prototypes

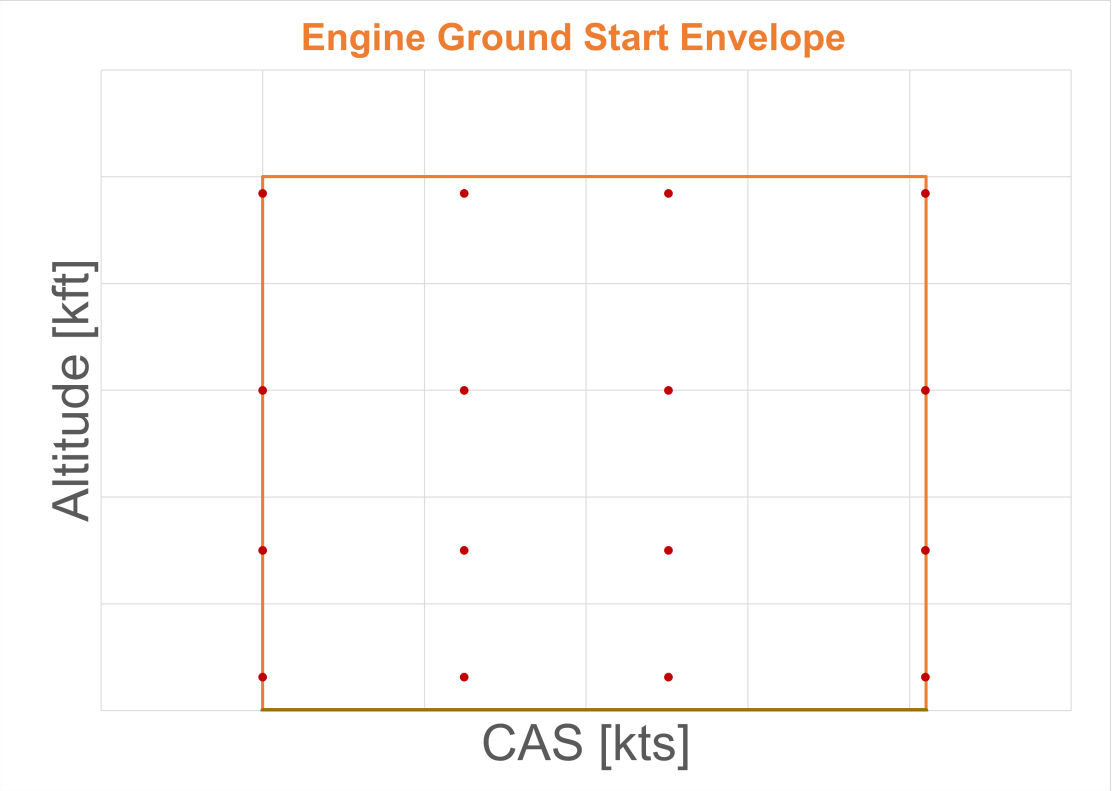

Figure 3.6: Ground Start Operating Envelope with Test Points

of many parameters at the same time, it was based on an approximate reconstruction starting from data from a real flight test; however, to remain conservative, we limited ourselves to a portion of the maneuvering envelope around the available conditions

- Burst & Chop - The dwelling time when the commanded power is reached is such as to allow the engine to reach a steady state at all operating points of its envelope, regardless of the ambient conditions. There are two drives, one high-power and one maximum: the latter is a power regime that is rarely exploited in classic missions, but is representative of the engine's operational maximum

- Slow Ramp - There are two maneuvers to test two different ramp time profiles, with twice the duration of each other

- Air Start - Also in this case there are two maneuvers: in the first, at *high rpm*, the time between the voluntary shutdown of the engine and its re-ignition is such as to allow the gas generator to slow down roughly below a minimum

NG threshold such that the FADEC can control the restart safely and avoid too abrupt pressure and/or temperature peaks; the second one, at *low rpm*, slows the engine below an even more critical threshold to observe its dynamic behavior in a more disadvantageous situation. The lower constraint on the altitude was obtained from a real flight test

Ground Start

The *Ground Start* maneuver is the continuous transition from a static condition, with the aircraft stationary on ground and the engine cold (or hot, in the case of ignition immediately following a phase with the engine active), to a ground IDLE regime stabilized and protected by the FADEC. Initially, the aircraft is parked, with brakes engaged, the area in front of the propeller is clear, and the configuration of the accessory systems is verified. If temperatures are very low, the manufacturer may require the oil to be preheated to a minimum temperature, typically not less than -40 °C, to allow starting and ensure acceptable viscosity. [36]

At this stage, the FADEC is already powered by the on-board electrical system: it performs the initialization of logical channels and the verification of critical sensors, preparing to automatically manage the start sequence. The pilot sets the power lever to the position corresponding to the ground IDLE and moves the fuel selector to RUN (or FUEL ON, according to the engine's specific nomenclature). The subsequent action on the START command engages the starter, an electric APU (Auxiliary Power Unit) or air-turbine that drives the gas generator up to a predefined NG value, while the free turbine and the propeller remain substantially unloaded or constrained by appropriate pitch devices (propeller in feather position, to limit torque). The first part of acceleration is generally a *dry motoring* phase: the rotor is dragged without fuel, with the aim of verifying that NG increases, that the oil pressure rises above zero within a time limit, and that no obvious mechanical anomalies emerge. [36]

When the compressor speed exceeds a set threshold, the FADEC enables the ignition system (igniters) and commands the opening of the fuel delivery valve to the nozzles, applying an ignition flow rate calculated to maintain the stability range in the combustion chamber without exceeding the turbine temperature limits. Light-off is recognized by the increase in turbine gas temperature (ITT) within a prescribed time window. In parallel, the compressor's air management system positions variable vanes and bleed valves in a start-up configuration to maximize the margin with respect to sub-idle surge conditions. [37]

Once the correct light-off has taken place, the thermal energy developed in the chamber allows the gas generator to accelerate beyond the threshold guaranteed by the starter. The fuel control law passes under acceleration conditions, in which the

FADEC simultaneously limits the NG gradient and the ITT, balancing the demand to reduce start-up time with the need to contain thermomechanical loads on hot components. The starter continues to contribute to the torque up to a cut-out speed, above which the turbine is able to support the compressor autonomously. Once this threshold is reached, the FADEC disengages the starter, keeps the ignition still active for a short safety interval, and then deactivates the igniters, leaving combustion to continue by autoignition. [37]

Consequently, the power turbine hit by the gases leaving the gas generator begins to accelerate and, through the gearbox, transmits torque to the propeller. To avoid excessive loads in a phase when the oil may still be cold, the propeller control unit (PCU) keeps the propeller pitch in a dedicated start position (feather or controlled end of step, depending on the design philosophy) in order to reduce the resistive torque on the power turbine. Only when the engine has reached a speed close to idle and the oil pressure is stabilized, the PCU allows the transition of the pitch towards the values provided for taxiing, coordinating with the FADEC which controls the torque through the fuel flow: the balance between the available energy of the generator gas and the propulsive speed is thus maintained, keeping Nprop at the target value through pitch variations. [37]

Once NG, Nprop, and ITT have been stabilized, the control logic abandons the start mode and moves to the idle regime of government. With the aircraft on the ground and PLA in the minimum position, the ground idle is automatically selected: the FADEC adjusts the fuel flow rate to keep NG at a minimum value compatible with full combustion stability and an adequate margin with respect to surge, taking into account any open bleeds (air for cabin conditioning, anti-icing, on-board services). Meanwhile, the propeller control imposes a propulsive speed of IDLE on the ground, typically lower than that used in flight, obtained by bringing the propeller pitch to a small positive angle (or slightly negative to compensate for the residual thrust of the core) so as to minimize traction during taxiing operations. At this point, the system is ready for warm-up at idle and for the subsequent transition to flight idle and take-off, climb, and cruise power ratings, which are also managed according to thrust/torque management laws derived from the position of the power lever. [37]

During Ground Start, the FADEC monitors the status of the engine and adjusts its parameters to ensure its performance and safety: at any time, it is able to interrupt the procedure autonomously when it detects abnormal starting conditions.

For thermal protection purposes, the FADEC tightly controls the gas temperature in the turbine or exhaust, using it as a limiting variable to modulate the fuel flow rate during ignition and acceleration ramp. It also uses characteristic pressures (e.g., high-pressure compressor outlet pressure, P3) to monitor the development

of the air flow rate and derive surge margin indices, thus adapting the fuel law to remain in a safe operating envelope.

A second critical issue is the management of the dynamics coupled between the gas generator, the power turbine and, in the case of turboprops, the propeller: the ignition of combustion takes place while the starter imposes a minimum speed on the gas generator, and the subsequent transition from external drag to self-sustaining must take place without dangerous oscillations or overshoots of speed and temperature. In addition, the surge margin of the compressor is minimal in the early stages of acceleration, so the fuel law must avoid dangerous air/fuel flow combinations that would lead to surge or flame out.

In the presence of auxiliary actuators (Inlet Vane or bleed valves), the FADEC coordinates their position to improve the surge margin during start-up and promote a smoother transition to idle mode, always keeping critical parameters (speeds, temperatures, stage pressures) within certified limits. [38]

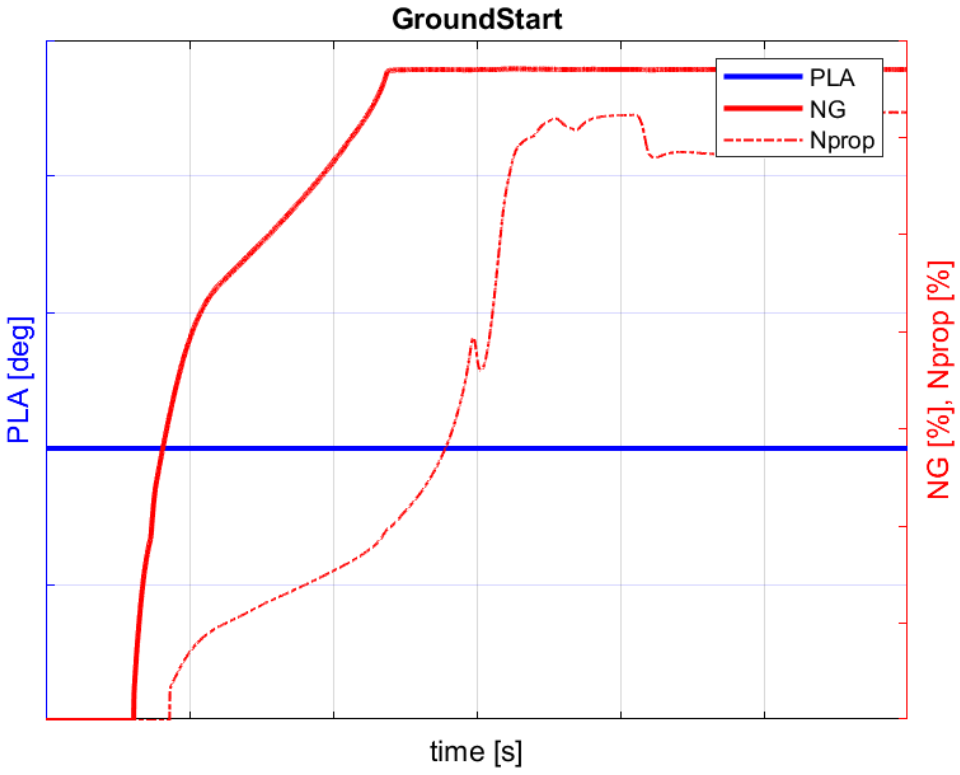

Figure 3.7: Ground Start maneuver

The example in **Figure 3.7** shows the time profiles of throttle PLA, engine rpm

NG and propeller rpm Nprop, during the *Ground Start* maneuver: it is easy to see how the procedure is completed without pilot intervention on PLA which remains stably at 0°, in the ground IDLE position, NG which follows its acceleration ramp up to its IDLE value and Nprop which similarly follows an increasing profile up to its IDLE regime, except for some intermediate oscillations related to control dynamics during the start-up phase that are automated and fully controlled by the FADEC.

Take Off & Climb

In the case of a single-engine aircraft, the *TakeOff* maneuver is probably the most critical phase of the flight, since the implications for safety are significant: the redundancy of the digital channels of the FADEC becomes essential, as well as the implementation of fault-tolerant logics that allow the continuation of the flight even in the presence of partial failures of the control system. The FADEC's ability to continuously monitor engine health and adapt control strategies to external conditions and component deterioration is a critical benefit for operational safety. [39]

During this phase, the pilot and the FADEC are required to have the integrated management of thermodynamic, mechanical, aerodynamic and stability constraints in a rapid and high-power transient regime: the pilot must monitor torque, ITT, NG (gas generator speed), Nprop (propeller speed) and aircraft speed, while the FADEC autonomously manages fuel flow, propeller pitch angle and any air bleed systems. In the most modern systems with single-lever control, the FADEC completely assumes the management of these parameters, simplifying the pilot interface but increasing the dependence on the correctness of the control software. [40]

The procedure begins with the configuration obtained from the previous Ground Start sequence, i.e., with the engine running and at idle: the pilot positions the throttle lever in the extreme forward position to obtain maximum engine rotational speed. The FADEC receives these inputs and automatically calculates the appropriate torque and ITT targets as a function of environmental conditions, site altitude, take-off speed, and aircraft weight. [39]

Subsequently, during the take-off run, the FADEC continuously monitors the fuel flow to maintain the target torque while monitoring the ITT to avoid exceeding thermal limits, balancing the balance between providing the maximum available power and not exceeding the thermomechanical limits of the engine. In parallel, it automatically adjusts the pitch angle of the blades to absorb the available power while keeping the propeller rotation speed constant (during take-off, it is typically at the maximum possible). [40]

As can be guessed, the main operational criticality during take-off concerns the

control of torque in relation to temperature limits. In turboprop engines, torque is indicative of the effort that the propeller exerts on the mechanical transmission to produce the required traction: at low altitude and low ambient temperature, the high density of the air is favorable to both combustion and propeller efficiency, allowing mechanical torque limits to be quickly reached. However, at higher altitudes and temperatures, the operating limit becomes the thermal limit of the ITT, which is a critical redline for engine integrity. [41]

However, the motor may be subject to other effects that must be taken into account in the design of the control:

- during the runway, the acceleration of the aircraft increases the total pressure of the air entering the engine (a phenomenon called *ram air*), which consequently increases the power delivered even with the same throttle position, risking an *overtorque* condition [42]
- the *compressor surge* occurs when the flow of air through the compressor becomes unstable, causing a reversal of the flow with sudden expulsion of the previously compressed air; during take-off, conditions of high power demand, low initial velocity and possible ingestion of foreign object debris (**FOD**) or birds make the engine particularly vulnerable to surge [PLACEHOLDER BIBLIO]
- the risk of *propeller overspeed* is particularly accentuated during rapid power transients and can cause excessive structural stress on the blades and hub, with the risk of structural failure [43]

The FADEC, for its part, must implement protection logics that limit the pilot's authority to prevent dangerous operating conditions. During takeoff, these protections are guaranteed by acceleration schedules that implement: [39]

- torque and acceleration limiters of rotating components (NG, Nprop) to counteract the effects of ram air and reduce mechanical stress on the gear transmission and propeller shaft [42]
- pressure limiters in the combustor that limit the maximum flow of fuel to prevent surge conditions, ensuring adequate stability margins during the rapid transients typical of take-off [40]
- temperature limiters to prevent thermal damage from exceeding the maximum ITT, as excessive temperatures can irreparably damage turbine blades, rings, fixed components, and combustion chamber elements [44]

These protections operate transparently with respect to the pilot, as the FADEC automatically selects the most restrictive limiter at all times. However, this control

architecture has as its counterpart the impossibility for the pilot to exceed the limits even in emergency situations. [39]

For fixed-wing aircraft (including many mono turboprops certified according to similar criteria to transport), the *climbing* path is often conceptually divided into segments [45]:

- first segment: from about 35 ft AGL[6] (screen height or lift-off altitude) up to fully retracted landing gear
- second segment: retracted landing gear, take-off configuration, V2 climb up[7] to approximately 400 ft AGL
- third segment: acceleration and retraction of flaps and/or slats, from about 400 ft AGL up to final climb speed
- fourth segment: from clean configuration and final climb rate up to 1500 ft AGL, which conventionally represents the end of the *takeoff flight path*

Therefore, from a performance-regulatory point of view, takeoff is finished as soon as the aircraft has completed the initial climb up to 1500 ft above-ground-level in a clean configuration (retracted lift devices) and with continuous climb power; from there on it enters the ascent phase towards cruising.

The example in **Figure 3.8** shows the time profiles of the throttle PLA, engine rpm NG and propeller rpm Nprop, during the *TakeOff & Climb* maneuver, starting with the engine already running: the PLA throttle is brought in a very short time almost to the end of the stroke in the very first takeoff phase and actual ascent ramp of the aircraft and so Nprop is also pushed to its maximum value; similarly, NG rapidly rises almost to its operational limit. In a second phase, the throttle is reduced to a value that maximizes the rate of climb (max climb), and Nprop stabilizes at its cruising operating value. Once the climb is complete, PLA is returned to IDLE, and NG stabilizes at its Flight IDLE value.

[6] AGL: above-ground-level

[7] V2 is defined as the minimum speed that must be reached at 35 ft AGL and maintained in the first phase of climb, such as to ensure an adequate margin above stall and good control/maneuverability characteristics in the take-off configuration. In the texts and performance tables of SETs (single-engine turboprops), V2 is more of a reference speed for the initial climb with all engines operating, than a real parameter linked to OEI (one engine inoperative) scenarios, such as for twin-engine engines

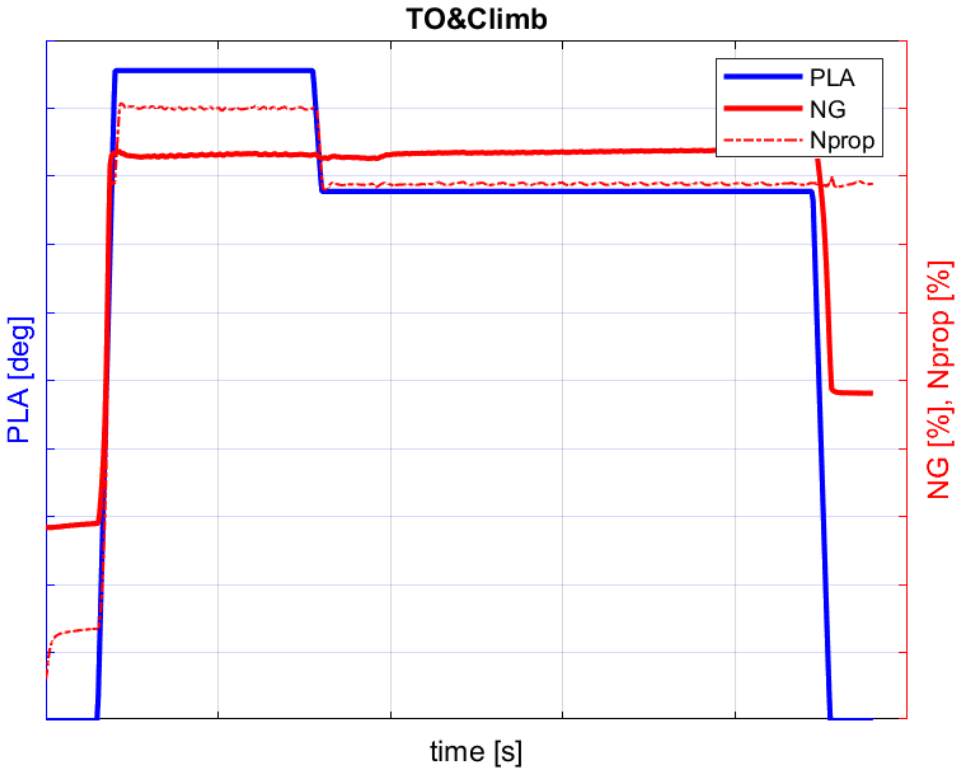

Figure 3.8: TakeOff & Climb maneuver

Stair Steps

The *Stair Steps* maneuver is characterized by discretized, controlled, and rapid variations in the operating speeds of the engine and propeller, and can be representative of a test for the analysis of the dynamic response of the propulsion system. [46]

In the configuration of a turboprop aircraft, the typical maneuver involves the gradual increase (or decrease) of the power required through a series of steps, and each level is maintained for a set time (dwell time) necessary for the system to stabilize and reach pseudostationary conditions before moving on to the next level. The procedure may also include the reverse and symmetrical decrement (or increase) maneuver. [46]

This test also allows the mapping of the engine performance throughout the flight envelope, providing the data necessary for the calibration of the power maps and for the verification of the linearity of the response to the throttle command [37]. The risks that must be faced in any case, and which then affect the design of

the control system are:

- control of thermodynamic transients during the acceleration steps, the ITT can go beyond the reference redline: the FADEC must therefore implement logics to limit the rate of increase in the fuel flow to prevent damage to the turbine [37]
- combustion instability - rapid transitions can cause flameouts or combustion instabilities, especially at intermediate power regimes where the fuel-to-air ratio is critical: again, the FADEC will have to manage the rate of change in the fuel flow to avoid these events [37]
- mechanical stresses on the rotors - the torque variations generated by the steps create torsional transients on the crankshaft and propeller – a stair-step endurance test can be specifically designed to induce these loads and assess fatigue strength [46]
- compressor depressurization - during rapid decelerations, the risk of compressor stall or surge increases significantly: the control system must manage the air bleed valves and the deceleration rate to maintain the stall margin [37]

For FADEC in short, the *stair steps* maneuver is useful for verifying:

- the simultaneous management of overlapping limits: rotor speed, turbine temperature, torque, and fuel flow; during the maneuver, these limits can be reached in rapid sequence, consequently requiring an appropriate priority selection logic [37]
- the accuracy of setpoint tracking and characterization of control loop timing [47]

The example in **Figure 3.9** shows the time profiles of throttle PLA, engine rpm NG and propeller rpm Nprop during the *Stair Steps* maneuver: the PLA and NG profiles are similar in the two symmetrical rising and falling step phases, with the NG variation less abrupt than the PLA counterpart because it is transparently regulated by the FADEC with respect to the pilot; Nprop remains substantially constant net of small transitory fluctuations at the steps.

Slow Ramps

The *Slow Ramp* maneuver in some ways represents a complement to the *Stair Steps* maneuver for the complete validation of turboprop propulsion systems. While the *Stair Steps* focuses on maximum transient stresses and robustness to large transients, the *Slow Ramp* highlights phenomena of long duration, thermal accumulation, possible control delays, and convergence of predictive models. [48]

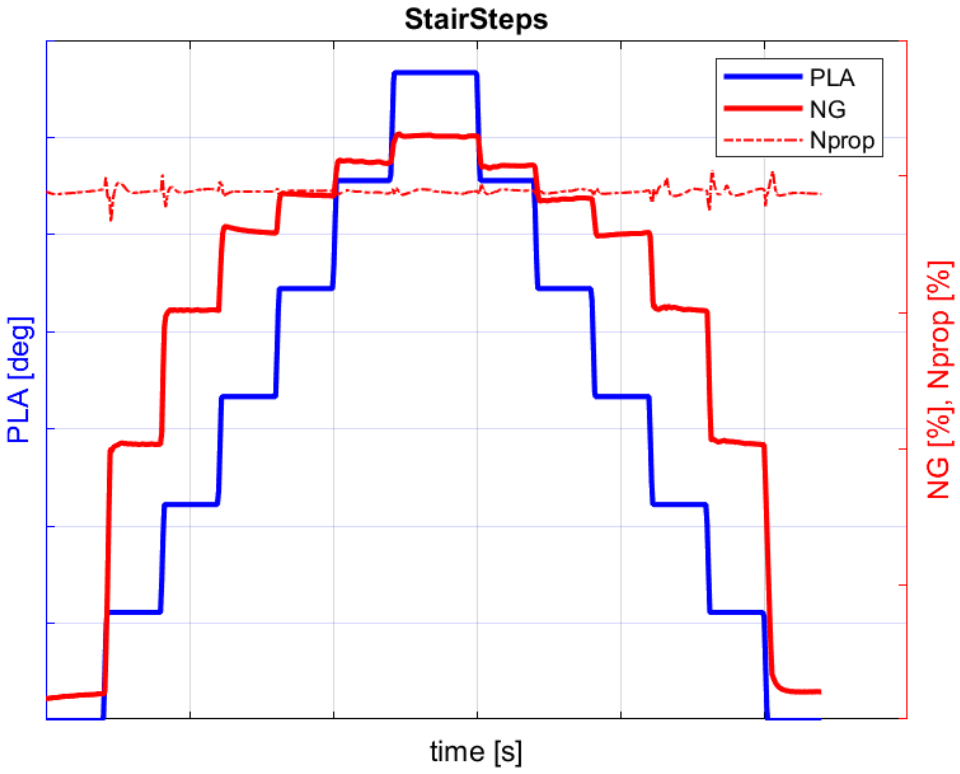

Figure 3.9: Stair Steps maneuver

Unlike the *Stair Steps* maneuver, which uses discretized variations, the *Slow Ramp* is characterized by continuous and gradually controlled temporal variations of the operating parameters of the engine and propeller.

The typical configuration includes:

- a monotonically increasing (or decreasing) acceleration (or deceleration) profile, according to a ramped profile with a predetermined and constant slope (linear) or a variable-controlled by the test system one
- progressive modification of the propeller pitch angle to keep its rotation speed constant
- pseudostationary conditions maintained along the entire ramp, allowing the study of the dynamic transient without discontinuity [48]

Usually, the throttle covers the entire power range, from idle to maximum/take-off power (and vice versa), in an assigned time interval, causing a relatively low rate

of thrust variation (usually 5-20 seconds for the full transition, but under test conditions it can be as high as 60 seconds) [48]

During the maneuver, the engine will come up against:

- thermal heat soak: the prolonged *slow ramp*, especially if repeated at short intervals, leads to an accumulation of heat inside the engine, causing a thermal effect - known as *hot re-slam* - which significantly changes the behavior of the system. These effects, critical for turboprops, cause: [48]
  - reduction of boundary layer thickness in compressors
  - changing the position of the operating line towards the stall boundary
  - unpredictable change in the available stall margin
- slow changes in fuel-to-air ratio during slow ramps can excite natural combustor frequencies, causing: [48]
  - combustion roughness (pressure fluctuations in the combustor)
  - flame extinction
  - inhomogeneous temperature in the combustor due to uneven air distributions

For FADEC, on the other hand, the *slow ramp* is essential to verify:

- the accuracy of thermodynamic predictive models, during the transient regime: if the model does not capture thermal heat soak effects, combustion reactions with delayed dynamics, and the variability of the air-fuel mixture, unforeseen violations of temperature limits may occur
- tracking the desired thrust profile without oscillations or instability
- communication delays, control latencies, and model errors without the masking due to fast transients, since the delay in the control loop could be comparable to the ramp time and bring out delays between the pilot command and the actual available thrust response or overshoot/undershoot
- similarly to the *stair steps*, the *slow ramp* also allows to verify the transition without discontinuity in the fuel flow control [49] between the different FADEC control modes, having to deal with the management of overlapping limits during the transition: overspeed, ITT, torque, air bleed valves. The priority selection logic must manage these limits in real time and continuously, without fluctuations [48]

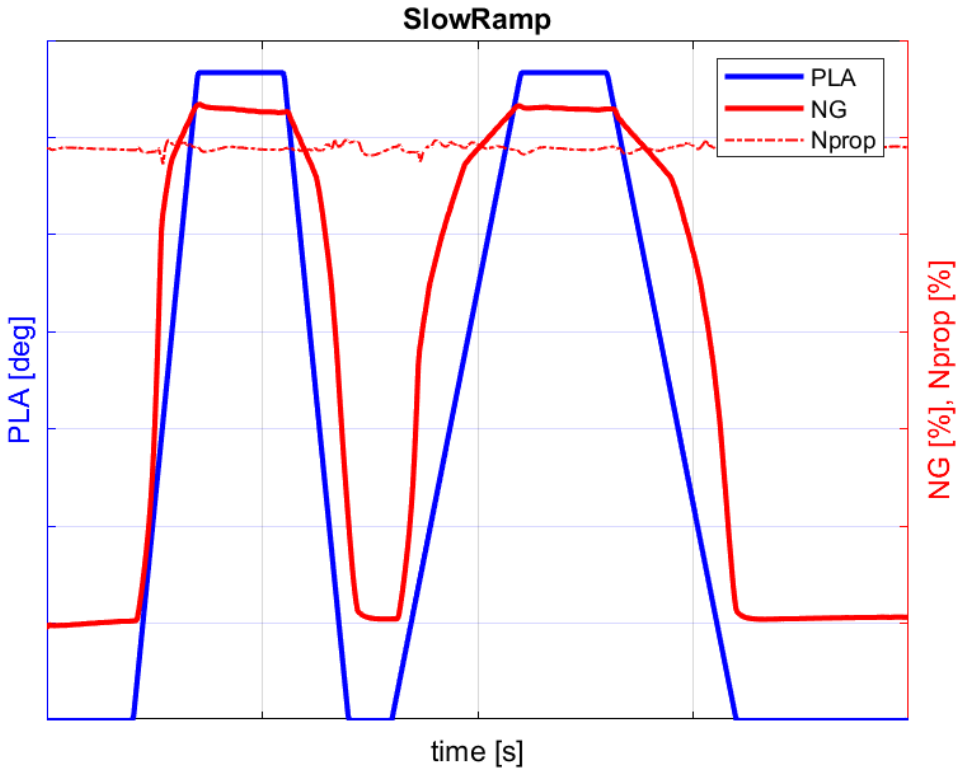

Figure 3.10: Slow Ramp maneuver

The example in **Figure 3.10** shows the time profiles of throttle PLA, engine rpm NG and propeller rpm Nprop, during the *Slow Ramp* maneuver: the PLA and NG profiles are similar in the ascending and decreasing sections, from IDLE to high power and return; Nprop remains substantially constant net of small oscillations at power transients. In the test cases, two slow ramps are carried out, the second with twice the duration of the first.

Burst & Chop

It is a transient test maneuver that is used in aeronautics fields to evaluate the performance and control systems of turbine engines, particularly turboprops. It consists of two symmetrical but opposite activations of the throttle (*PLA – Power Lever Angle*) by the pilot, from IDLE to maximum power (burst) and vice versa (chop); their peculiarity is the extreme speed with which they are completed, just a few seconds - i.e., the maximum actuation speed that the throttle lever physically allows. In the test phase, the time interval between the two parts may

vary depending on the need for the test itself, while in flight, the time will be determined by the specific needs or intentions of the pilot; the sequence of throttle activations can also be repeated several times in a row, depending on the specific need of the moment.

The maneuver helps to test the response of the control system in extreme transient conditions and thus verify the effectiveness of the FADEC in managing engine operating limits or as a stress test for control models or engine management algorithms. In terms of performance, it is also used to evaluate the stability of the compressor during rapid acceleration and deceleration. [50]

The maneuver has several critical aspects: [51]

- During acceleration (*burst*)
  - the High-Pressure Compressor (**HPC**) is at risk of stalling
  - the temperature at the inlet (T41) or inside (T45) of the turbine may exceed the structural limits
  - the core can experience overspeed, i.e., exceeding the speed limits of the shafts
  - thermal imbalance between contiguous mechanical parts, with rapid differential thermal expansions
- During deceleration (*chop*)
  - the Low Pressure Compressor (**LPC**) is at risk of stalling
  - risk of combustor blowout, i.e., shutting down the combustion chamber due to insufficient fuel flow
  - fluid-dynamic instabilities due to the temporary reversal of the air flow in the compressor

From the point of view of FADEC, the critical issues to be managed during the maneuver are [51]:

- the control of the limits on
$$\phi = \frac{W_f}{P_3}$$
i.e., the ratio between fuel flow and static pressure at the combustor inlet, to be maximized during the *burst* to prevent **HPC** stalling and turbine overtemperature, and to be minimized during the *chop* to prevent combustor shutdown
- the maintenance of stall margins on the **HPC** during acceleration and on the **LPC** during deceleration

In this way, the *burst and chop* maneuver helps to demonstrate: the response of the core speed within the limits, the activation of the limiters, the maintenance of the safety margins of the parameters involved, and the response time.

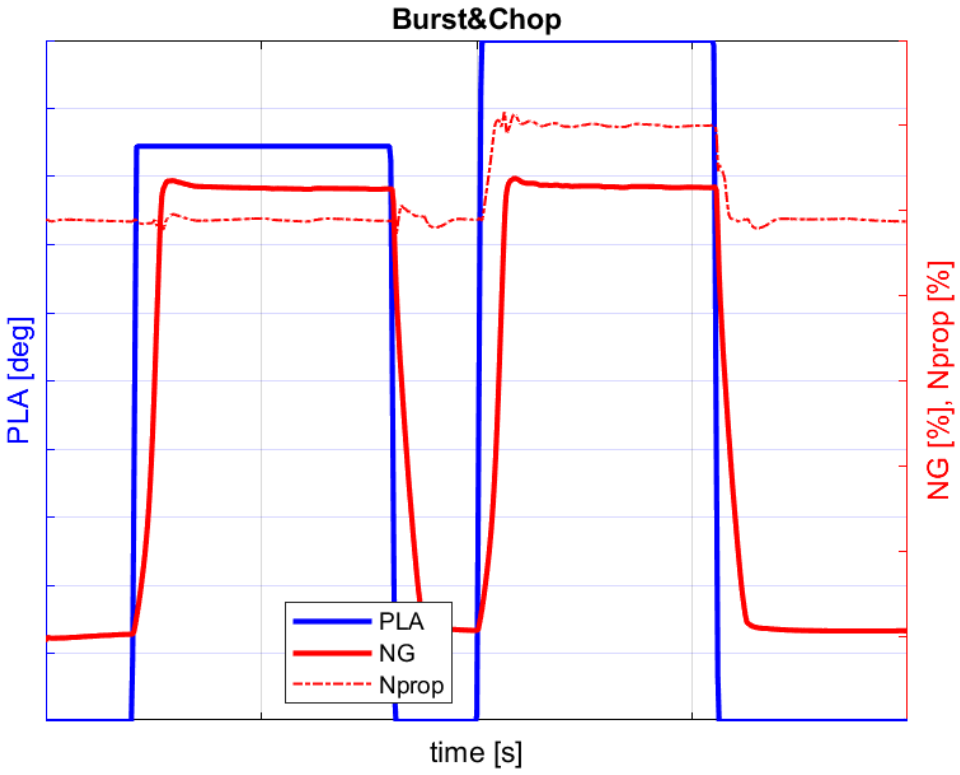

Figure 3.11: Burst&Chop maneuver

The example in **Figure 3.11** shows the time profiles of throttle PLA, engine rpm NG and propeller rpm Nprop during the *Burst & Chop* maneuver: the PLA and NG profiles are similar in the rising and falling sections, but PLA varies abruptly while NG follows a less steep ramp, regulated by FADEC to avoid stalling and flame-out phenomena. Two similar maneuvers are carried out: in the first a high power speed is reached, in the second the maximum level allowed by the throttle beyond the end of the stroke (overshoot) which, however, does not correspond to a similar increase beyond the NG threshold due to internal limitations to the control logics and the simulation model, but instead increases Nprop up to its maximum takeoff level.

Air Start

The *Air Start* (or more appropriately *Air Restart*) maneuver is a procedure for restoring engine operation during flight in the event of accidental (flameout) or controlled shutdown. For single-engine turboprop aircraft, the reliability and predictability of this maneuver are of crucial importance for the safety of the pilot, the payload, and the continuity of the flight. Unlike the *Ground Start* procedure, the *Air Start* represents a thermodynamically complex operation for the control system, and it has more stringent constraints related to the operating altitude, the Mach number, and the thermal conditions of the engine at the time of shutdown [52]

The procedure begins by verifying that the flight conditions fall within the certified restart envelope, i.e., assigned altitude and speed conditions [53]. The verification also includes: checking the pressurization of the fuel for its correct atomization and combustion; the amount of fuel available in the tank; quantity and pressure of engine oil in the hydraulic system - critical for the control of the propeller pitch and the lubrication of mechanical components [37]. For the rest, the *Air Start* procedure coincides with the sequence previously described in *Ground Start*, when it is carried out manually by the pilot.

In the event that the FADEC, based on instantaneous flight parameters, automatically determines that the gas generator RPM is sufficient for spontaneous combustion (windmilling relight), the procedure allows operation without the aid of the starter, so as to reduce the operational dependence on any pneumatic systems (APU or cross-bleed) and to increase operational efficiency, at the cost of more restrictive altitudinal envelopes. [54]

The certified windmilling relight envelope represents the intersection of two physical constraints: the minimum speed of the compressor for ignition, and the combustor load parameter to maintain flame stability. For representative turboprop engines, the typical envelope [52] is defined by:

- lower speed limit expressed in Mach number range, below which the dynamic flow does not provide sufficient ram pressure[8] to the compressor;

[8]The ram pressure at the compressor indicates the total pressure increase at the compressor inlet. The airflow in the inlet duct is slowed down (ideally in a quasi-isentropic manner) and part of the dynamic pressure $p_d = \frac{1}{2}\rho V^2$ it is converted into an increase in total pressure with respect to the undisturbed atmosphere (ρ is the density of the air fluid, V is the flight speed) due to the conversion of the dynamic flow pressure into static/total pressure due to the effect of the flight speed (ram effect or ram compression) [55]

- upper altitude limit, function of maximum combustor load[9];

During windmilling relight, the compressor works by stirring the air, generating a significantly lower increase in pressure and temperature at the combustor inlet than with an assisted starter, without performing efficient compression, making ignition more difficult at high altitudes. [57]

The ignition phase of the fuel in the combustor represents the critical and most decisive point for the success or failure of the maneuver. From a thermodynamic point of view, combustion conditions vary significantly with altitude and speed: low altitude and low Mach number are favorable conditions for ignition, high altitude and low Mach number are adverse conditions until critical margins for ignition are reached

This is because the operating altitude changes the conditions of entry to the combustor according to the following

$$p_{30} = p_2 \cdot \frac{p_3}{p_2}$$

$$T_{30} = T_2 \cdot \frac{T_3}{T_2}$$

where the pressure and temperature ratios depend themeselves by rotation speed of the compressor and the flight Mach number [56]

Similar to *Ground Start*, during *Air Start*, the FADEC has complete control over fuel ignition and regulation, accessory valves, propeller pitch, diagnostics, and engine limit protection [39]

- gas generator speed (NG), used as a fuel scheduling parameter and to monitor core acceleration
- Interstage Turbine Temperature (ITT), to monitor both the maximum operating limit and as an incipient hot start index
- compressor discharge pressure (p_3), to monitor its variation as a function of incipient stall detection and to derive the $\frac{p_3}{p_2}$ ratio, parameter for combustor load

[9]The combustor load defines the stability margins of the flame

$$L = \frac{W_{a,p} \cdot p_{30}^{1.8}}{\vee_{comb}}$$

where $W_{a,p}$ is the mass flow rate of air in the primary zone, p_{30} is the compressor discharge pressure and $\vee$ is the volume of the primary zone [56]

- propeller speed (*Nprop*), adjusted to the engine architecture by controlling the propeller pitch

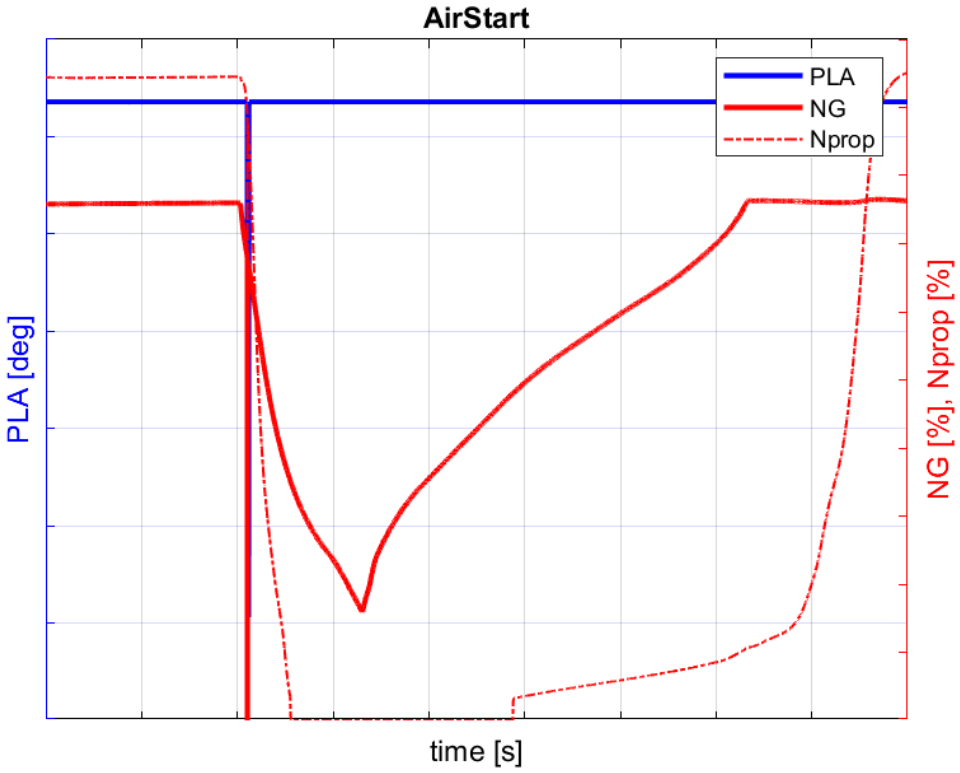

Figure 3.12: Air Start maneuver

The example in **Figure 3.12** shows the time profiles of the throttle PLA, engine rpm NG and propeller rpm Nprop, during the *Air Start* maneuver: the entire maneuver takes place without the pilot intervening on the PLA trigger, but only on the *start* control (not shown in the figure); in the first quarter of the image, the reset of the signals for a time unit during the engine shutdown is recognizable, coinciding with the collapse of the NG and Nprop values while the engine and propeller slow down due to their intrinsic mechanical resistance (the propeller even comes to a complete stop because it is exposed to the flow of outside resistant air); at the cusp point it is the moment of restarting, with the following increase in the number of rpm, until it returns to IDLE conditions. Again in this case, two conditions were simulated, high rpm (HiNg) and low rpm (LoNg): they are distinguished by the dwelling time between switching off and on again, thus obtaining two different initial NG values for the *Air Start* and thus testing the robustness of the maneuver

control.

3.2 Numerical Propulsion System Simulation

The test case simulations were performed with proprietary software from the same company that designed the turboengine, developed in an **NPSS** (*Numerical Propulsion System Simulation*) environment [58]. It is a non-linear, object-oriented thermo-fluid dynamics modeling environment developed for the simulation of propulsion cycles (aeronautical gas turbines, liquid rocket engines, supercritical CO_2 systems, etc.). [59]

NPSS was originally developed in the mid-1990s at *NASA's Glenn Research Center (GRC)* by the team of propulsion and software engineers, as part of NASA-industry cooperation programs. It is therefore a collective product with the participation of industry partners (GE, Pratt&Whitney, Boeing, Honeywell, Rolls-Royce, etc.). [59]
Nowadays, NPSS has evolved from a NASA environment for the virtual study of aircraft engines in research, to a standardized industrial platform, managed by a consortium and used today in a wide spectrum of applications, including digital twins and advanced energy cycles [59]

The NPSS software, therefore, implements numerical models of the thermodynamic performance of the engine and integrates them with pilot commands, FADEC control logic, and external environmental conditions.

3.2.1 List Engine Operations

A *List Engine Operations (LEO)* text file is used to provide the computational inputs to the NPSS software. This file contains all the instructions useful for the code to perform the simulation: the environmental conditions in which the aircraft operates, the pilot's throttle control, the control and protection adjustments of the FADEC; the code thus generates an output that contains the response of the system in terms of thermodynamic variables and FADEC signals.

A *LEO* file consists of three parts:

- the first contains general instructions on the format of the simulation output file, on the type of simulation environment (whether in a test cell or on a complete aircraft), and on the initial conditions of the engine (if initially off or already running and at *idle*); in this section it is also possible to insert instructions to punctually modify the FADEC control logic in case it is needed to study the effect of software modifications or simulate off-design engine conditions, but this will not be covered in this analysis;

- the second contains the list of all the variables that can be monitored by the FADEC and by the on-board (or cell) avionics, that are wanted to be in the output file: it is important to take care of this input section because it directly influences the simulation time and the size of the output, so it is a sensitive step to optimize the analysis;

- the third contains the complete and detailed description, time-stamp by time-stamp, of the maneuver to be simulated, including the pilot's commands, the ambient conditions, and any critical events that the simulation should include, always with a view to studying the response of the control system to external off-design stimuli.

3.3 MATLAB codes

After generating all the simulation outputs, the data were analyzed with codes written in MATLAB specifically for this thesis work.

`Lc55.m` is the main code: it contains all the instructions for the preliminary acquisition of data and formatting to be provided for the analyses carried out by the following functions, which it calls depending on the type of maneuver to examine.

- `Sam310.m` analyzes the *Ground Start*. It reports the maximum values of NG and ITT, and the rise time of NG to its reference IDLE value, for both Ruggedized and noRuggedized engine versions, comparing them and making sure that they fall within the engine-to-engine variability range

- `Mt82.m` analyzes the *Take Off & Climb*. It reports the maximum values of NG and ITT, the average value of PWR, and the rise times of NG and Nprop to their respective reference values in the phase of maximum PLA request, for both Ruggedized and noRuggedized engine versions, comparing them and making sure that they fall within the engine-to-engine variability range

- `Gv668.m` analyzes the *Slow Ramp*. It reports the maximum value of ITT and the average value of PWR in the phase of maximum PLA, and the rise time of NG to its reference value, for both Ruggedized and noRuggedized engine versions, comparing them and making sure they fall within the engine-to-engine variability range

- `Sal222` analyzes the *Stair Steps*. It reports the maximum value of ITT, the average value of PWR, and the average values of Nprop's derivative at every step, for both Ruggedized and noRuggedized engine versions, comparing them and making sure they fall within the engine-to-engine variability range

- `Mc440` analyzes *Burst & Chop*. It reports the maximum value of NG, ITT, Nprop, and the average value of PWR in the phase of maximum PLA, and the rise times of NG and Nprop to their respective reference values, for both Ruggedized and noRuggedized engine versions, comparing them and making sure they fall within the engine-to-engine variability range

- `AB112` analyzes the *Air Start*. It reports the maximum values of NG, ITT, Nprop, and PWR, and the rise times of NG and Nprop to their respective reference values, for both Ruggedized and noRuggedized engine versions, comparing them and making sure that they fall within the engine-to-engine variability range

To these are added two accessory scripts:

- `AlexCyc.m` to generate in bulk and sequentially all the required LEOs, starting from the test point conditions defined in Section 3.1.2 and with the two Ruggedized and noRuggedized engine configurations

- `Jacopino.m` to convert output files to a `.mat` or `.csv` format depending on later usage in MATLAB or Excel

All the listed scripts contain references to sensitive data or functions developed *ad hoc* to deal with the original data format and will not be attached to this thesis, with the exception of the main code `Lc55` reported in Appendix A.

Chapter 4

Rugged analysis

4.1 What we did

In this chapter, the results of the so-called **Rugged** analysis will be presented, comparing for each test point described previously in Chapter 3 the results of each maneuver examined, between the noRuggedized (*noRugg*) version and the Ruggedized (*Rugg*) version of the engine. The results are presented in the form of Excel graphs: each graph presents the result of a quantity of interest, with the y-axis suitably muted, in accordance with the company's requests for confidentiality on the technical data, plus the series of percentage deviations of the same quantity. The difference is considered acceptable if the percentage deviation falls within the range of variability $\pm 1.5\%$: this threshold value is applied to all the metrics studied and has been selected to simplify the massive evaluation, as it is the most restrictive of the applicable values.

4.1.1 Ground Start

NG

Figure 4.1 shows the data related to NG during the Ground Start maneuver. This parameter allows to verify that no overshoots have occurred during the entire duration of the maneuver. The graph shows, for each ID Case on the x-axis, the respective maximum values of NG for the noRuggedized version and for the Ruggedized version on the primary y-axis, and on the secondary axis is shown the respective series of percentage deviations between the two previous values. The comparison shows that the percentage deviations remain in the range of variability $\pm 0.01\%$ and emphasizes the conformity of the parameter between the two versions.

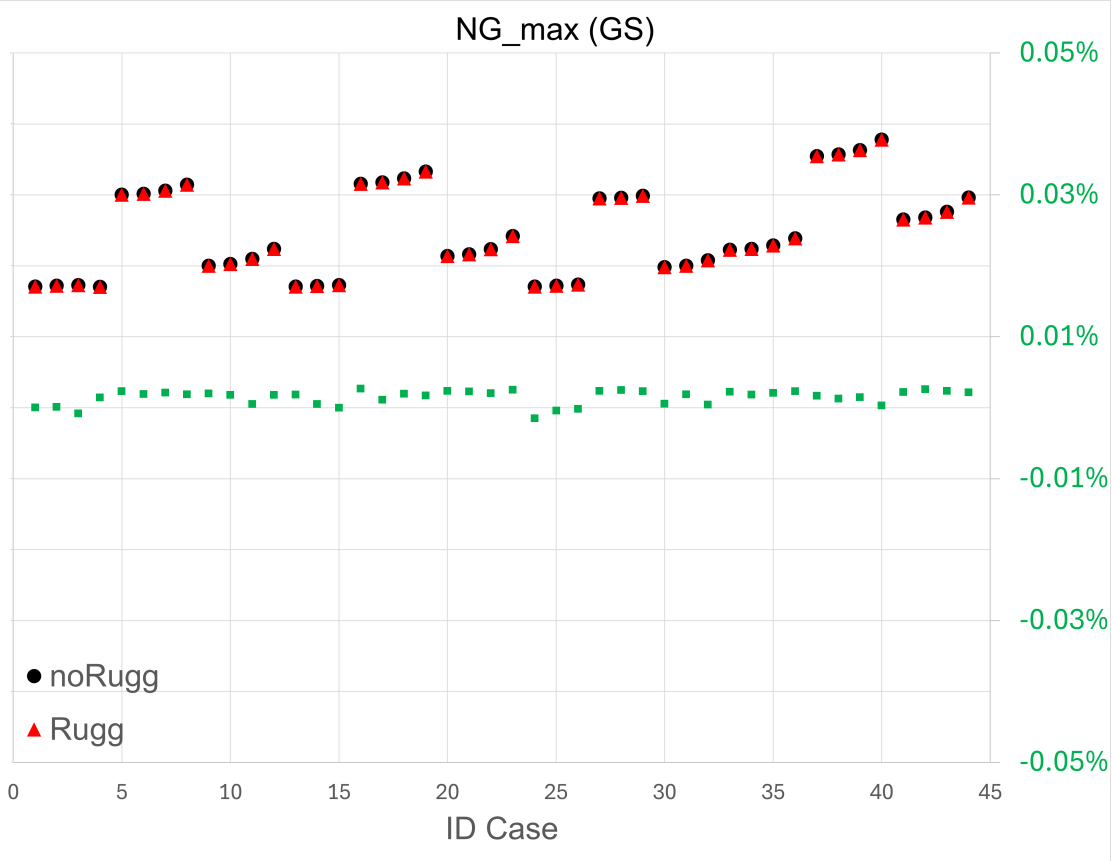

Figure 4.1: Ground Start - NG

ITT

Figure 4.2 shows the data related to ITT during the Ground Start maneuver. This parameter allows to verify that no overshoots have occurred during the entire duration of the maneuver. The graph shows for each ID Case on the x-axis the respective maximum values of ITT for the noRuggedized version and for the Ruggedized version on the primary y-axis, and on the secondary axis is shown the respective series of percentage deviations between the two previous values. The comparison shows that the percentage deviations remain in the range of variability $\pm 0.1\%$ and emphasizes the conformity of the parameter between the two versions.

Settling time

Figure 4.3 shows the data relating to the settling time of NG at its reference value during the Ground Start maneuver. This parameter allows to verify that the performance of the engine is guaranteed throughout the entire maneuver. The

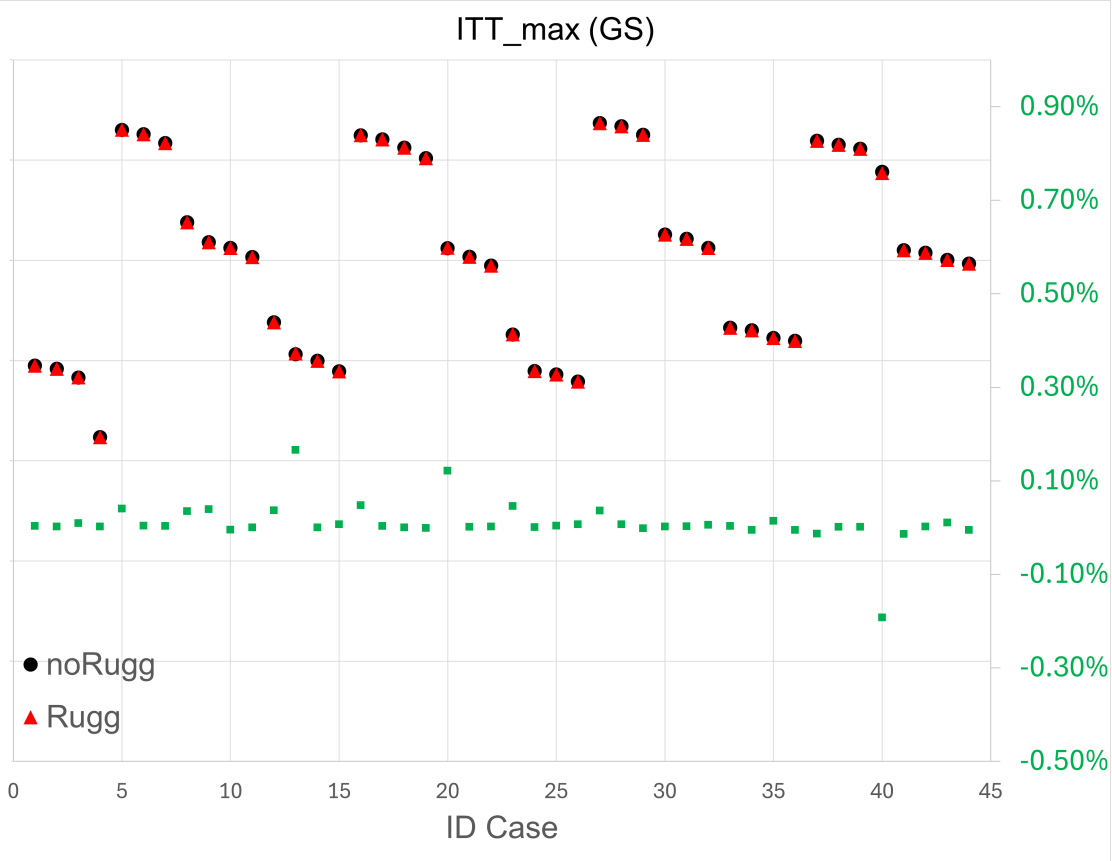

Figure 4.2: Ground Start - ITT

graph shows for each ID Case on the x-axis the respective rise values of NG for the noRuggedized version and for the Ruggedized version on the primary y-axis, and on the secondary axis is shown the respective series of percentage deviations between the two previous values. The comparison shows that the percentage differences remain in the range of variability $\pm 2.5\%$ and emphasizes the parameter conformity between the two versions.

4.1.2 Take Off & Climb

NG

Figure 4.4 shows the data relating to NG in the maximum throttle phase during the Take Off maneuver. This parameter allows to verify that no overshoots have occurred during the critical duration of the maneuver. The graph shows for each ID Case on the x-axis the respective maximum NG values for the noRuggedized version and for the Ruggedized version on the primary y-axis, and on the secondary axis

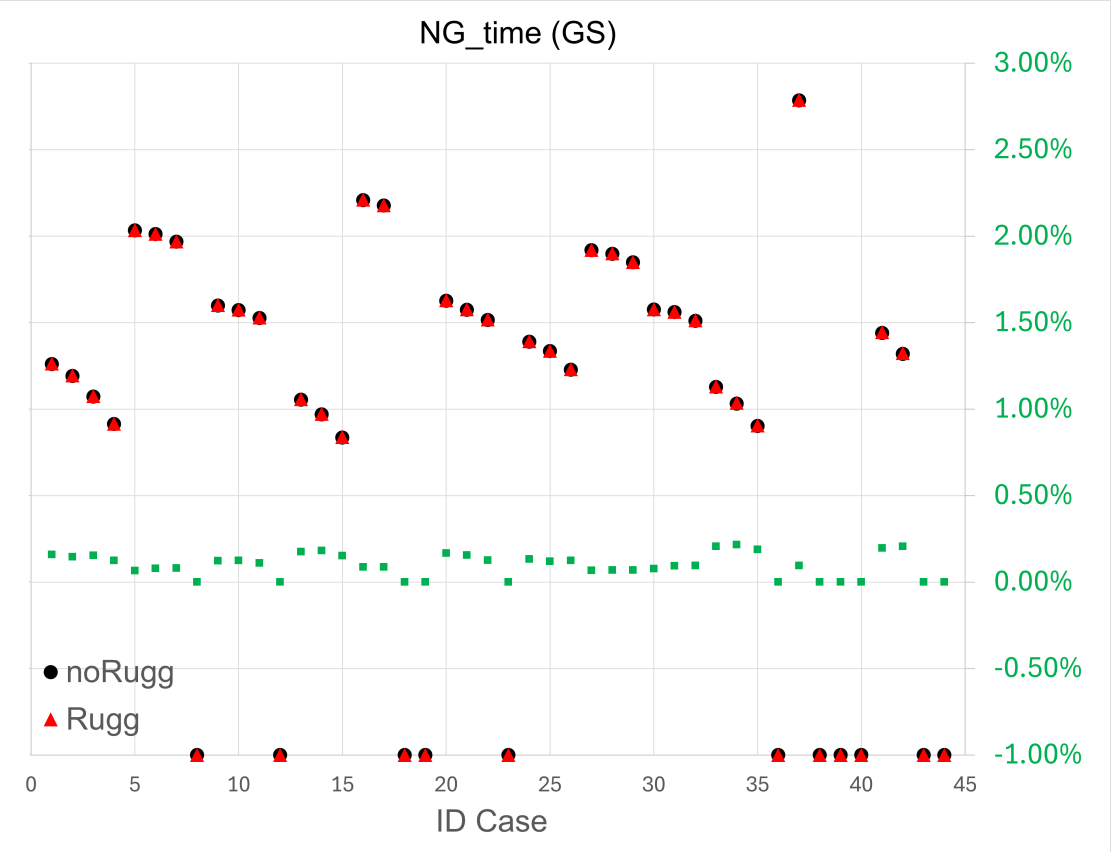

Figure 4.3: Ground Start - NG set time

is shown the respective series of percentage deviations between the two previous values. The comparison shows that the percentage deviations remain in the ±0.05% variability band and underlines the parameter compliance between the two versions.

ITT

Figure 4.5 shows the data relating to ITT in the maximum throttle phase during the Take Off maneuver. This parameter allows to verify that no overshoots have occurred during the critical duration of the maneuver. The graph shows, for each ID Case on the x-axis, the respective maximum ITT values for the noRuggedized version and for the Ruggedized version on the primary y-axis, and the secondary axis shows the respective series of percentage deviations between the two previous values. The comparison shows that the percentage deviations remain in the ±0.05% variability band and underlines the parameter compliance between the two versions.

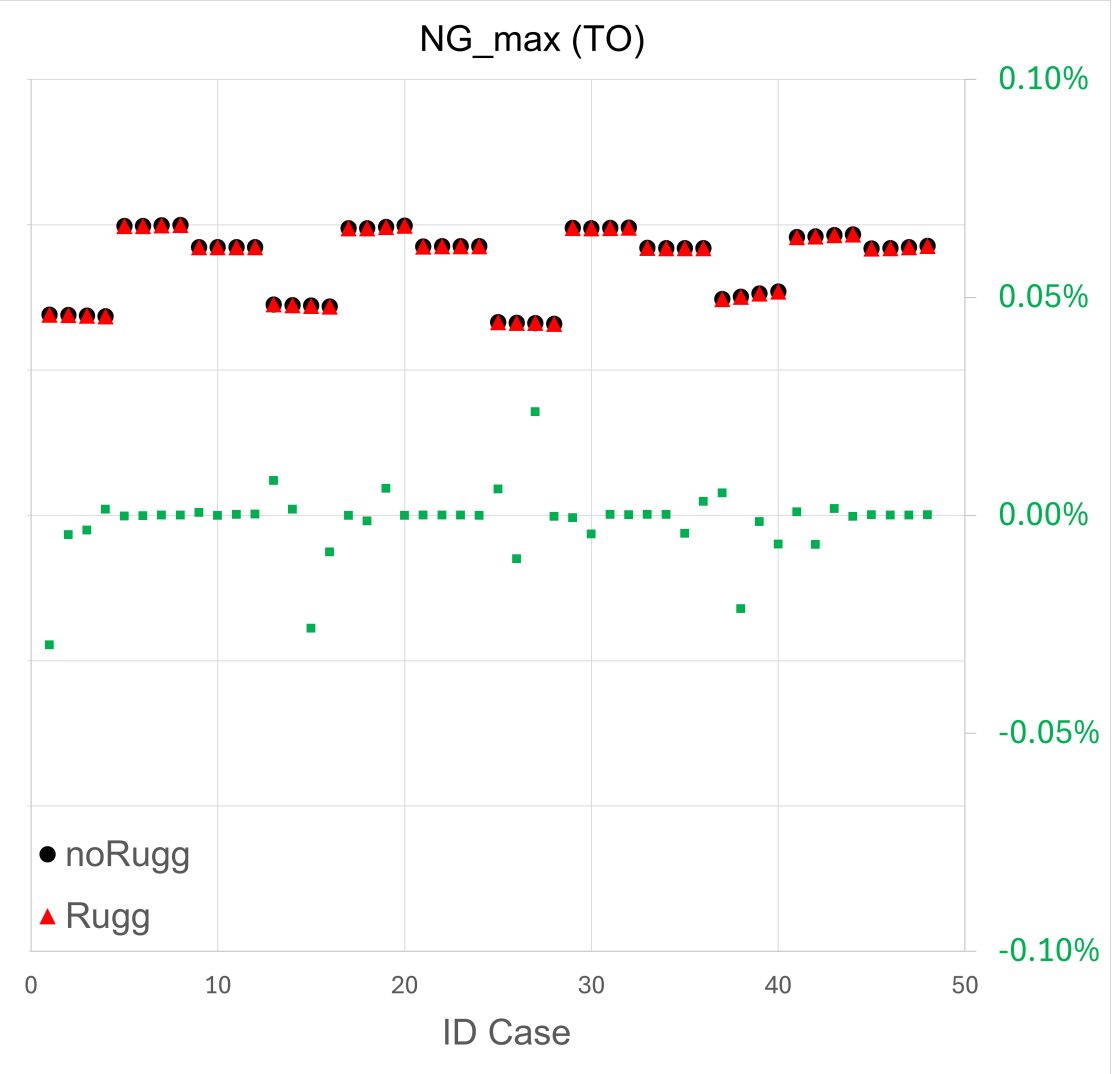

Figure 4.4: Take Off - NG

PWR

Figure 4.6 shows the PWR data in the maximum throttle phase during the Take Off maneuver. This parameter makes it possible to verify that the power delivered during the entire arc of the maneuver is adherent to the pilot's command. The graph shows, for each ID Case on the x-axis, the respective average PWR values for the noRuggedized version and for the Ruggedized version on the primary y-axis, and the secondary axis shows the respective series of percentage deviations between the two previous values. The comparison shows that the percentage deviations remain in the $\pm 0.01\%$ variability band and underlines the parameter compliance

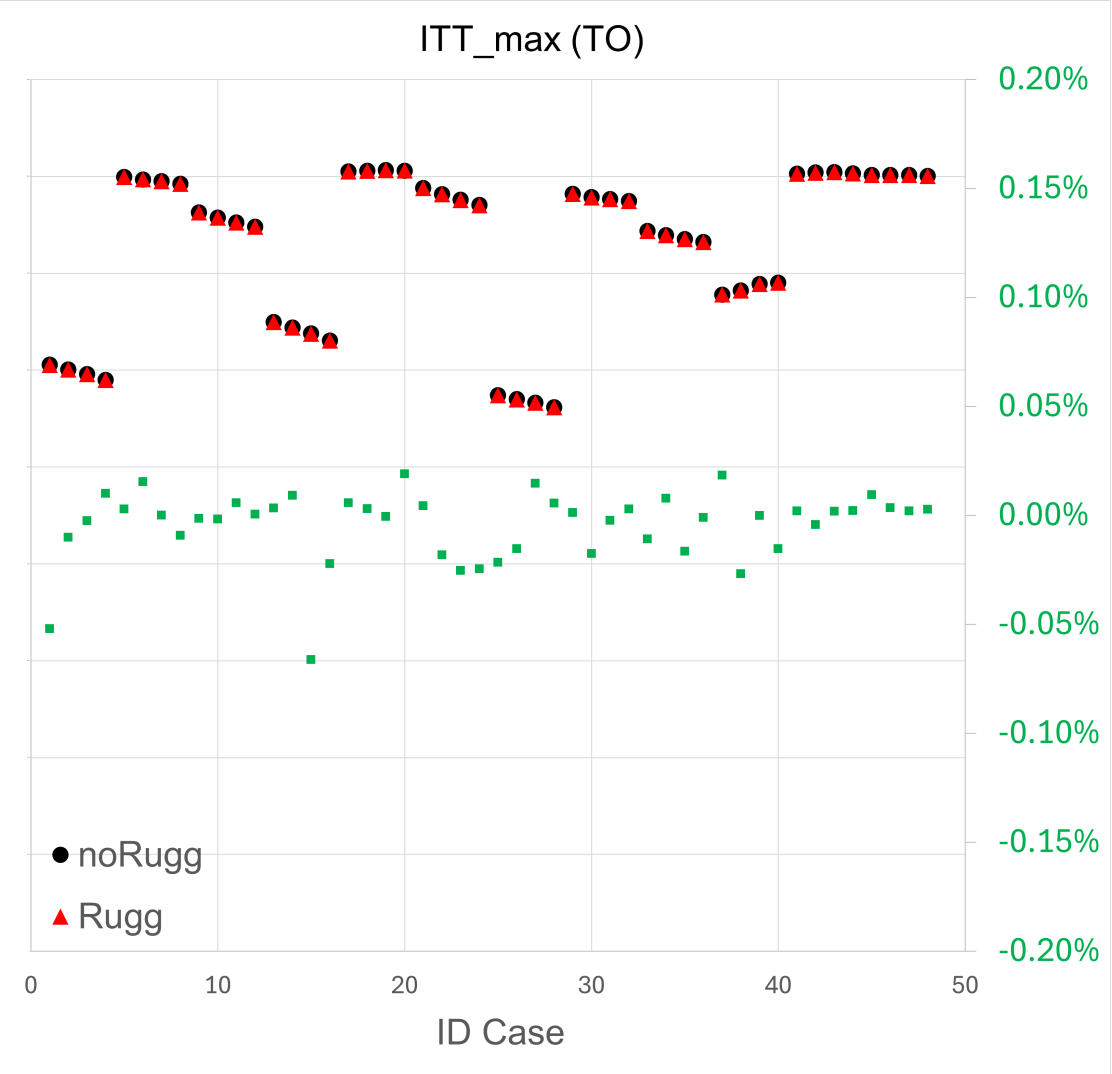

Figure 4.5: Take Off - ITT

between the two versions.

NG set time

Figure 4.7 shows the data relating to the settling time of NG at its reference value during the Take Off maneuver. This parameter allows to verify that the performance of the engine is guaranteed throughout the entire maneuver. The graph shows for each ID Case on the x-axis the respective rise values of NG for the noRuggedized version and for the Ruggedized version on the primary y-axis, and on the secondary axis is shown the respective series of percentage deviations between

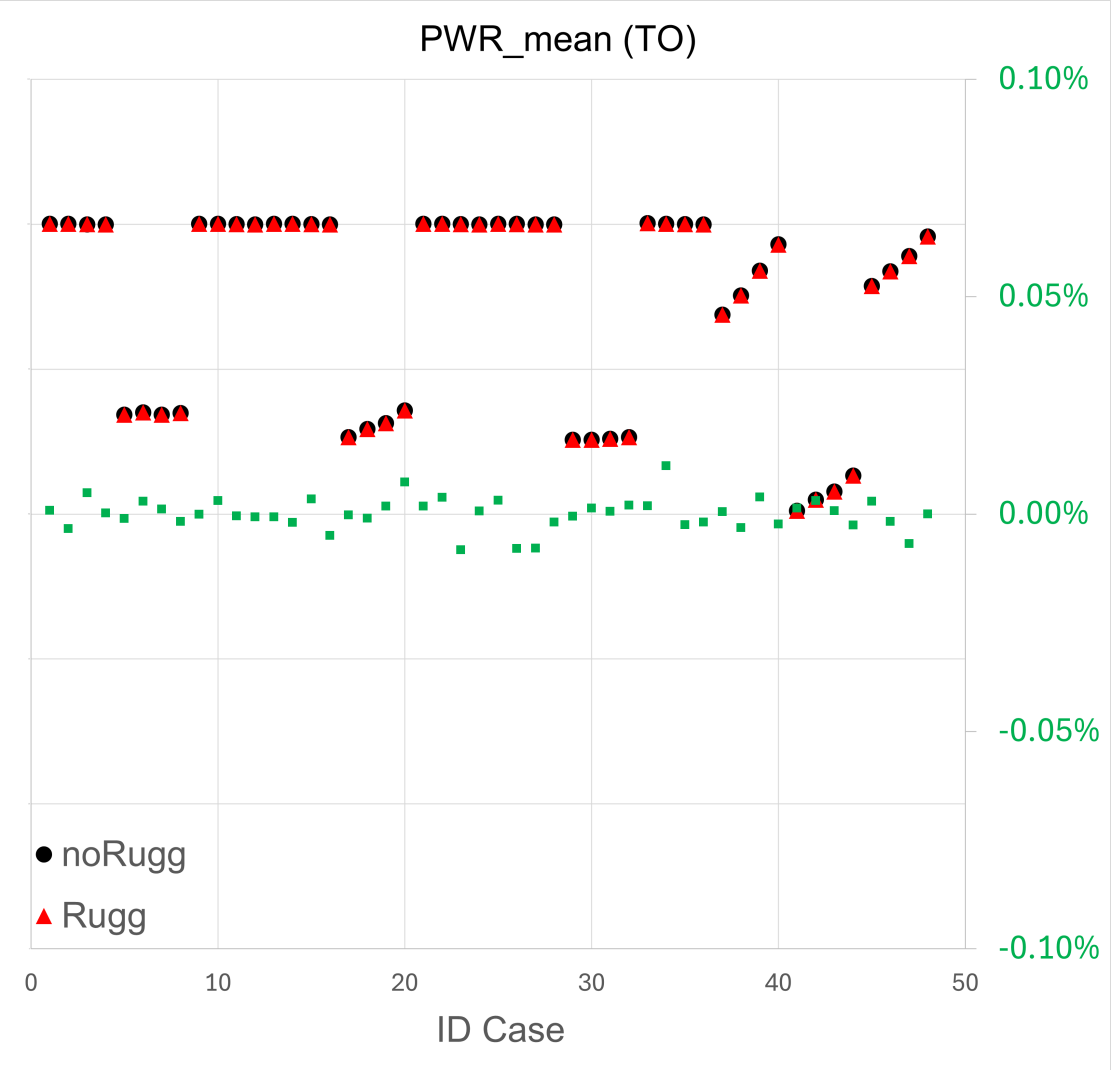

Figure 4.6: Take Off - PWR

the two previous values. The comparison shows that the percentage deviations remain in the $\pm 0.01\%$ variability band and underlines the parameter compliance between the two versions.

Nprop set time

Figure 4.8 shows the data relating to the settling time of Nprop at its reference value during the Take Off maneuver. This parameter allows to verify that the performance of the engine is guaranteed throughout the entire maneuver. The graph shows, for each ID Case on the x-axis, the respective Nprop rise values for

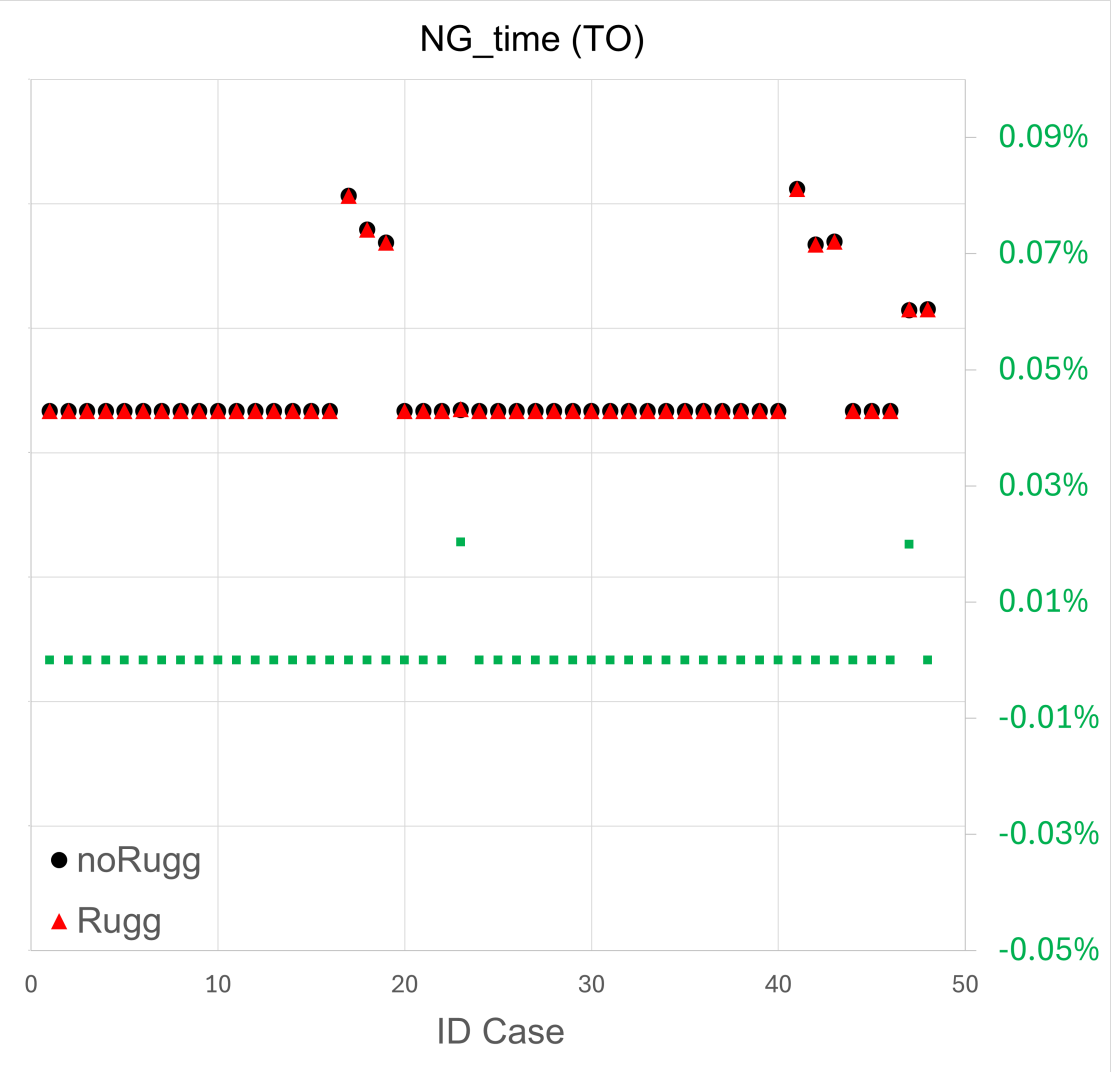

Figure 4.7: Take Off - NG set time

the noRuggedized version and for the Ruggedized version on the primary y-axis, and the secondary axis shows the respective series of percentage deviations between the two previous values. The comparison shows that the percentage deviations remain in the $\pm 0.1\%$ variability band and underlines the parameter compliance between the two versions.

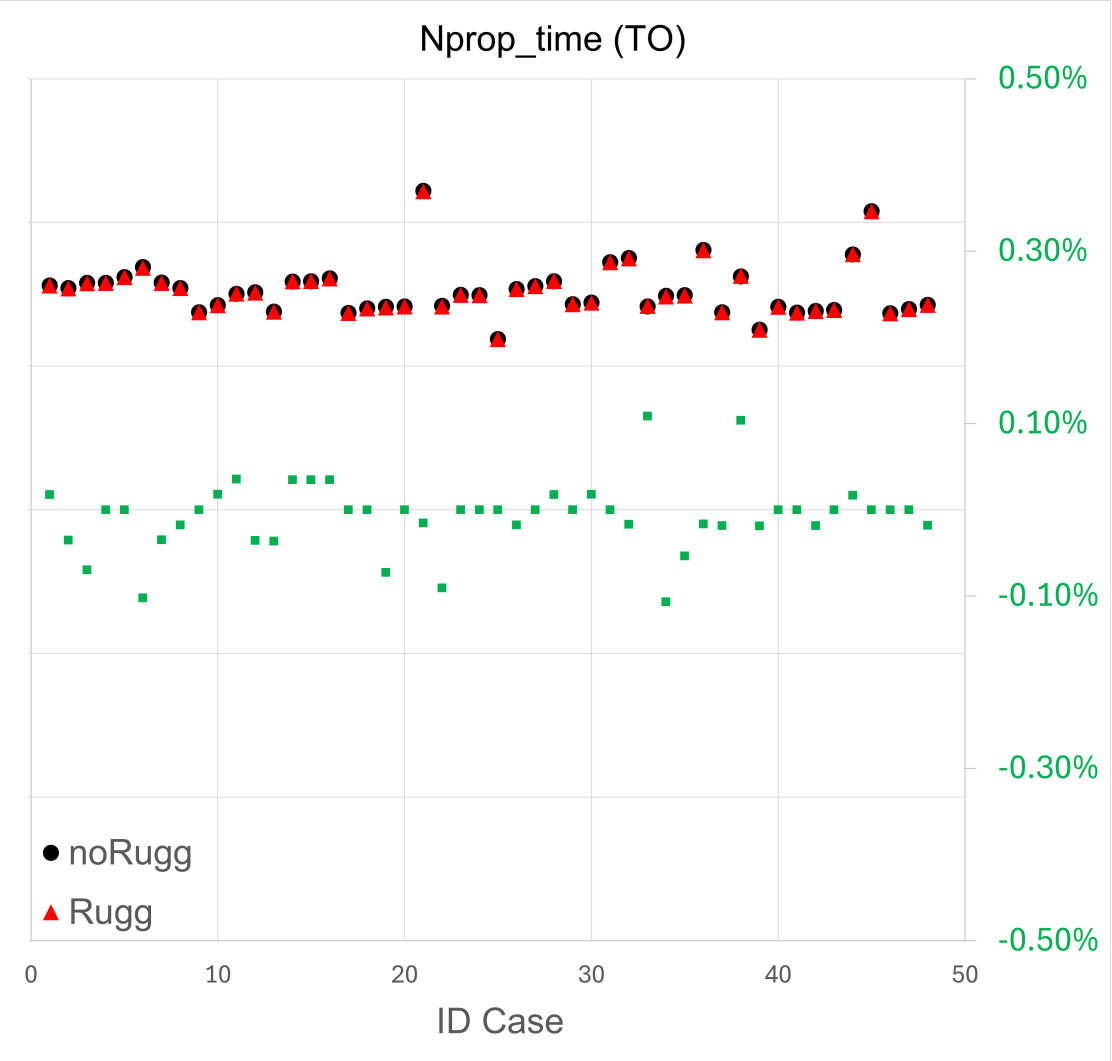

Figure 4.8: Take Off - Nprop set time

4.1.3 Slow Ramp - slow

ITT

Figure 4.9 shows the data relating to ITT in the maximum throttle phase during the Slow Ramp (slow) maneuver. This parameter allows you to verify that no overshoots have occurred during the critical duration of the maneuver. The graph shows for each Case ID on the x-axis the respective maximum ITT values for the noRuggedized version and for the Ruggedized version on the primary y-axis, and the secondary axis shows the respective series of percentage deviations between the two previous values. The comparison shows that the percentage deviations remain

in the ±0.05% variability band and underlines the parameter compliance between the two versions.

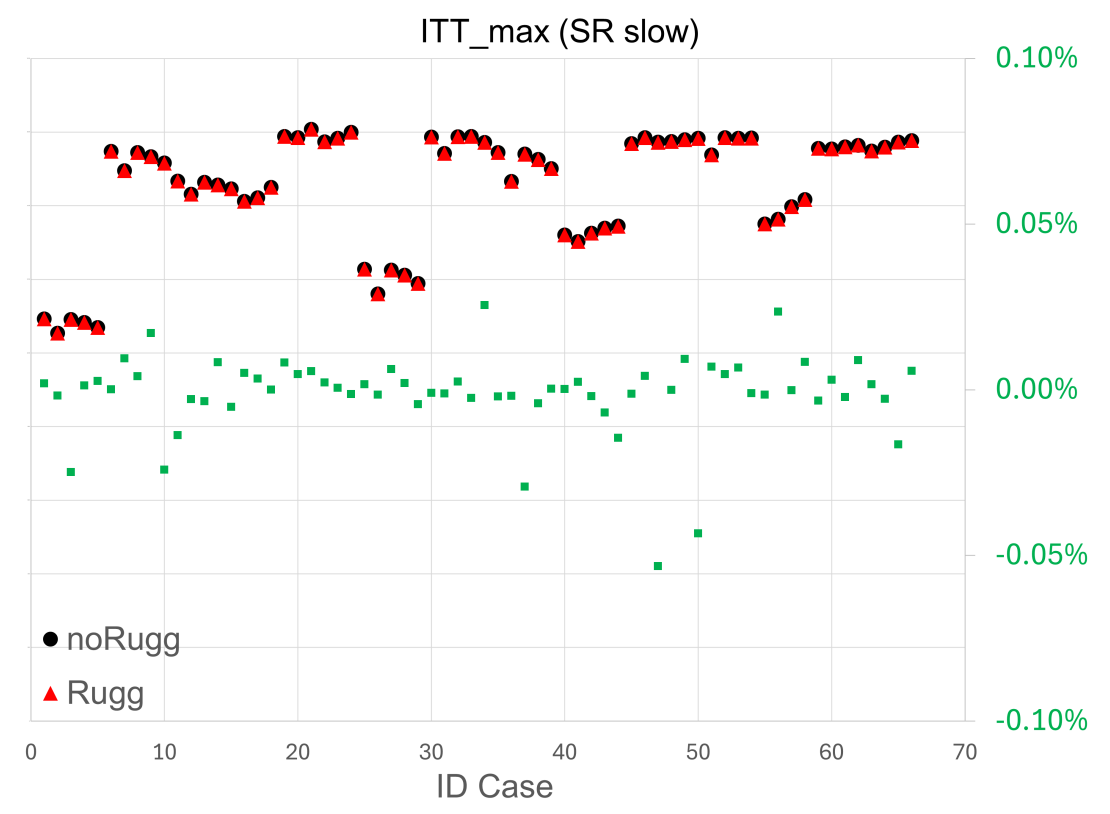

Figure 4.9: Slow Ramp (slow) - ITT

PWR

Figure 4.10 shows the PWR data in the maximum throttle phase during the Slow Ramp (slow) maneuver. This parameter makes it possible to verify that the power delivered during the entire arc of the maneuver is adherent to the pilot's command. The graph shows, for each ID Case on the x-axis, the respective average PWR values for the noRuggedized version and for the Ruggedized version on the primary y-axis, and the secondary axis shows the respective series of percentage deviations between the two previous values. The comparison shows that the percentage deviations remain in the ±0.01% variability band and underlines the parameter compliance between the two versions. Figure 4.11 shows the data relating to the settling time of NG at its reference value during the Slow Ramp (slow) maneuver. This parameter allows to verify that the performance of the engine is guaranteed throughout the

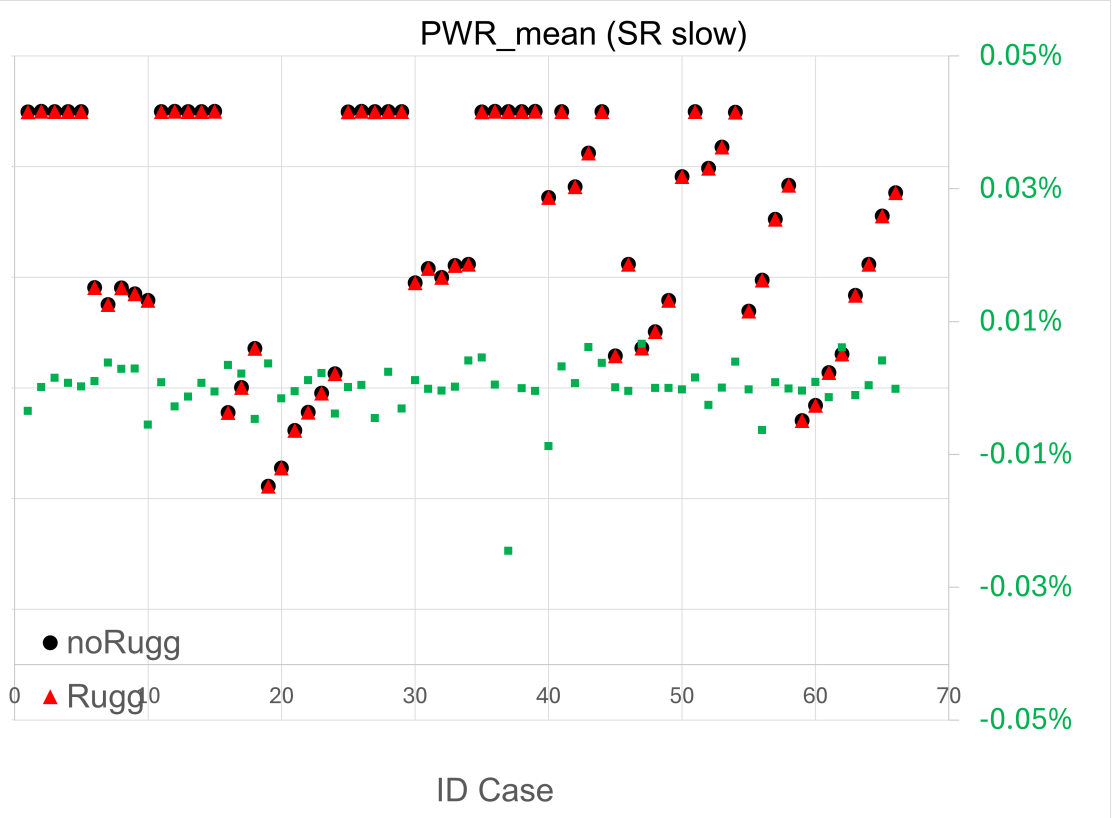

Figure 4.10: Slow Ramp (slow) - PWR

entire maneuver. The graph shows, for each Case ID on the x-axis, the respective rise values of NG for the noRuggedized version and for the Ruggedized version on the primary y-axis, and on the secondary axis is shown the respective series of percentage deviations between the two previous values. The comparison shows that the percentage differences are practically zero and underlines the compliance of the parameter between the two versions.

4.1.4 Slow Ramp - fast

ITT

Figure 4.12 shows the data relating to ITT in the maximum throttle phase during the Slow Ramp (fast) maneuver. This parameter allows to verify that no overshoots have occurred during the critical duration of the maneuver. The graph shows, for each ID Case on the x-axis, the respective maximum ITT values for the noRuggedized version and for the Ruggedized version on the primary y-axis, and the secondary axis shows the respective series of percentage deviations between the

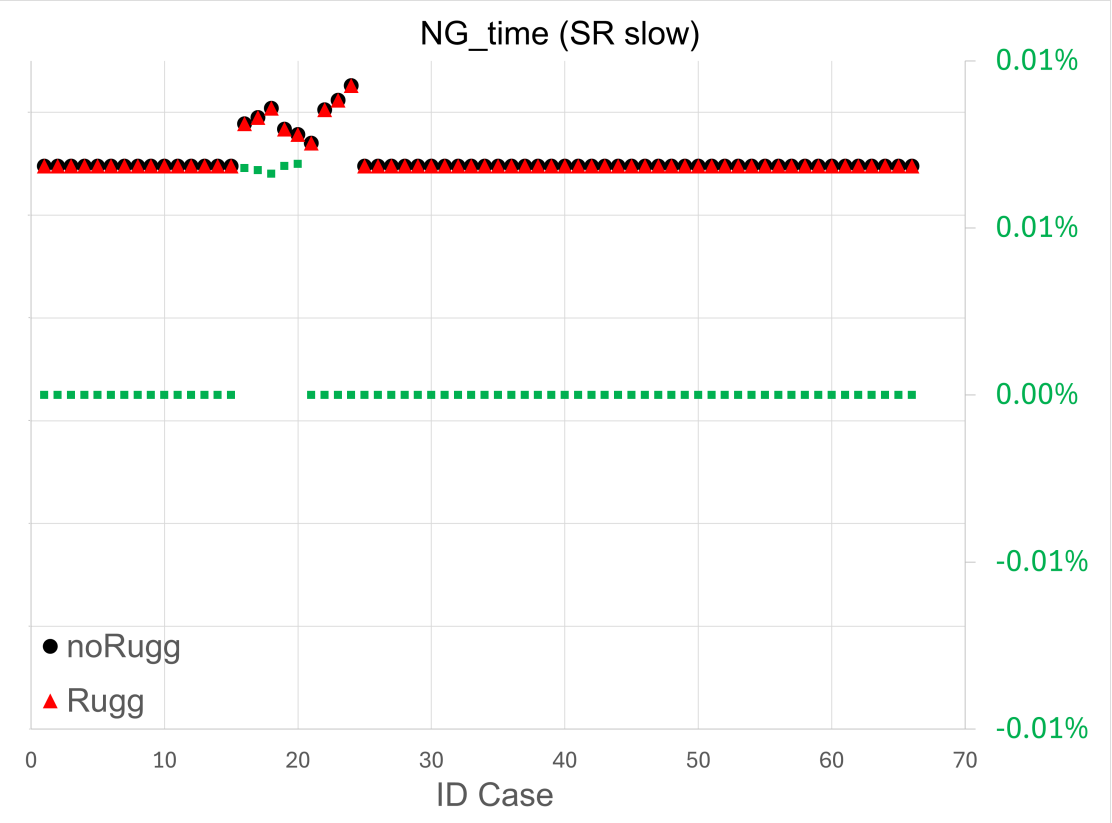

Figure 4.11: Slow Ramp (slow) - NG set time

two previous values. The comparison shows that the percentage deviations remain in the ±0.05% variability band and underlines the parameter compliance between the two versions.

PWR

Figure 4.13 shows the PWR data in the maximum throttle phase during the Slow Ramp (fast) maneuver. This parameter allows to verify that no overshoots have occurred during the critical duration of the maneuver. The graph shows, for each ID Case on the x-axis, the respective average PWR values for the noRuggedized version and for the Ruggedized version on the primary y-axis, and the secondary axis shows the respective series of percentage deviations between the two previous values. The comparison shows that the percentage deviations remain in the ±0.05% variability band and underlines the parameter compliance between the two versions.

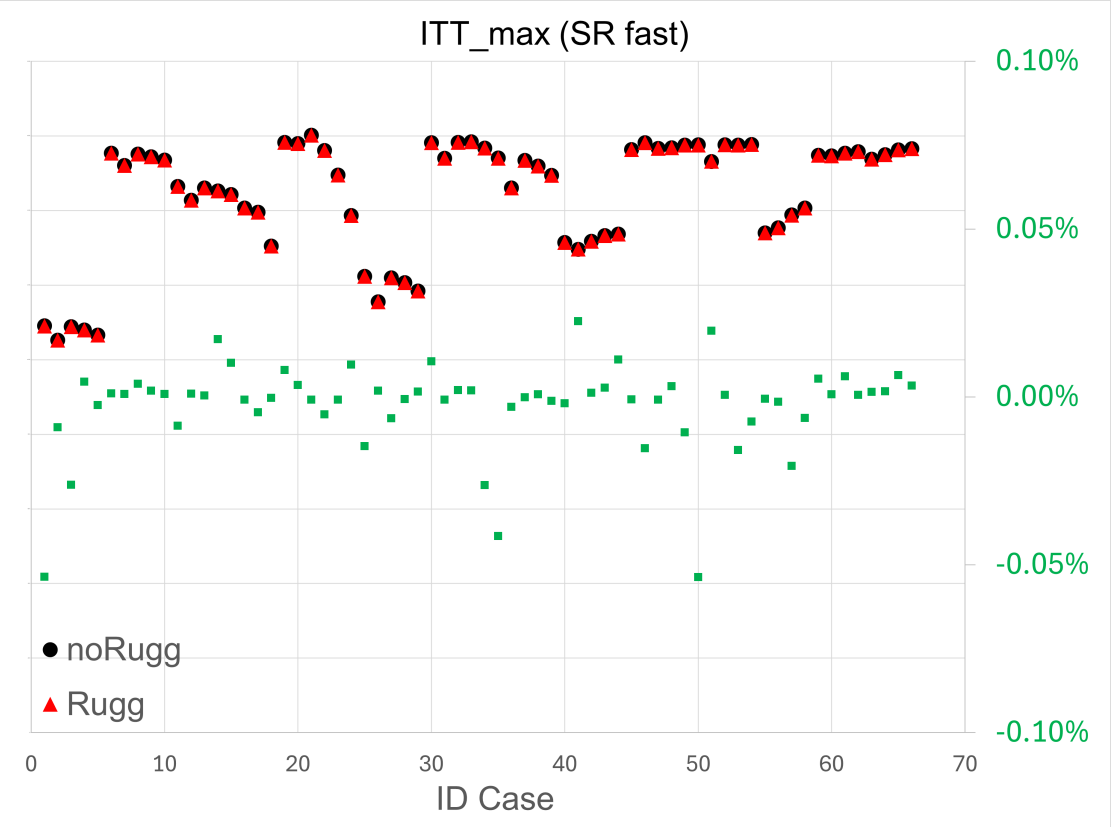

Figure 4.12: Slow Ramp (fast) - ITT

NG set time

Figure 4.14 shows the data relating to the settling time of NG at its reference value during the Slow Ramp (fast) maneuver. This parameter allows to verify that the performance of the engine is guaranteed throughout the entire maneuver. The graph shows, for each ID Case on the x-axis, the respective rise values of NG for the noRuggedized version and for the Ruggedized version on the primary y-axis, and on the secondary axis is shown the respective series of percentage deviations between the two previous values. The comparison shows that the percentage differences are practically zero and underlines the compliance of the parameter between the two versions.

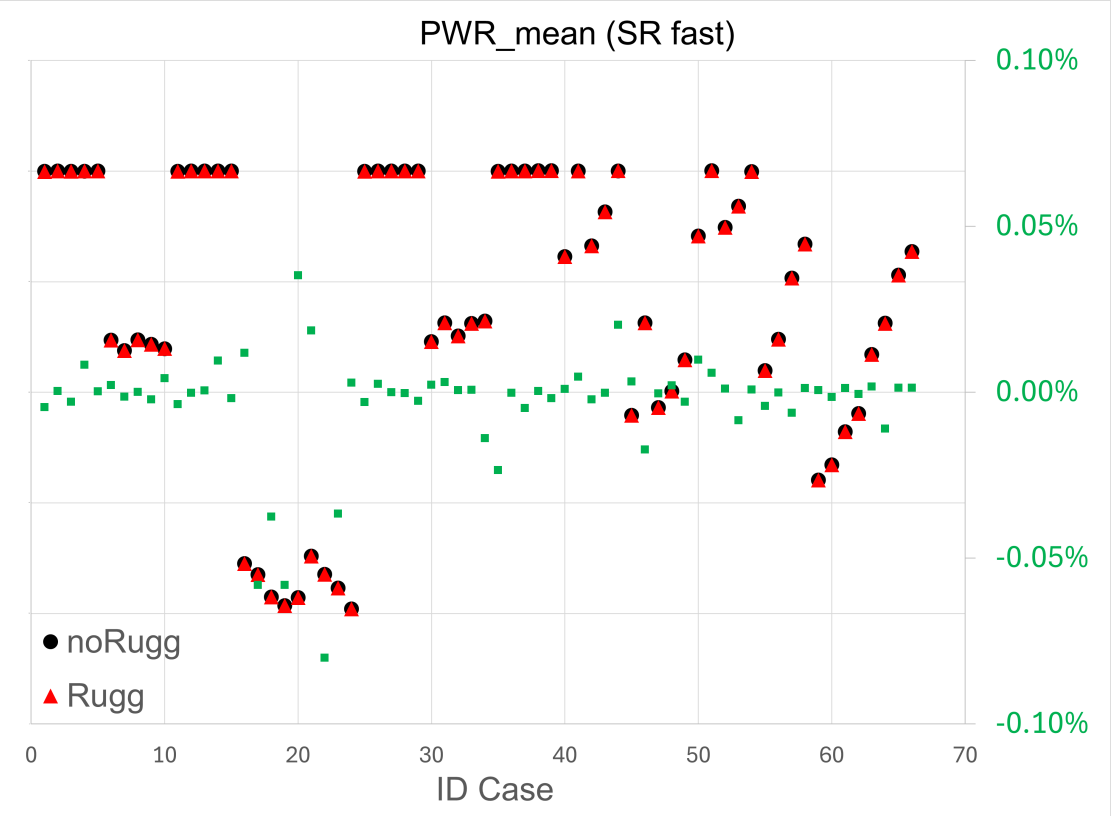

Figure 4.13: Slow Ramp (fast) - PWR

4.1.5 Stair Steps

ITT

Figures 4.15 and 4.16 show the ITT data in the phase of an upward step and a downward one, with the same final throttle value during the Stair Steps maneuver. This parameter allows to verify that no overshoots have occurred during a sample step of the maneuver. The graph shows, for each ID Case on the x-axis, the respective maximum ITT values for the noRuggedized version and for the Ruggedized version on the primary y-axis, and the secondary axis shows the respective series of percentage deviations between the two previous values. The comparison shows that the percentage deviations remain in the $\pm 0.05\%$ range of variability and underlines the compliance of the parameter between the two versions.

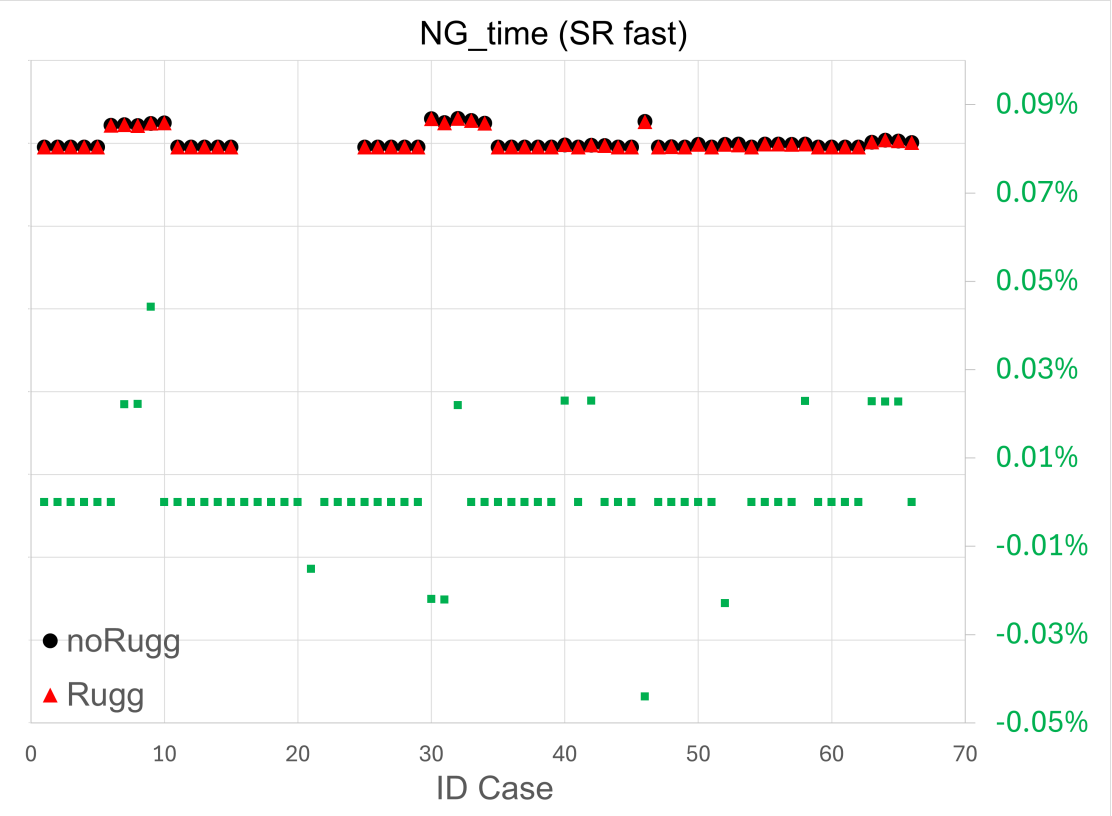

Figure 4.14: Slow Ramp (fast) - NG set time

PWR

Figures 4.17 and 4.18 show the PWR data in the phase of an upward step and a downward step, with the same final throttle value during the Stair Steps maneuver. This parameter makes it possible to verify that the power delivered during the entire arc of the maneuver is adherent to the pilot's command. The graph shows, for each ID Case on the x-axis, the respective average PWR values for the noRuggedized version and for the Ruggedized version on the primary y-axis, and the secondary axis shows the respective series of percentage deviations between the two previous values. The comparison shows that the percentage deviations remain in the $\pm 0.05\%$ range of variability and underlines the compliance of the parameter between the two versions.

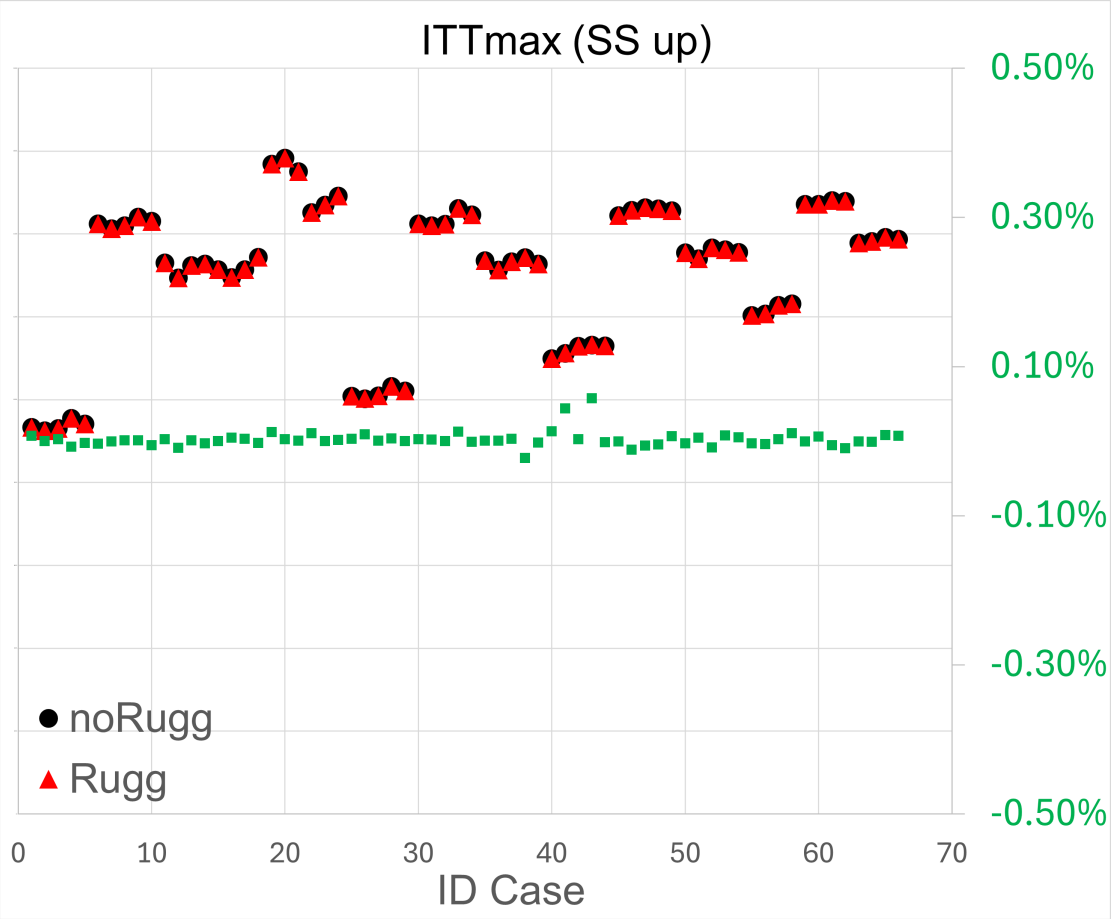

Figure 4.15: Stair Steps (up) - ITT

4.1.6 Burst & Chop

ITT

Figures 4.19 and 4.20 show the ITT data in the low throttle phase and the high throttle phase, during the Burst & Chop maneuver. This parameter allows you to verify that no overshoots have occurred during the critical phase of the maneuver. The graph shows, for each ID Case on the x-axis, the respective maximum ITT values for the noRuggedized version and for the Ruggedized version on the primary y-axis, and the secondary axis shows the respective series of percentage deviations between the two previous values. The comparison shows how the percentage deviations remain in the $\pm 0.01\%$ variability band and underlines the parameter compliance between the two versions.

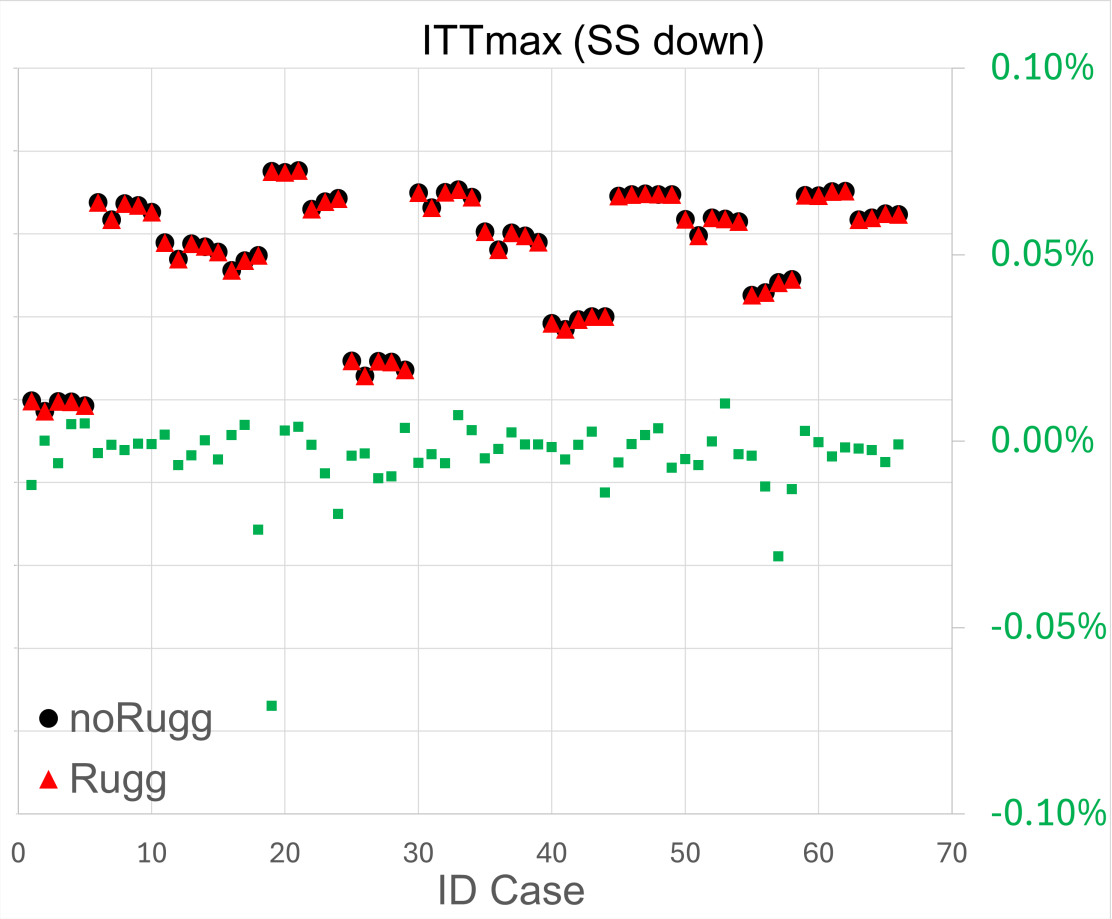

Figure 4.16: Stair Steps (down) - ITT

PWR

Figures 4.21 and 4.22 show the PWR data in the low throttle phase and the high throttle phase, during the Burst & Chop maneuver. This parameter makes it possible to verify that the power supplied during the critical phase of the maneuver is adequate for the pilot's command. The graph shows, for each ID Case on the x-axis, the respective average PWR values for the noRuggedized version and for the Ruggedized version on the primary y-axis, and the secondary axis shows the respective series of percentage deviations between the two previous values. The comparison shows how the percentage deviations remain in the $\pm 0.01\%$ variability band and underlines the parameter compliance between the two versions.

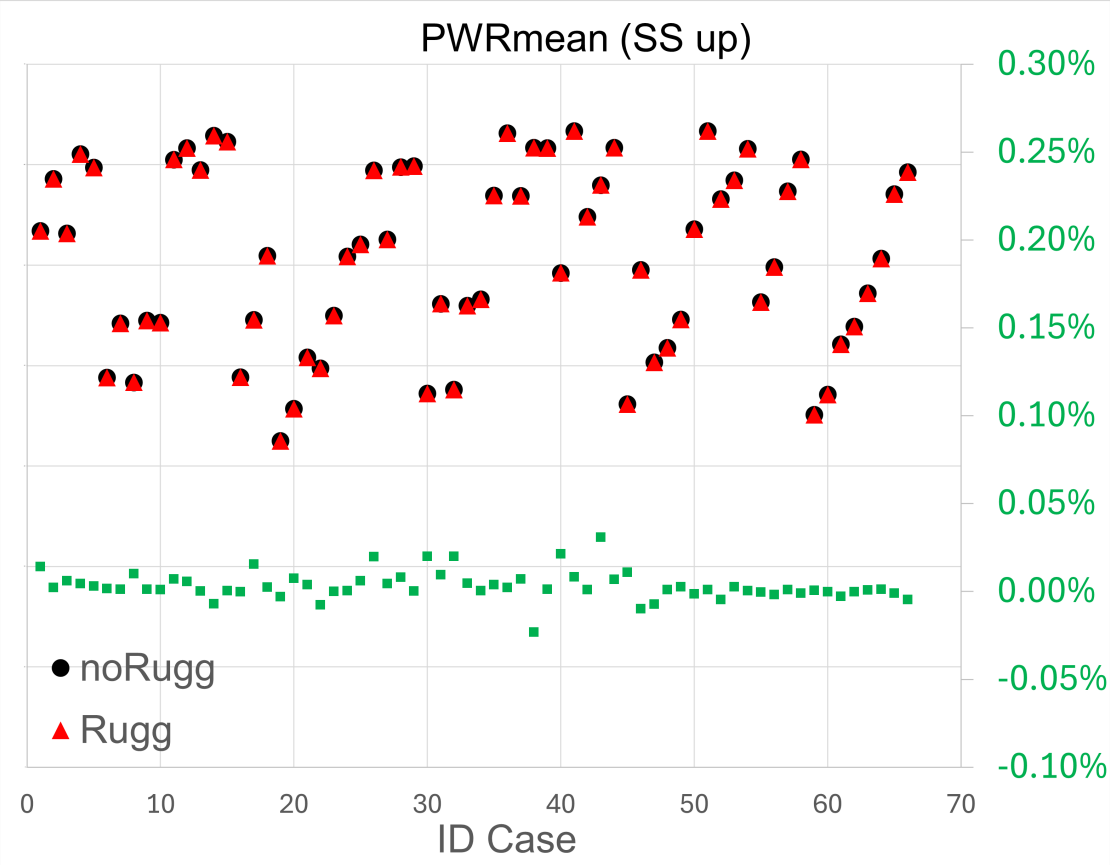

Figure 4.17: Stair Steps (up) - PWR

NG set time

Figures 4.23 and 4.24 show the data relating to the settling time of NG at its reference value during the Burst & Chop maneuver, at high power (low) and at maximum power (high). This parameter makes it possible to verify that the performance of the engine is guaranteed during the critical phase of the maneuver. The graph shows, for each ID Case on the x-axis, the respective rise values of NG for the noRuggedized version and for the Ruggedized version on the primary y-axis, and on the secondary axis is shown the respective series of percentage deviations between the two previous values. The comparison shows that the percentage differences are practically zero and underlines the compliance of the parameter between the two versions.

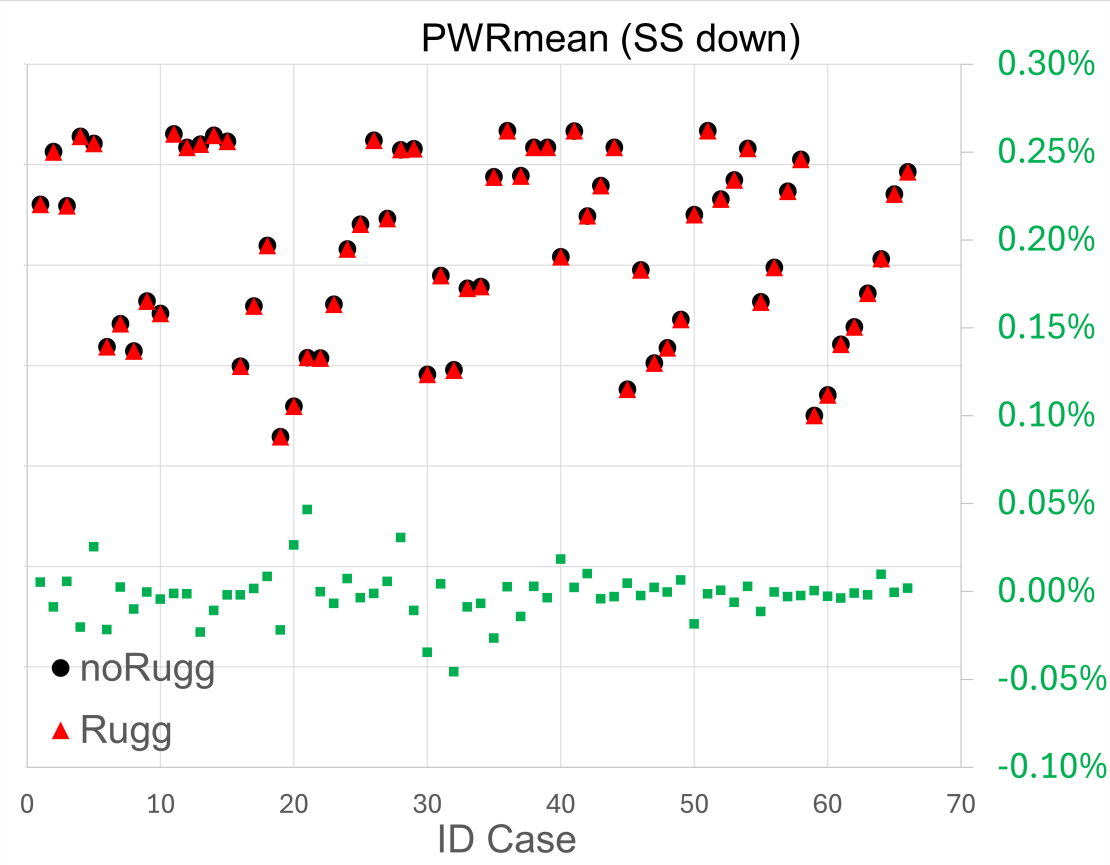

Figure 4.18: Stair Steps (down) - PWR

Nprop set time

Figures 4.25 and 4.26 show the data relating to the settling time of Nprop at its reference value during the Burst & Chop maneuver at high power (low) and at maximum power (high). This parameter makes it possible to verify that the performance of the engine is guaranteed during the critical phase of the maneuver. The graph shows, for each ID Case on the x-axis, the respective Nprop rise values for the noRuggedized version and for the Ruggedized version on the primary y-axis, and the secondary axis shows the respective series of percentage deviations between the two previous values. The comparison shows that the percentage differences are practically zero and underlines the compliance of the parameter between the two versions.

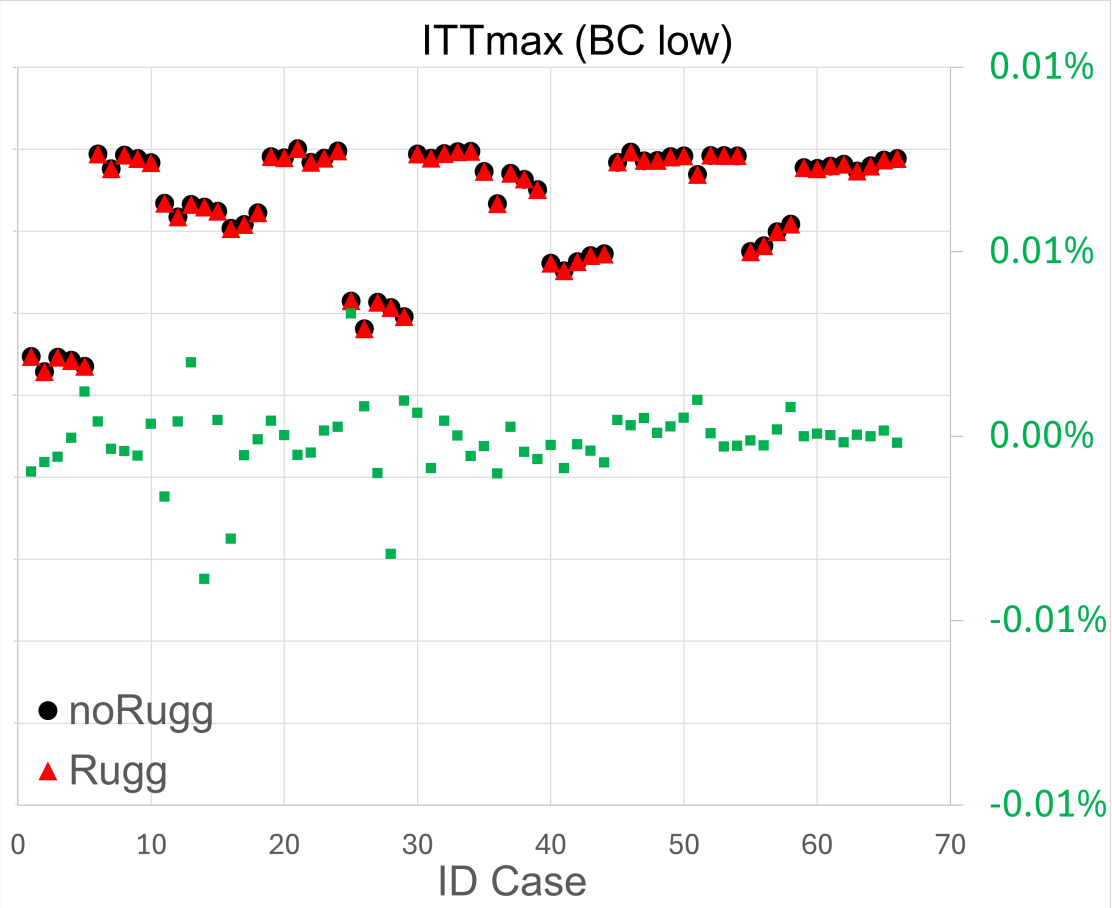

Figure 4.19: Burst & Chop (low) - ITT

4.1.7 Air Start

ITT

Figures 4.27 and 4.28 show ITT data during the Air Start maneuver, under high rpm (high) and low rpm (low) re-ignition conditions. This parameter allows to verify that no overshoots have occurred during the entire duration of the maneuver. The graph shows, for each ID Case on the x-axis, the respective maximum ITT values for the noRuggedized version and for the Ruggedized version on the primary y-axis, and on the secondary axis is shown the respective series of percentage deviations between the two previous values. The comparison shows that the percentage deviations of the high condition are purely zero, while those of the low condition remain in the $\pm 0.2\%$ variability band, emphasizing the parameter conformity between the two versions. Figures 4.29 and 4.30 show the data relating to the settling time of NG at its reference value during the Air Start maneuver, in high rpm and low rpm (low)

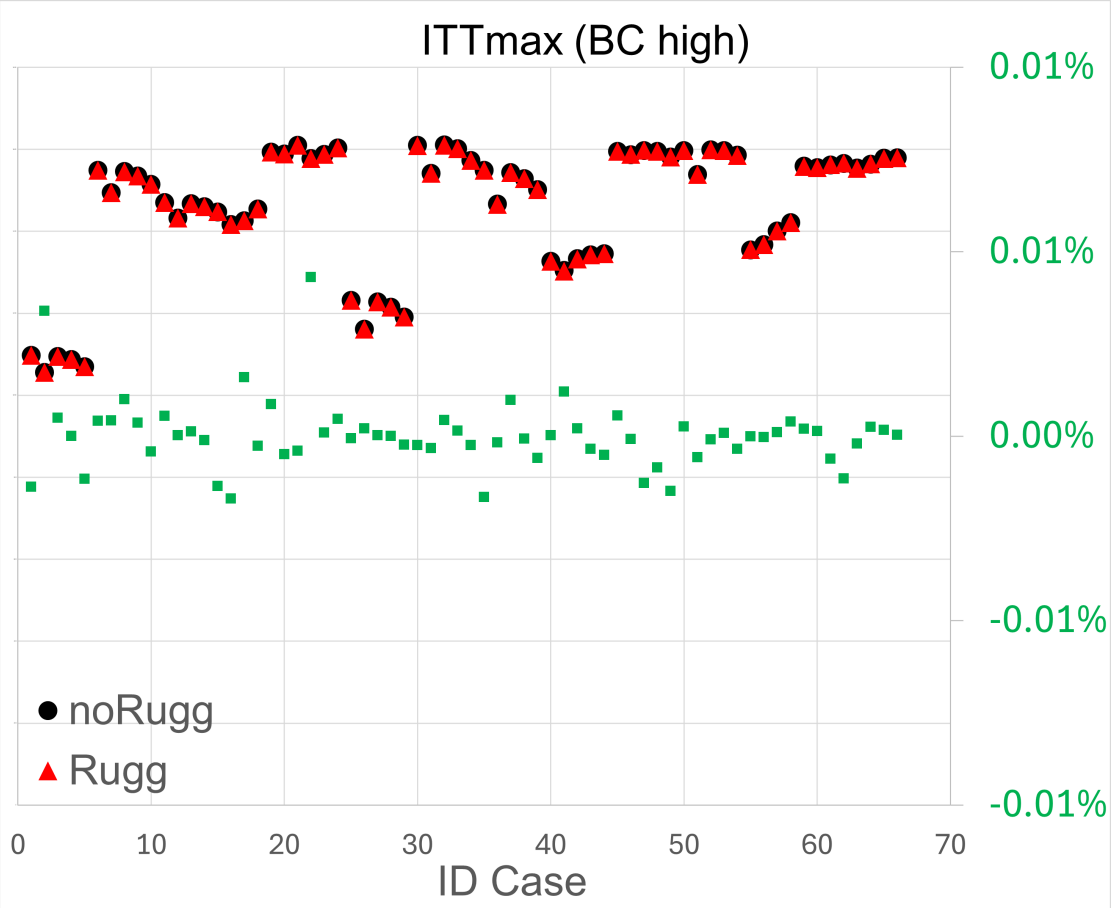

Figure 4.20: Burst & Chop (high) - ITT

re-ignition conditions. This parameter allows to verify that the performance of the engine is guaranteed throughout the entire maneuver. The graph shows, for each ID Case on the x-axis, the respective rise values of NG for the noRuggedized version and for the Ruggedized version on the primary y-axis, and on the secondary axis is shown the respective series of percentage deviations between the two previous values. The comparison shows that the percentage deviations of the high condition are purely zero, while those of the low condition remain in the range of variability between 0% and 0.2%, underlining the parameter conformity between the two versions.

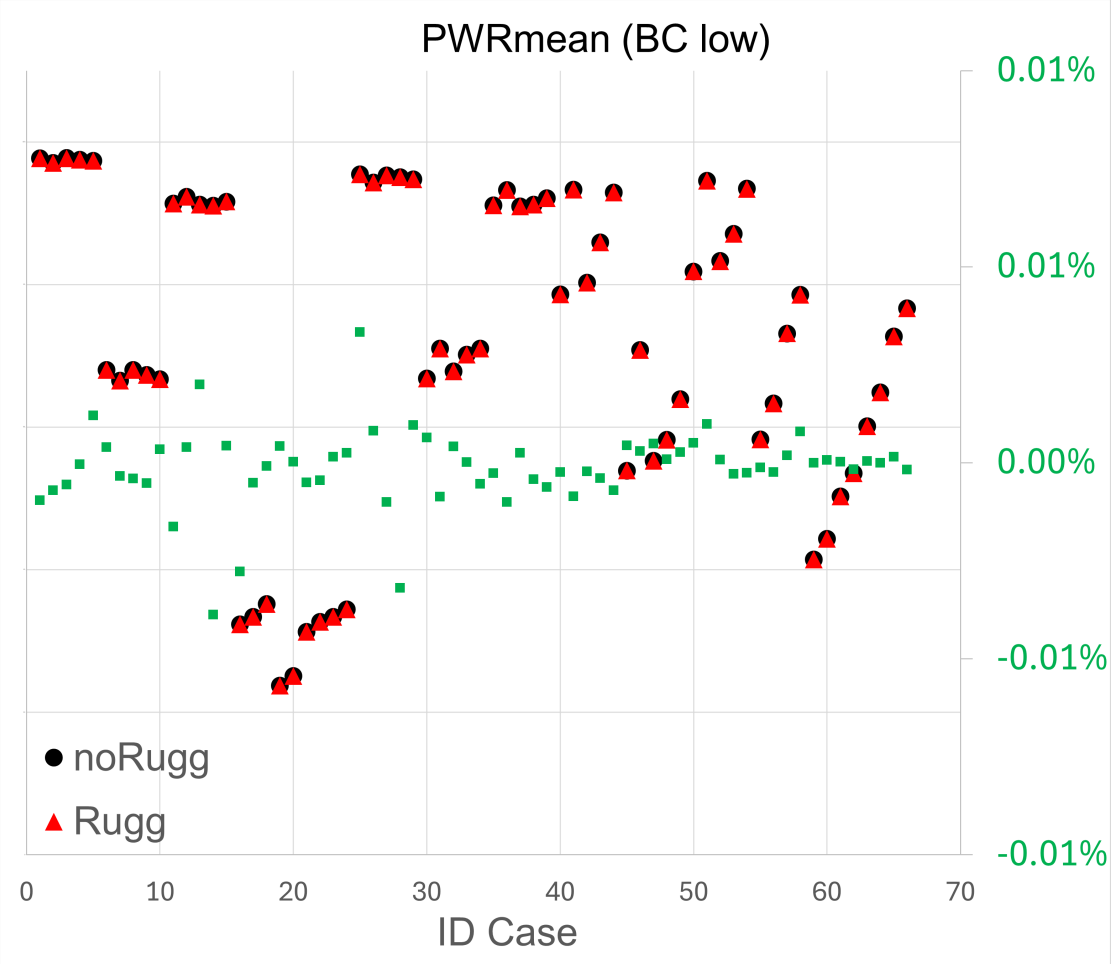

Figure 4.21: Burst & Chop (low) - PWR

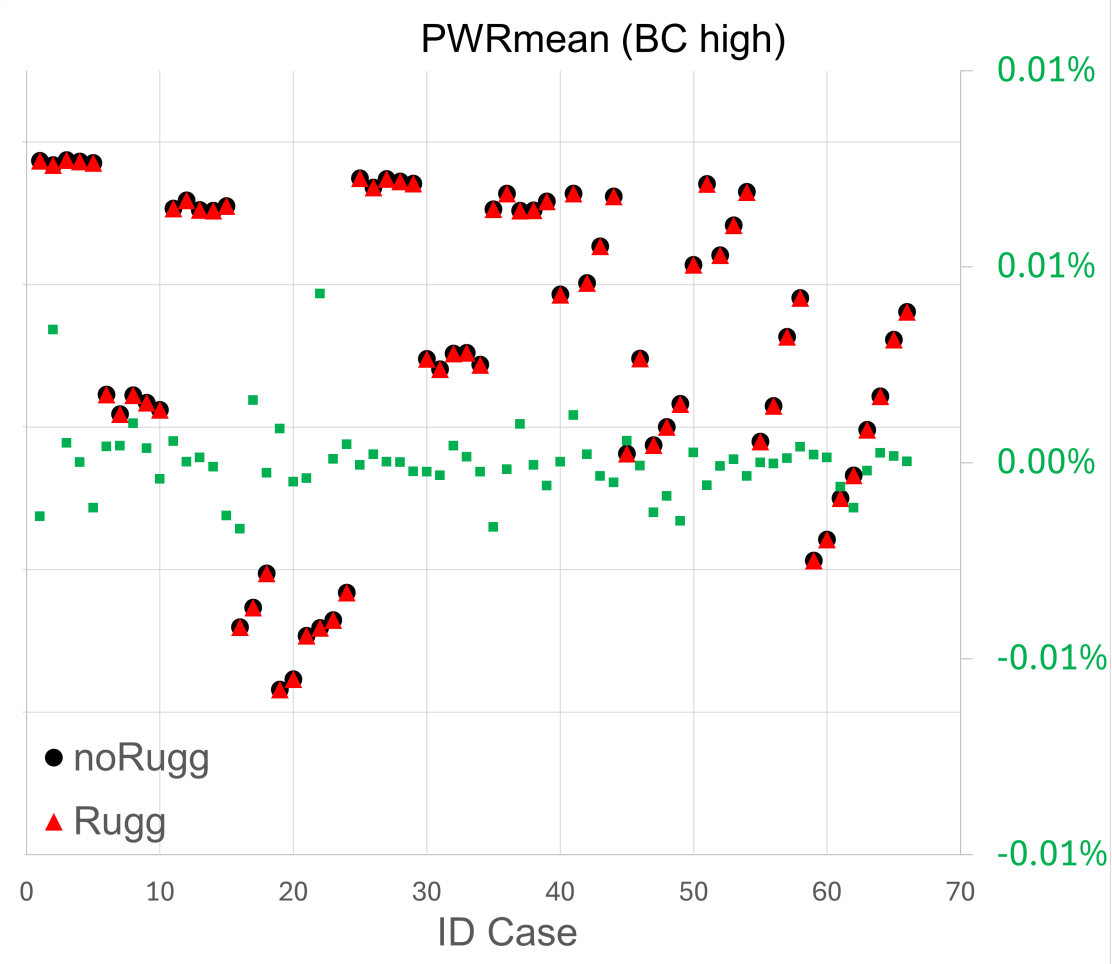

Figure 4.22: Burst & Chop (high) - PWR

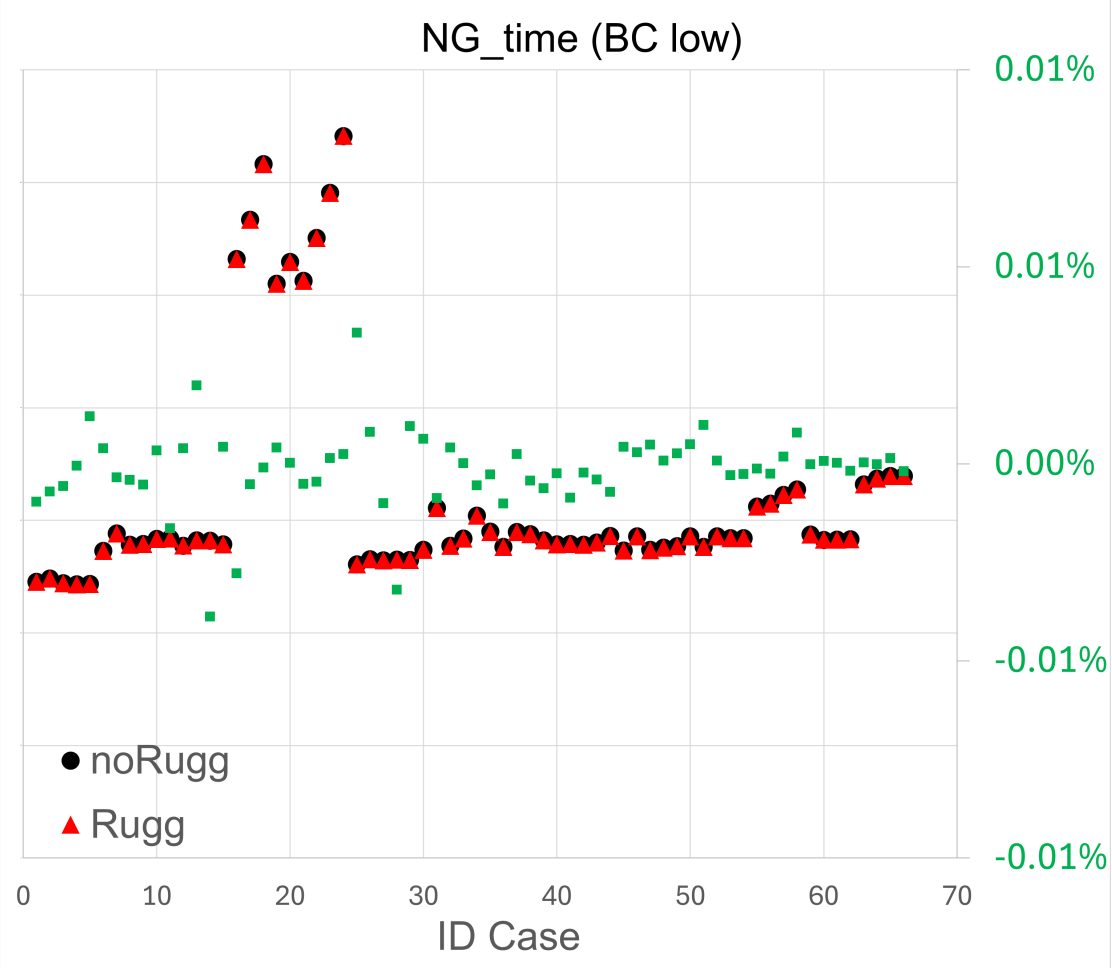

Figure 4.23: Burst & Chop (low) - NG set time

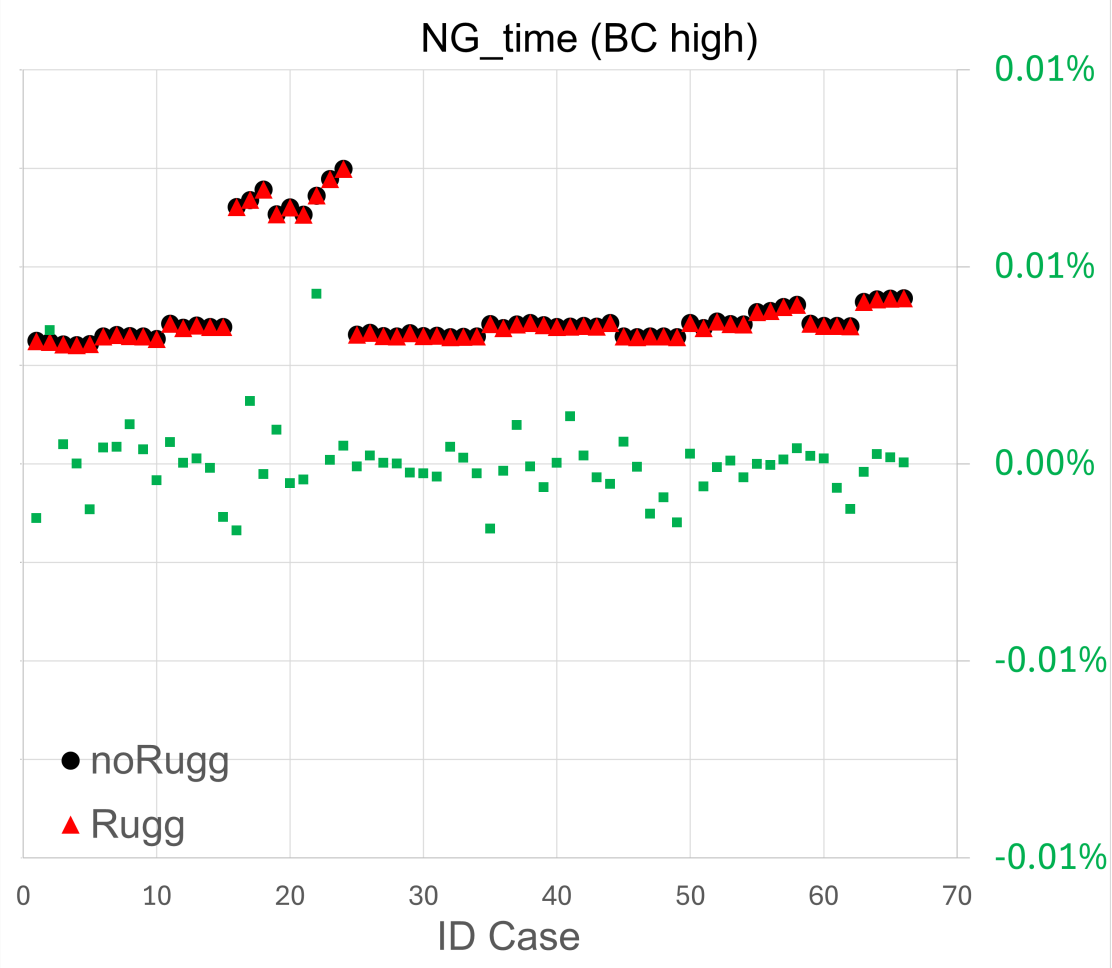

Figure 4.24: Burst & Chop (high) - NG set time

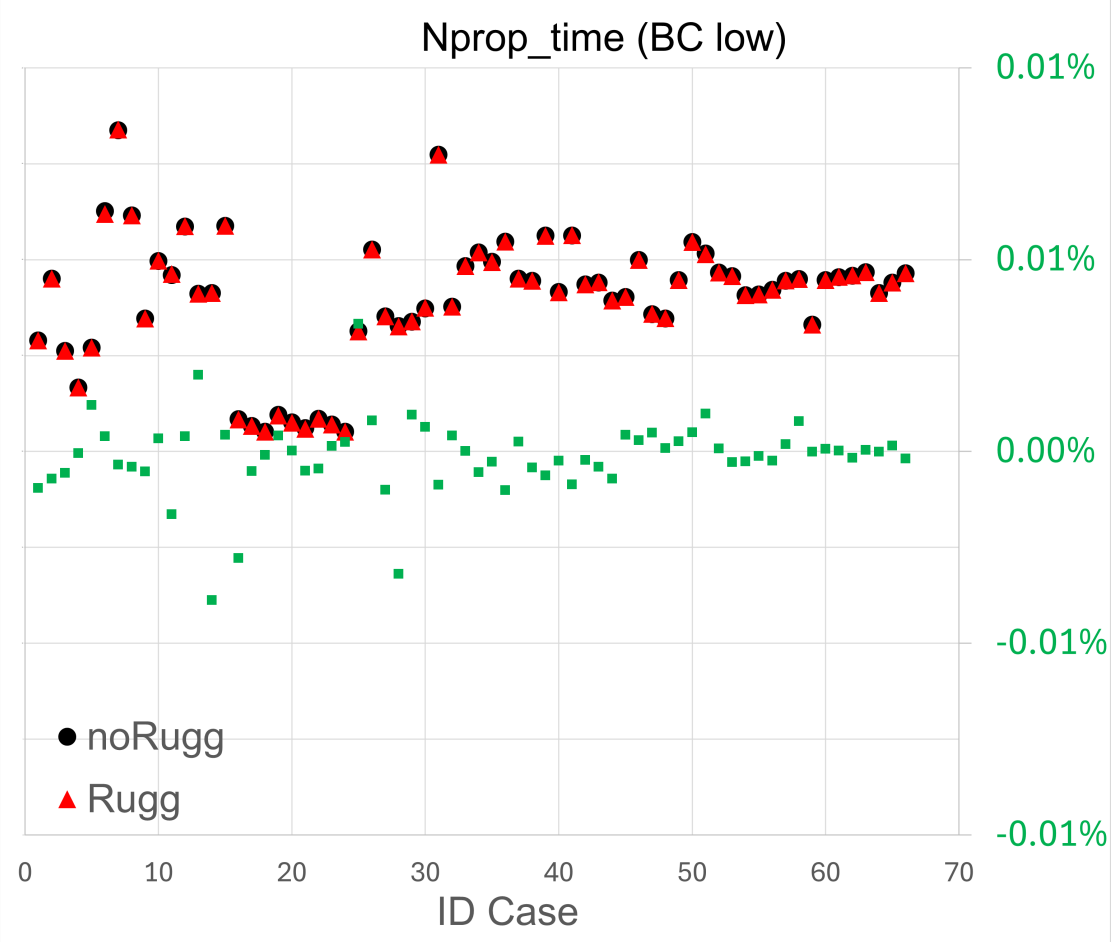

Figure 4.25: Burst & Chop (low) - Nprop set time

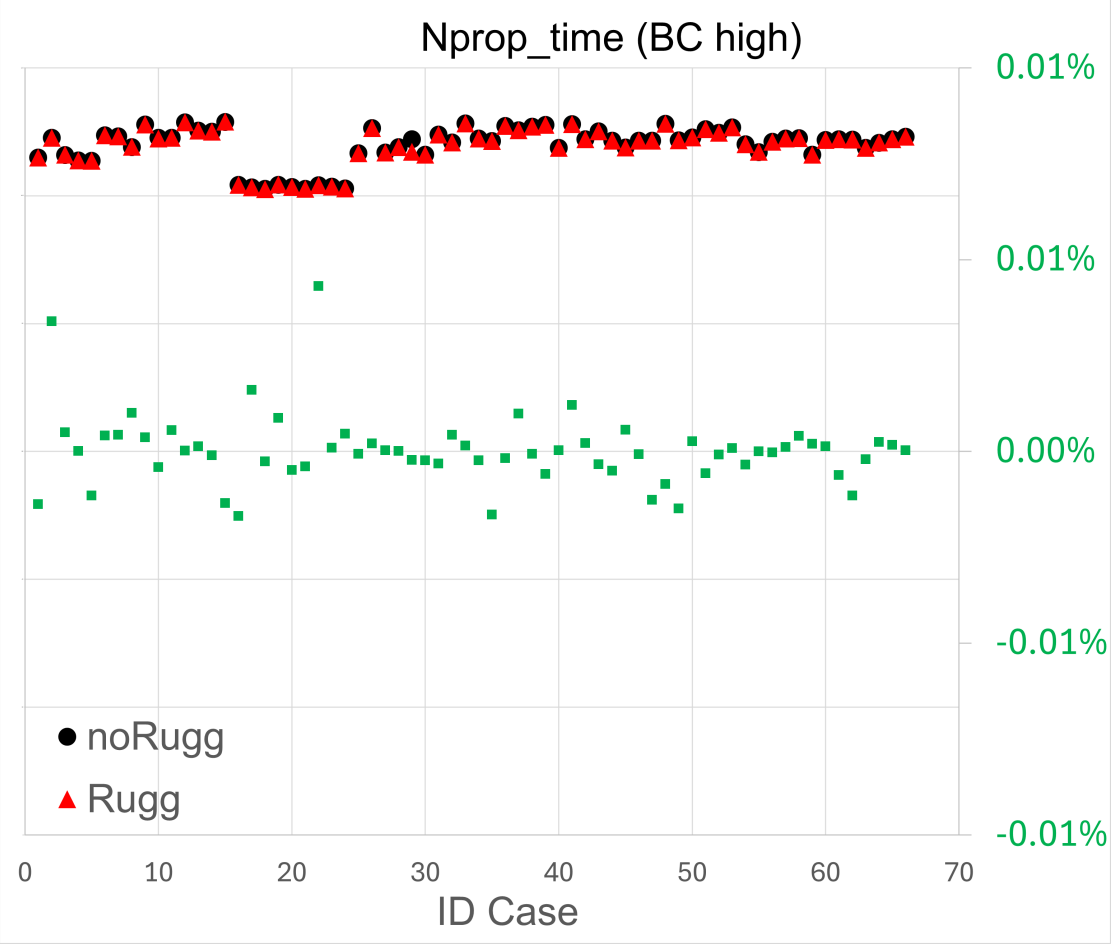

Figure 4.26: Burst & Chop (high) - Nprop set time

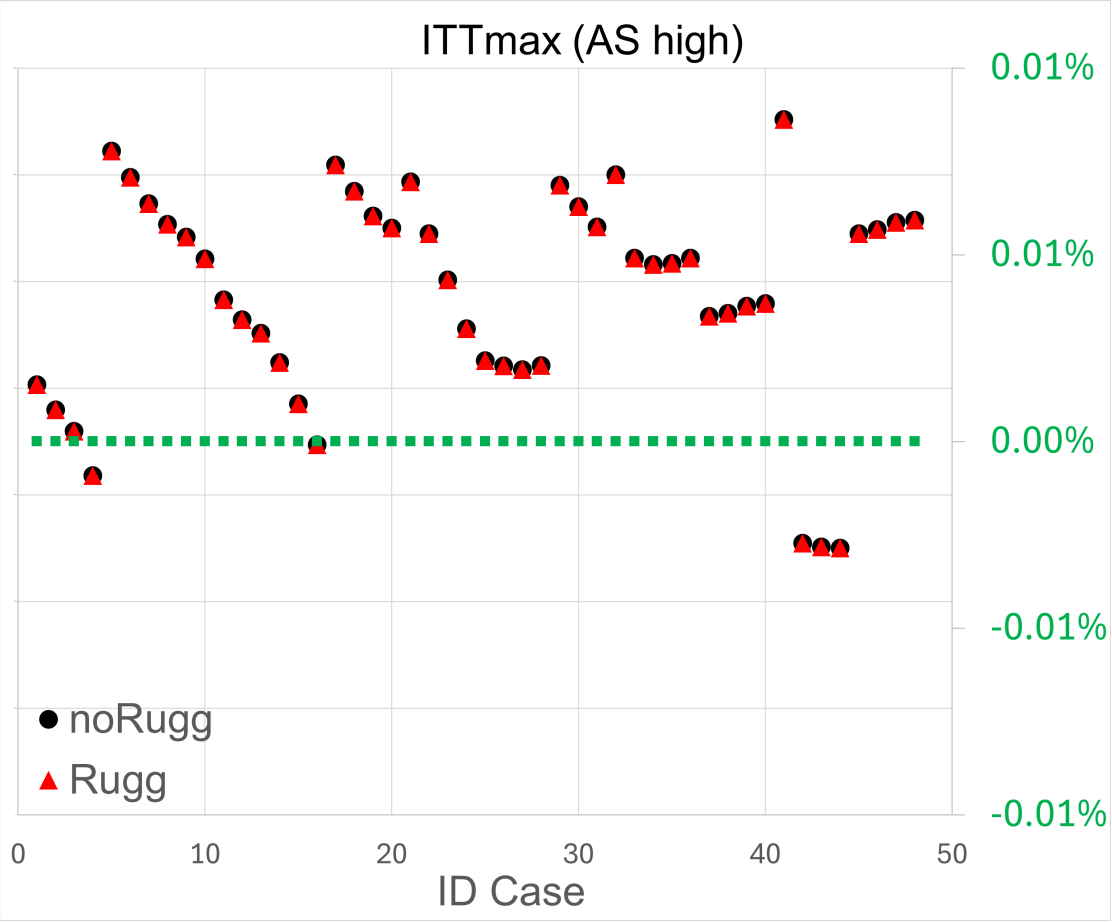

Figure 4.27: Air Start (high) - ITT

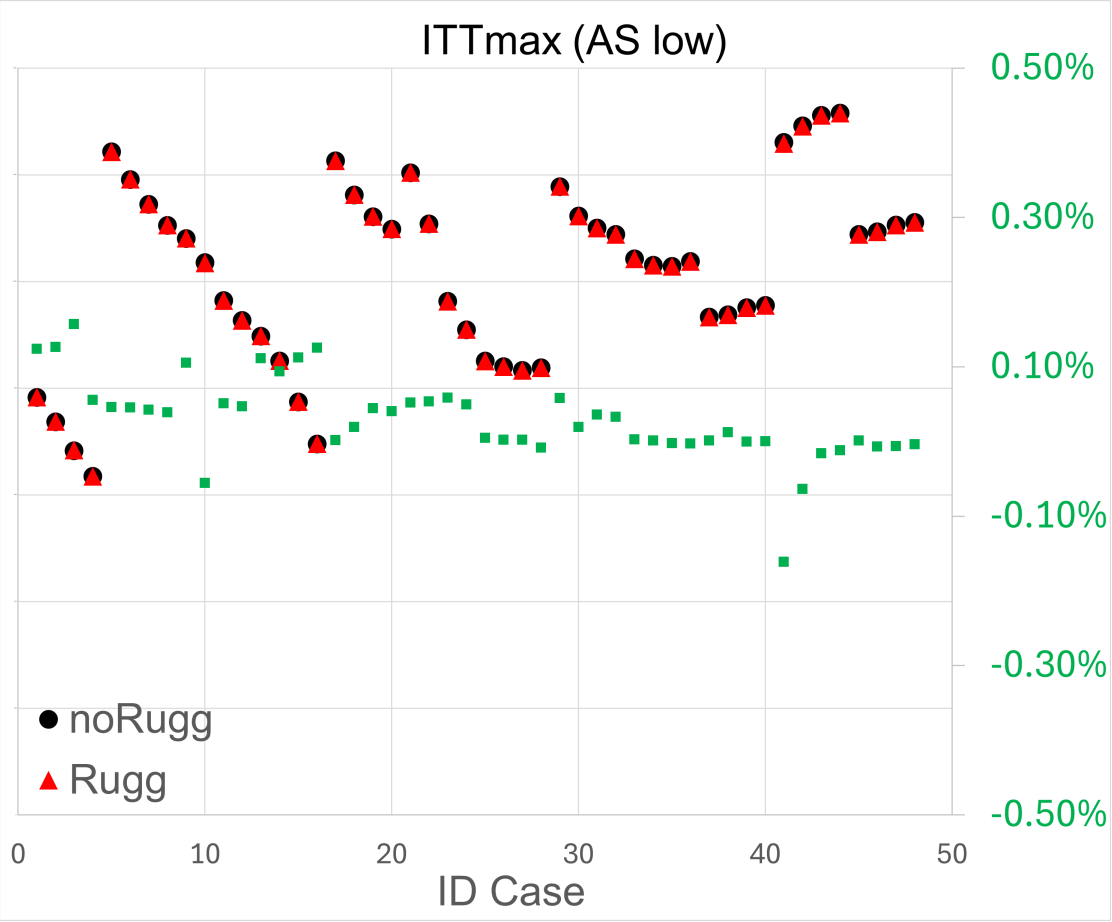

Figure 4.28: Air Start (low) - ITT

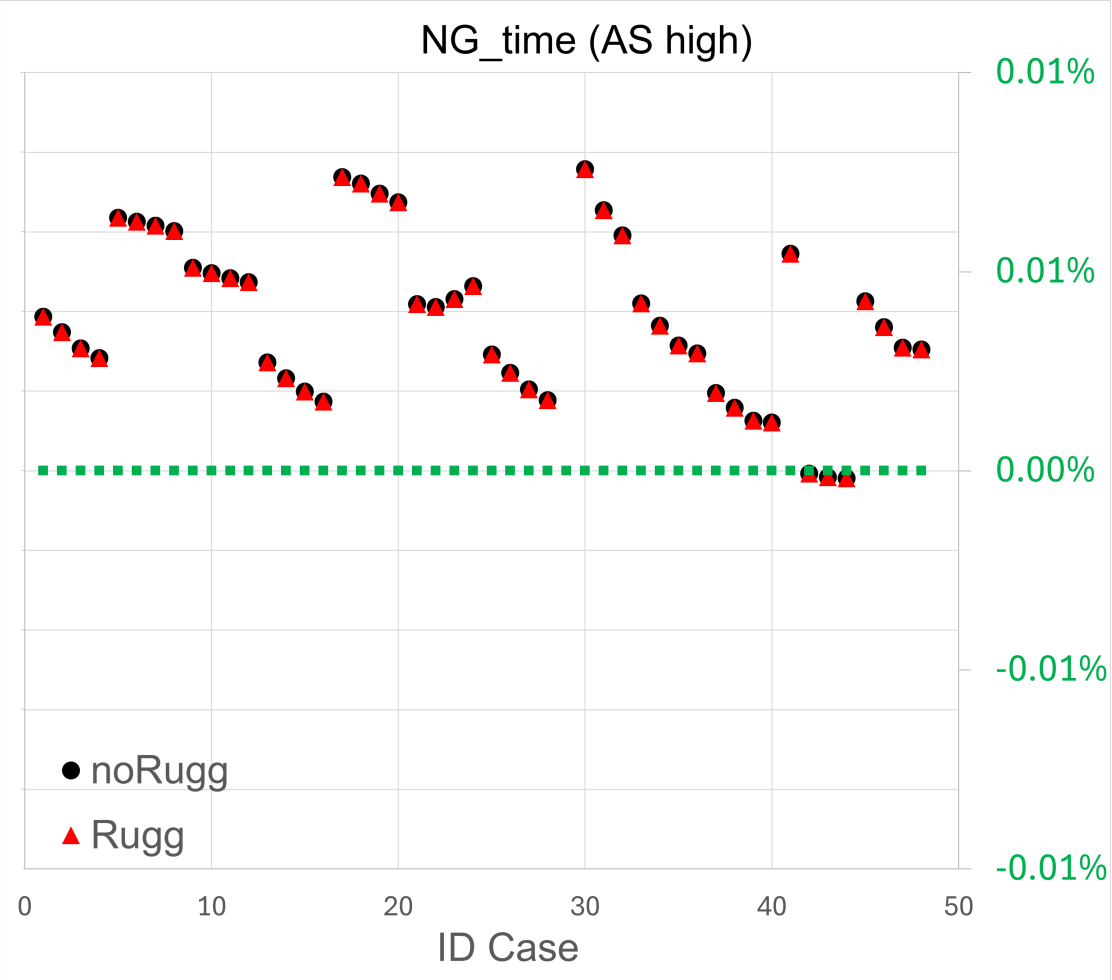

Figure 4.29: Air Start (high) - NG set time

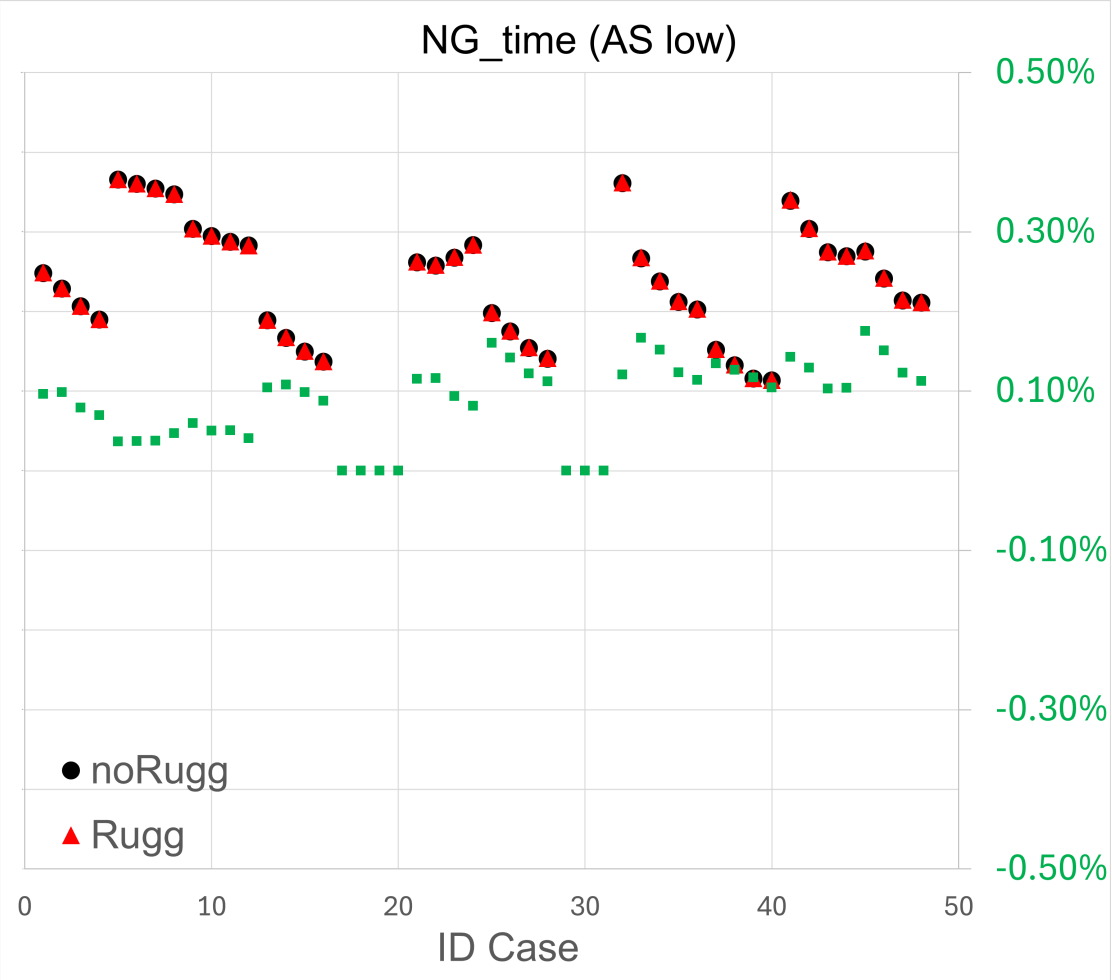

Figure 4.30: Air Start (low) - NG set time

Chapter 5

Parametric analysis

5.1 What we also did

In this chapter, the results of the so-called **Parametric** analysis will be presented.

The analysis aims to explore the robustness of the control software, varying the rotational inertia analyzed in Chapter 4 and now exploited as a parameter, in view of future use of the engine as a development platform for new generations of models with different characteristics and performance.

Taking as a basic reference the nominal value of the inertia increment Δi_0 of the **Ruggedized** configuration, theoretical increments of +50%, +100%, and +150% have been set, thus defining a total of 5 configurations, as shown in Table 5.1.

R0 (noRuggedized)	R1 (Ruggedized)	R2	R3	R4
$\Delta i = 0$	$\Delta i = \Delta i_0$	$\Delta i = 1.5\Delta i_0$	$\Delta i = 2\Delta i_0$	$\Delta i = 2.5\Delta i_0$

Table 5.1: Inertial parametric configurations

5.1.1 Test points

Three maneuvers were selected as a representative basis of the test, based on the thermo-mechanical load on the motor, simulating them all over the respective envelopes, as already performed in Chapter 4. The data have been processed by appropriately modifying scripts and functions presented in the Chapter 3. The results are presented in the form of Excel graphs: each graph represents the result of the quantity of interest, with the ordinate axis suitably muted, in accordance with the company's requests for confidentiality on technical data, plus the series of percentage deviations of the same quantity between the R0 and R4 versions. The

difference is again considered acceptable if the percentage difference falls within the range ±1.5% of variability, for the same reasons explained in Chapter 4. The results are presented hereafter.

5.1.2 Take Off & Climb

ITT

Figure 5.1 shows the data relating to ITT in the maximum throttle phase during the Take Off maneuver. This parameter allows to verify that no overshoots have occurred during the critical phase of the maneuver. The graph shows for each ID Case on the x-axis the respective maximum values of ITT for each version R on the primary y-axis, and on the secondary axis is shown the respective series of percentage deviations between the values R0 and R4. The comparison shows that the percentage deviations remain in the ±0.1% variability band and underlines the compliance of the parameter between the two versions.

NG set time

Figure 5.2 shows the data relating to the settling time of NG at its reference value during the Take Off maneuver. This parameter allows to verify that the performance of the engine is guaranteed throughout the entire maneuver. The graph shows for each ID Case on the x-axis the respective rising values of NG for each version R on the primary y-axis, and on the secondary axis is shown the respective series of percentage deviations between the two values R0 and R4. The comparison shows that the percentage deviations are purely zero with the exception of an outlier value - which does not cause concern if we look at the real values of the quantities - and underlines the conformity of the parameter between the two versions.

Nprop set time

Figure 5.3 shows the data relating to the settling time of Nprop at its reference value during the Take Off maneuver. This parameter allows you to verify that the performance of the engine is guaranteed throughout the entire maneuver. The graph shows for each ID Case on the x-axis the respective rising values of Nprop for each version R on the primary y-axis, and on the secondary axis is shown the respective series of percentage deviations between the two values R0 and R4. The comparison shows that the percentage deviations remain in the ±0.05% variability band and underlines the compliance of the parameter between the two versions.

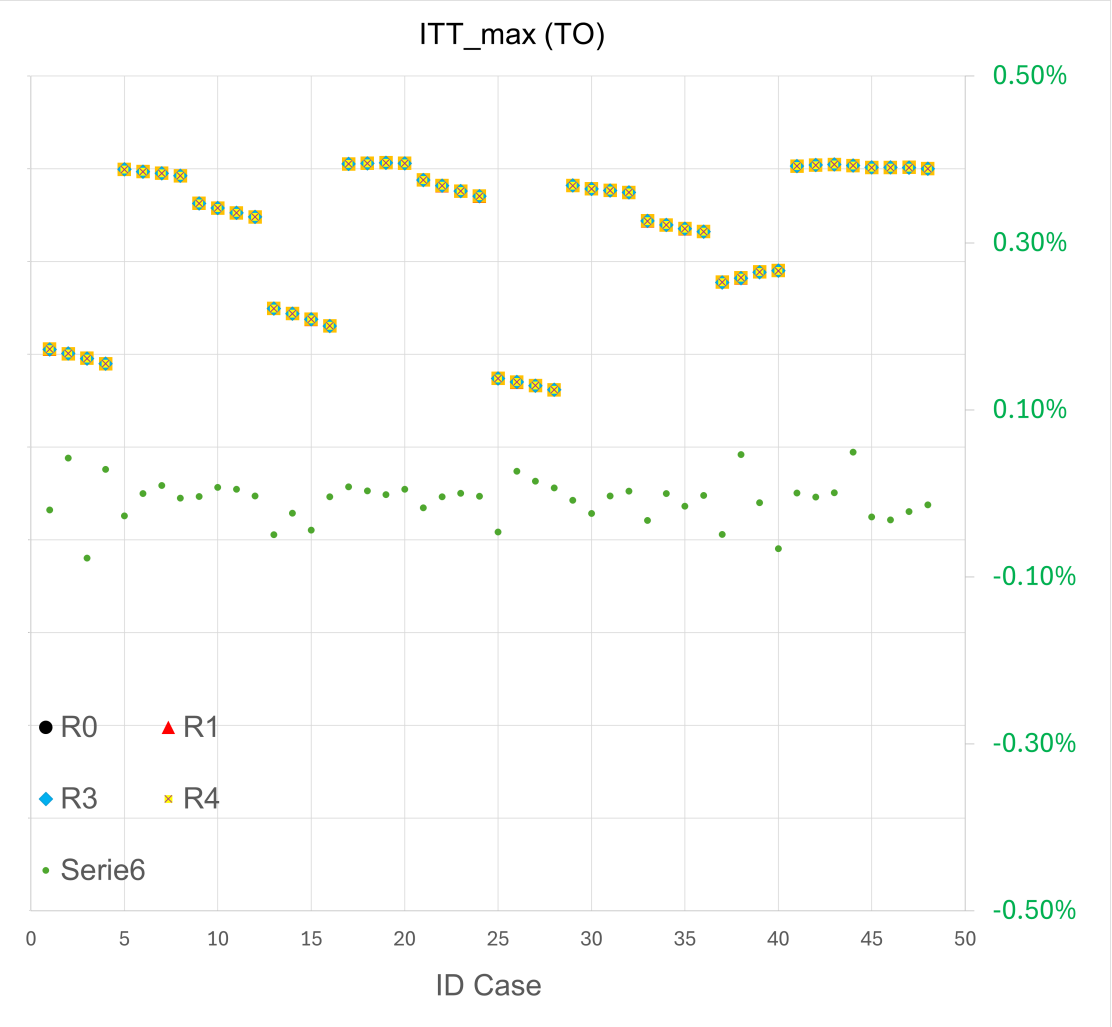

Figure 5.1: Take Off parametric - ITT

5.1.3 Burst & Chop (high)

ITT

Figure 5.4 shows the ITT data in the maximum throttle phase during the Burst & Chop maneuver. This parameter allows to verify that no overshoots have occurred during the critical phase of the maneuver. The graph shows for each ID Case on the x-axis the respective maximum values of ITT for each version R on the primary y-axis, and on the secondary axis is shown the respective series of percentage deviations between the values R0 and R4. The comparison shows that the percentage deviations remain in the $\pm 0.1\%$ variability band and underlines the compliance of the parameter between the two versions.

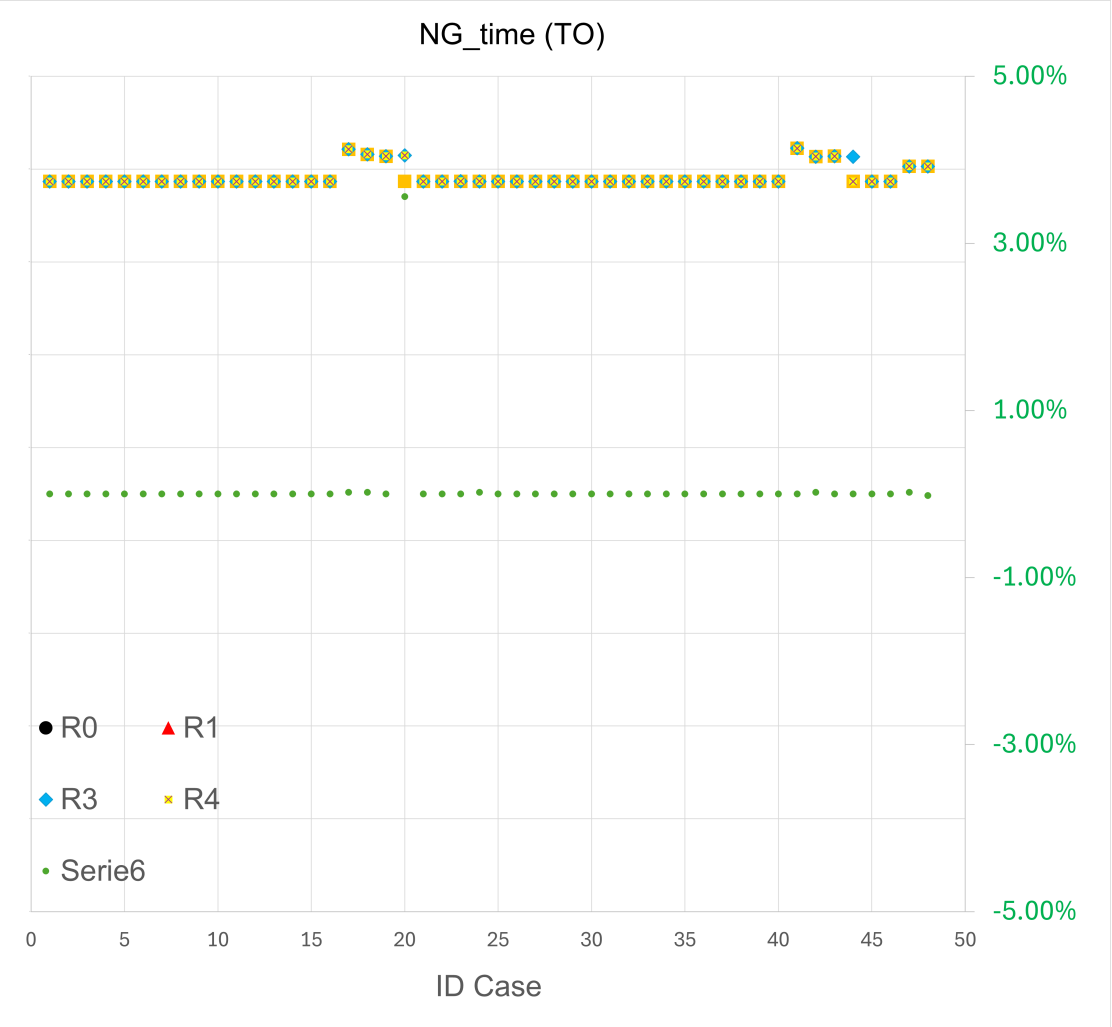

Figure 5.2: Take Off parametric - NG set time

NG set time

Figure 5.5 shows the data relating to the settling time of NG at its reference value during the Burst & Chop maneuver. This parameter allows to verify that the performance of the engine is guaranteed throughout the entire maneuver. The graph shows for each ID Case on the x-axis the respective rise values of NG for each version R on the primary y-axis, and on the secondary axis is shown the respective series of percentage deviations between the two values R0 and R4. The comparison shows how the percentage deviations remain in the $\pm 0.02\%$ variability band and underlines the compliance of the parameter between the two versions.

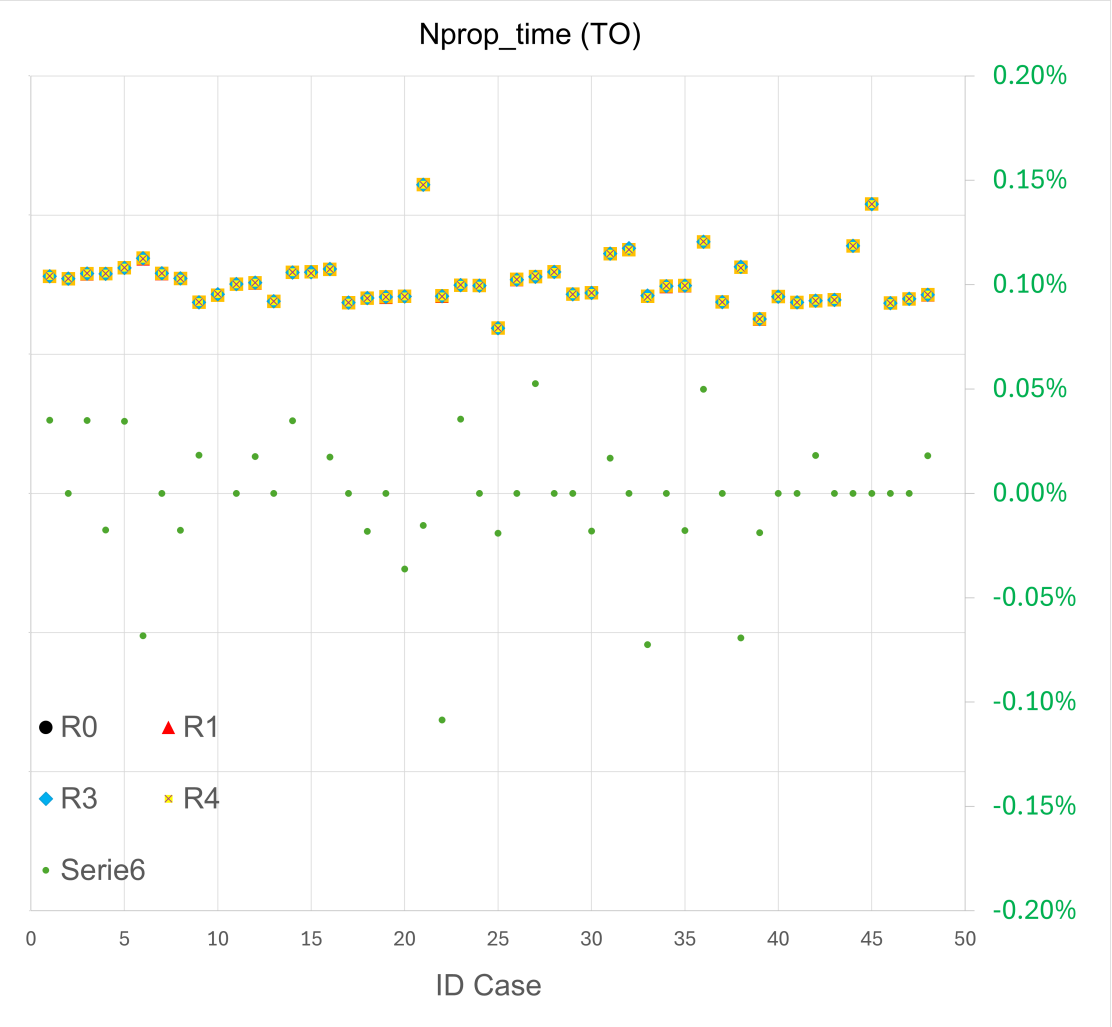

Figure 5.3: Take Off parametric - Nprop set time

Nprop set time

Figure 5.6 shows the data relating to the settling time of Nprop at its reference value during the Burst & Chop maneuver. This parameter allows to verify that the performance of the engine is guaranteed throughout the entire maneuver. The graph shows for each Case ID on the x-axis the respective Nprop rise values for each version R on the primary y-axis, and on the secondary axis is shown the respective series of percentage deviations between the two values R0 and R4. The comparison shows that the percentage deviations remain in the $\pm 0.05\%$ variability band and underlines the compliance of the parameter between the two versions.

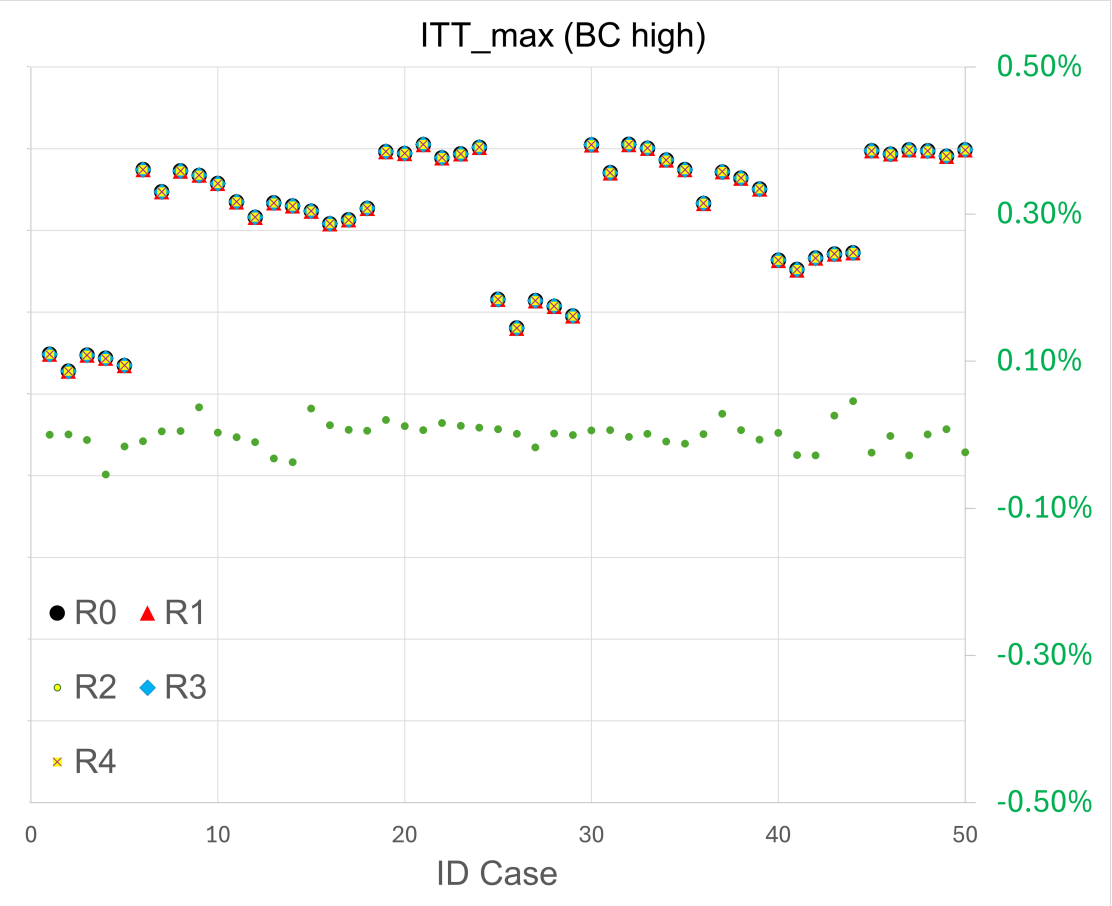

Figure 5.4: Burst & Chop (high) parametric - ITT

5.1.4 Air Start (low)

ITT

Figure 5.7 shows the ITT data during the Air Start (low) maneuver. This parameter allows to verify that no overshoots have occurred during the entire span of the maneuver. The graph shows for each ID Case on the x-axis the respective maximum values of ITT for each version R on the primary y-axis, and on the secondary axis is shown the respective series of percentage deviations between the values R0 and R4. The comparison shows that the percentage deviations remain in the $\pm 0.5\%$ variability band, showing a slight tendency to positive differences, but still emphasizing the compliance of the parameter between the two versions.

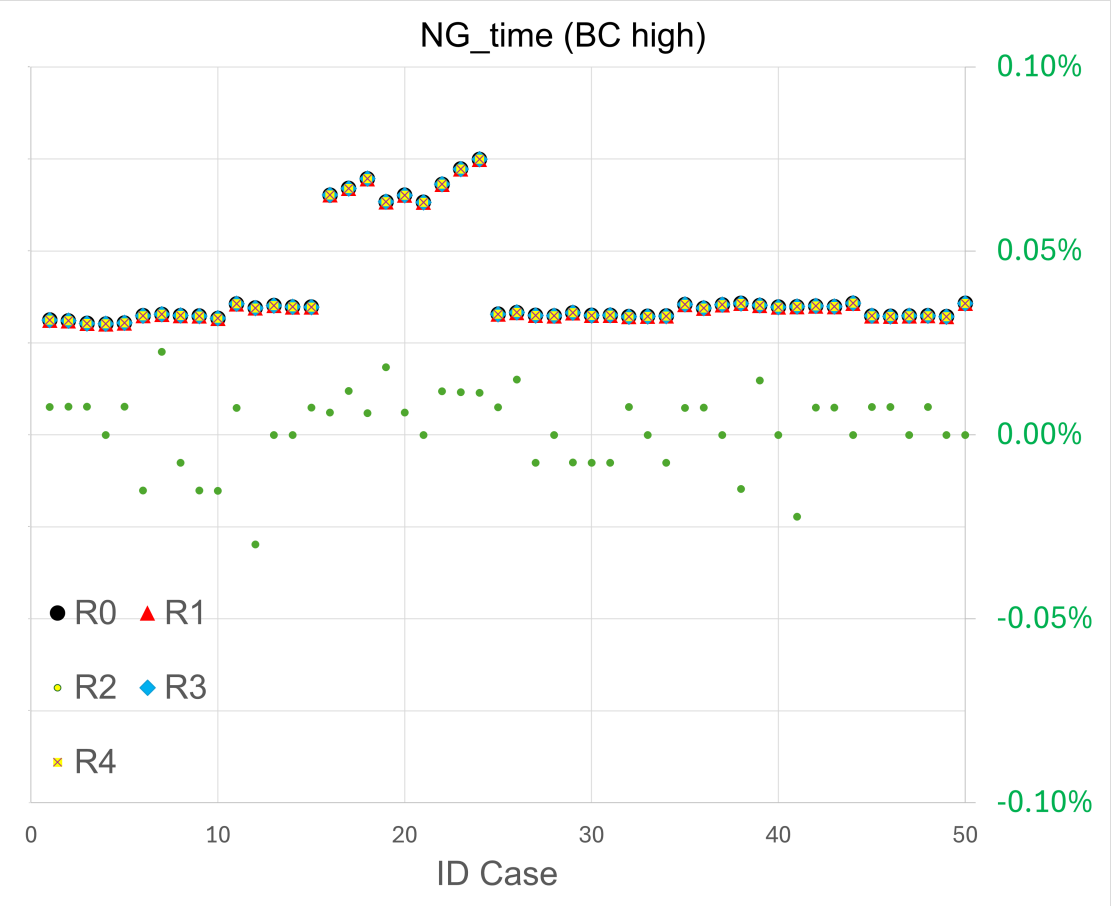

Figure 5.5: Burst & Chop (high) parametric - NG set time

NG set time

Figure 5.8 shows the data relating to the settling time of NG at its reference value during the Air Start maneuver. This parameter allows to verify that the performance of the engine is guaranteed throughout the entire maneuver. The graph shows for each ID Case on the x-axis the respective rise values of NG for each version R on the primary y-axis, and on the secondary axis is shown the respective series of percentage deviations between the two values R0 and R4. The comparison shows that the percentage deviations remain in the $\pm 0.4\%$ variability band, showing a slight tendency to positive differences, but still emphasizing the compliance of the parameter between the two versions.

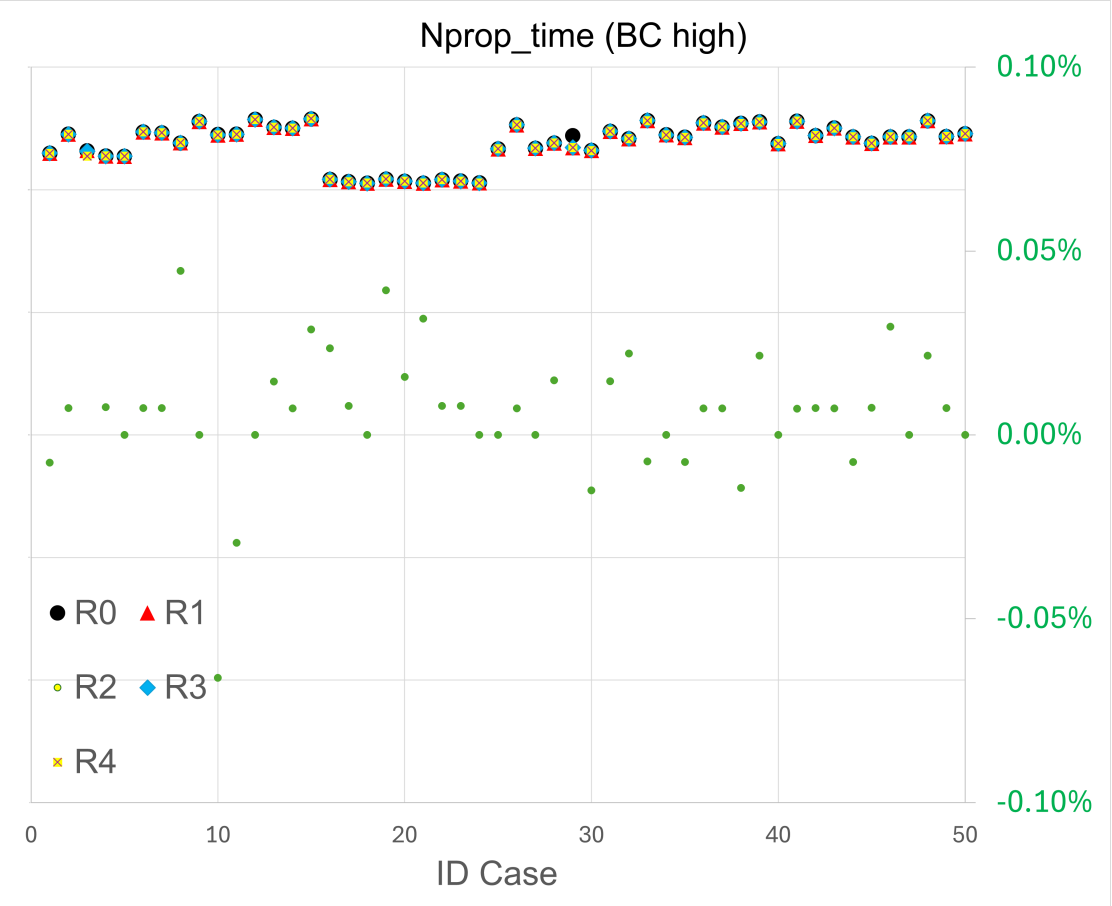

Figure 5.6: Burst & Chop (high) parametric - Nprop set time

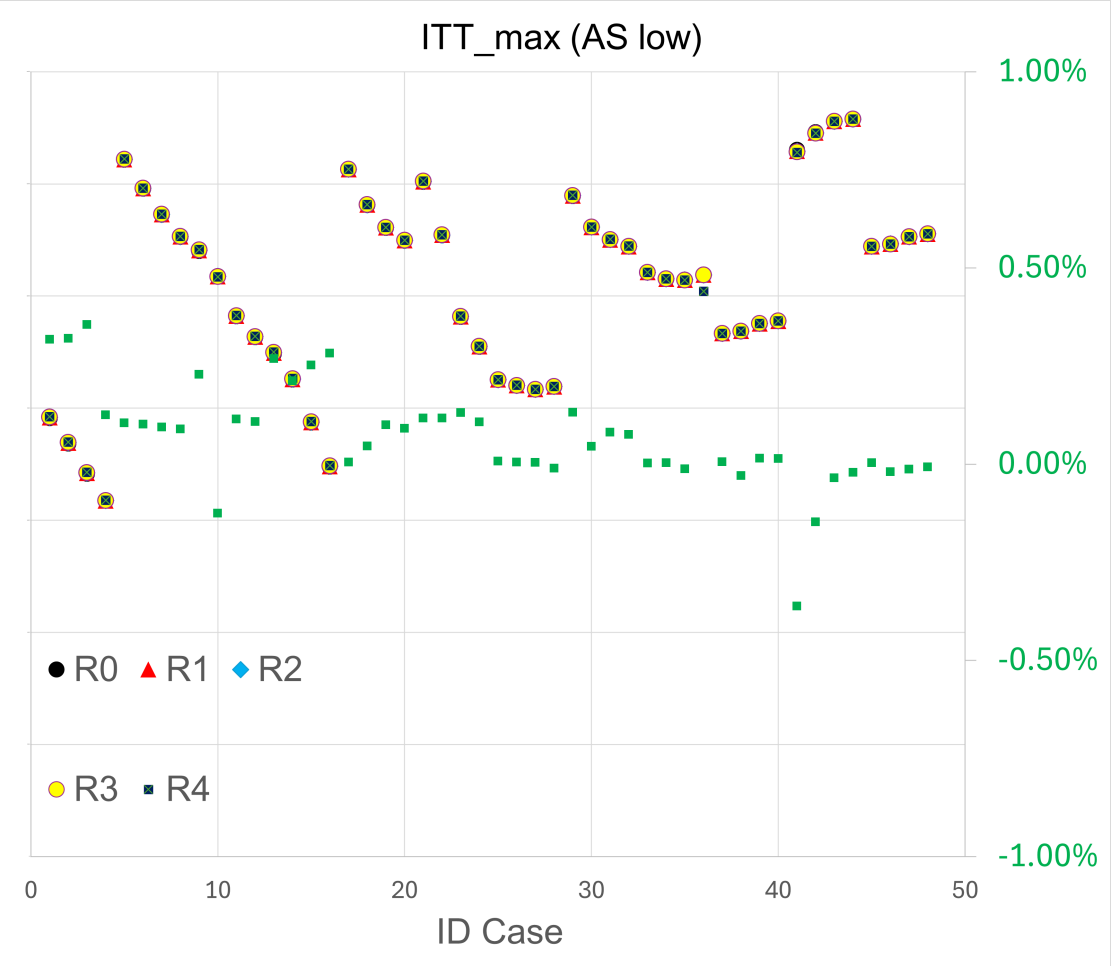

Figure 5.7: Air Start (low) parametric - ITT

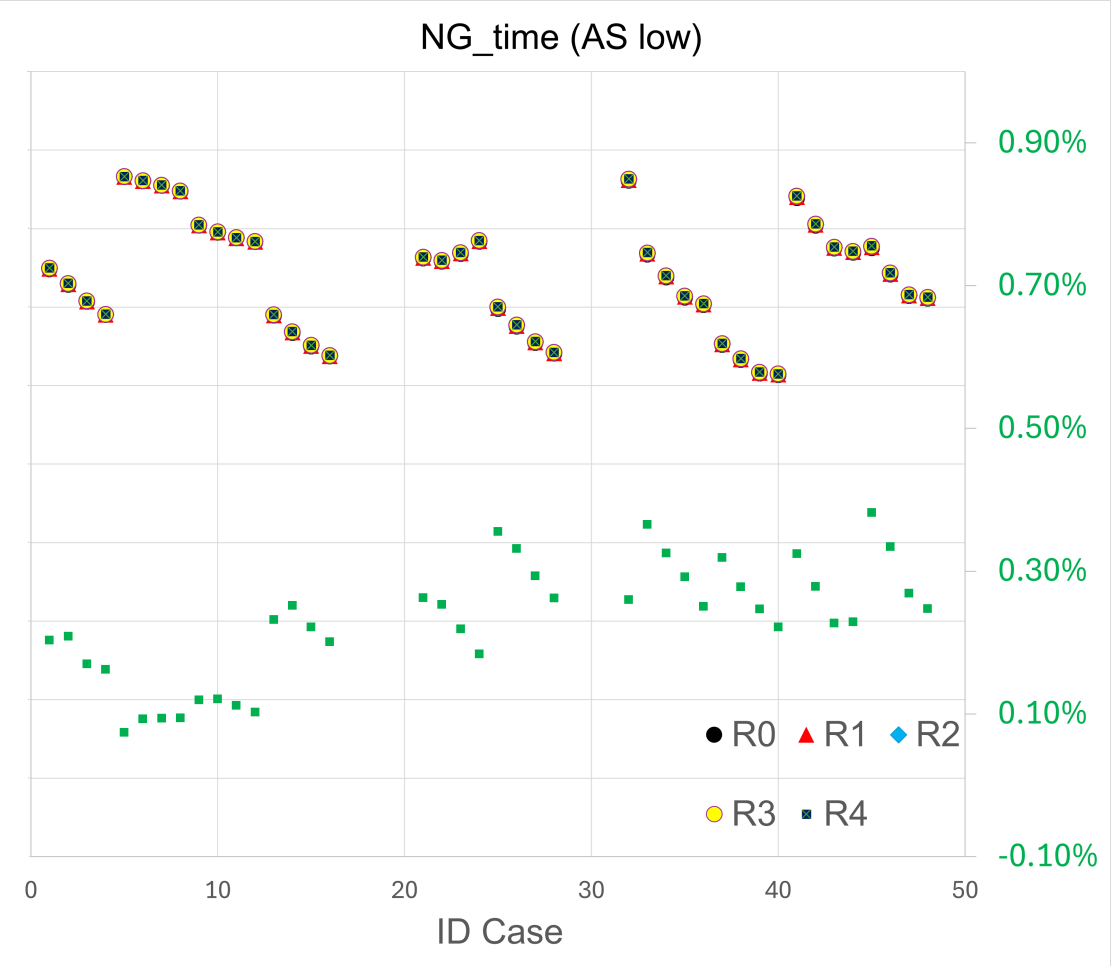

Figure 5.8: Air Start (low) parametric - NG set time

Chapter 6

Conclusions

6.1 What we know

In light of the conducted analyses, Rugged and Parametric, the results show a consistent behavior in line with the premises of the project, despite the different maneuvers, test points, and external conditions. Specifically, the differences observed between basic configuration and Ruggedized configurations systematically fall within the expected variability band.

- No ITT overshoot occurs
- No mechanical NG/Nprop overshoot, no response delays
- No abnormalities of motor-supplied PWR occur

This consistency of results indicates that the hardware change does not introduce a significant impact on engine controllability and/or its performance.

In addition, the control system showed its robustness as test conditions changed, maintaining a stable response behavior that complied with the original design conditions.

Based on this evidence, it can be concluded that the hardware modification does not require further modification of the control system, which has proven to be robust and reliable. The motor and its control system can then go trough the next steps of testing and certification in safe conditions.

Appendix A

Lc55 code

```
clear all
close all
clc

tic;

analysis = input('Insert analysis type (Rugg = 1, Param = 2): ');
codeMan = input('Insert maneuver code (GS, TO, SS, SR, BC, AS): ', 's'); % 's' = string
codeMan = upper(strtrim(codeMan)); % cleaning: remove spaces and use capital letters

files = dir('*.mat');

switch analysis

    % ========================================================
    % ANALYSIS 1: Rugg (2 lists: noRugg = R0, Rugg = R1)
    % ========================================================
    case 1
    % Initialize two lists (empty struct array)
    noRugg = struct('name', {}, 'folder', {}, 'date', {}, 'bytes', {}, 'isdir', {}, 'datenum', {});
    Rugg = noRugg;

    for k = 1:numel(files)
        nameFile = files(k).name;
        % Find .mat location
        [~, nameBase, est] = fileparts(nameFile);
        if ~strcmpi(est, '.mat')
            continue; % safety
```

```
29          end
30
31          if isempty(nameBase)
32              continue;  % stranger file
33          end
34
35          lastDigit = nameBase(end);
36
37          if lastDigit == '0'
38              noRugg(end+1) = files(k); %#ok<AGROW>
39          elseif lastDigit == '1'
40              Rugg(end+1) = files(k); %#ok<AGROW>
41          else
42              fprintf('Warning: "%s" does not end with "0" or "1",
    skipped.\n', nameFile);
43          end
44      end
45
46      switch codeMan
47              case 'GS'
48                  Sam310_Rugg(noRugg, Rugg);
49
50              case 'TO'
51                  Mt82_Rugg(noRugg, Rugg);
52
53              case 'SS'
54                  Sal222_Rugg(noRugg, Rugg);
55
56              case 'SR'
57                  Gv668_Rugg(noRugg, Rugg);
58
59               case 'BC'
60                   Mc440_Rugg(noRugg, Rugg);
61
62               case 'AS'
63                   AB112_Rugg(noRugg, Rugg);
64
65              otherwise
66                  error('Maneuver code "%s" not valid.', codeMan);
67      end
68
69      % ========================================================
70      % ANALYSIS 2: Param (5 lists: R0, R1, R2, R3, R4)
71      % ========================================================
72      case 2
73      % Initialize five lists (empty struct array)
74      R0 = struct('name', {}, 'folder', {}, 'date', {}, 'bytes', {}, '
    isdir', {}, 'datenum', {});
75      R1 = R0;
```

```
76      R2 = R0;
77      R3 = R0;
78      R4 = R0;
79
80      for k = 1:numel(files)
81              nameFile = files(k).name;
82              % Find .mat location
83              [~, nameBase, est] = fileparts(nameFile);
84              if ~strcmpi(est, '.mat')
85                  continue;  % safety
86              end
87
88              if isempty(nameBase)
89                  continue;  % stranger file
90              end
91
92              lastDigit = nameBase(end);
93
94              if lastDigit == '0'
95                  R0(end+1) = files(k); %#ok<AGROW>
96              elseif lastDigit == '1'
97                  R1(end+1) = files(k); %#ok<AGROW>
98              elseif lastDigit == '2'
99                  R2(end+1) = files(k); %#ok<AGROW>
100             elseif lastDigit == '3'
101                 R3(end+1) = files(k); %#ok<AGROW>
102             elseif lastDigit == '4'
103                 R4(end+1) = files(k); %#ok<AGROW>
104             else
105                 fprintf('Warning: "%s" does not end with a valid
    digit (0-4), skipped.\n', nameFile);
106             end
107         end
108
109     switch codeMan
110             case 'GS'
111                 Sam310_Param(R0, R1, R2, R3, R4);
112
113             case 'TO'
114                 Mt82_Param(R0, R1, R2, R3, R4);
115
116             case 'SS'
117                 Sal222_Param(R0, R1, R2, R3, R4);
118
119             case 'SR'
120                 Gv668_Param(R0, R1, R2, R3, R4);
121
122              case 'BC'
123                  Mc440_Param(R0, R1, R2, R3, R4);
```

```
124
125                 case 'AS'
126                     AB112_Param(R0, R1, R2, R3, R4);
127
128                 otherwise
129                     error('Maneuver code "%s" not valid.', codeMan);
130     end
131
132     otherwise
133         error('Analysis type "%s" not valid. Use 1 (Rugg) or 2 (Param
    ).', num2str(analysis));
134 end
135
136
137
138 disp('Run completed')
139
140 RunTime = [num2str(toc), ' sec']
```

Bibliography

[1] JS Morlu LLC. *Understanding De-risking: Strategies, Examples, and Best Practices*. JS Morlu LLC. 2024. URL: https://www.jsmorlu.com/financial-business-guides/de-risking-strategies/ (visited on 03/23/2026) (cit. on p. 2).

[2] Eric J. Klein. *Design Phase Risk Mitigation Tools and Methods*. Long International, Inc. 2022. URL: https://www.long-intl.com/articles/design-phase-risk-mitigation/ (visited on 03/23/2026) (cit. on p. 3).

[3] IBM. *What is Risk Mitigation?* International Business Machines Corporation. 2024. URL: https://www.ibm.com/it-it/think/topics/risk-mitigation (visited on 03/23/2026) (cit. on p. 3).

[4] Stefano Patelli. *Risk Management: come valutare e mitigare il rischio aziendale*. Polo Innovativo. 2025. URL: https://www.poloinnovativo.it/risk-management (visited on 03/23/2026) (cit. on p. 3).

[5] Dileepa Wijayanayake. *Ways Automation Can Improve Your Daily Life*. FlowWright. 2024. URL: https://www.flowwright.com/how-automation-can-improve-your-daily-life (visited on 03/23/2026) (cit. on p. 4).

[6] PatSnap Eureka. *Feedforward vs. Feedback Control: Key Differences and Use Cases*. PatSnap. 2025. URL: https://eureka.patsnap.com/article/feedforward-vs-feedback-control-key-differences-and-use-cases (visited on 03/23/2026) (cit. on p. 4).

[7] I. Marques, J. Silva, M. Campos, and A. Lima Filho. «Home Automation and Simulation of Presence in Empty Houses». In: *MATEC Web of Conferences*. Vol. 139. 2017, p. 02007. URL: https://www.matec-conferences.org/articles/matecconf/pdf/2017/39/matecconf_cscc2017_02007.pdf (visited on 03/23/2026) (cit. on p. 4).

[8] Q-NEX Technology. *What Are Examples of Control Systems?* Q-NEX Technology. 2024. URL: https://qnextech.com/it/blog/what-are-examples-of-control-systems/ (visited on 03/23/2026) (cit. on p. 4).

[9] Stuart Bennett. «A Brief History of Automatic Control». In: *IEEE Control Systems Magazine* 16.3 (1996), pp. 17–25. URL: https://elmoukrie.com/wp-content/uploads/2022/06/a-brief-history-of-automatic-control.pdf (visited on 03/23/2026) (cit. on p. 4).

[10] NASA Glenn Research Center. *Turboprop Engine*. 2021. URL: https://www.grc.nasa.gov/www/k-12/airplane/aturbp.html (visited on 03/23/2026) (cit. on p. 5).

[11] Taylor & Francis. *Turboprop*. Taylor & Francis Group. 2026. URL: https://taylorandfrancis.com/knowledge/Engineering_and_technology/Aerospace_engineering/Turboprop/ (visited on 03/23/2026) (cit. on p. 5).

[12] Global Charter. *How Does a Turboprop Engine Work?* Accessed via Global Charter aviation informational article. 2024. URL: https://www.globalcharter.com/post/how-does-a-turboprop-engine-work (visited on 03/23/2026) (cit. on p. 6).

[13] Monroe Aerospace. *Pros and Cons of Reverse-Flow Turboprop Engines*. Monroe Aerospace. 2026. URL: https://monroeaerospace.com/blog/pros-and-cons-of-reverse-flow-turboprop-engines/ (visited on 03/23/2026) (cit. on p. 6).

[14] Reddit user: /u/[username]. *Some Guide to Aircraft Engines*. Accessed for image reference. 2013. URL: https://www.reddit.com/r/aviation/comments/1iixn91/some_guide_to_aircraft_engines/ (visited on 03/23/2026) (cit. on p. 6).

[15] SKYbrary Aviation Safety. *Full Authority Digital Engine Control (FADEC)*. EUROCONTROL. 2026. URL: https://skybrary.aero/articles/full-authority-digital-engine-control-fadec (visited on 03/23/2026) (cit. on p. 7).

[16] Dennis E. Culley, Randy Thomas, and Joseph Saus. *Concepts for Distributed Engine Control*. Tech. rep. NASA/TM-2007-214994. NASA Glenn Research Center, 2007. URL: https://ntrs.nasa.gov/api/citations/20070038167/downloads/20070038167.pdf (visited on 03/23/2026) (cit. on p. 7).

[17] Federal Aviation Administration. *Full Authority Digital Engine Control (FADEC)*. Tech. rep. Federal Aviation Administration, 2022. URL: https://www.faa.gov/sites/faa.gov/files/2022-01/Full%20Authority%20Digital%20Engine%20Control%20%28FADEC%29.pdf (visited on 03/23/2026) (cit. on p. 7).

[18] Silver Atena GmbH. *FADEC – Digital Engine Management for Aircraft*. Silver Atena GmbH. 2026. URL: https://www.silver-atena.com/product-references/aerospace/propulsion/fadec (visited on 03/23/2026) (cit. on p. 7).

[19] Bill Cox. *FADEC Comes Of Age*. Plane & Pilot Magazine. 2010. URL: https://planeandpilotmag.com/fadec-comes-of-age/ (visited on 03/23/2026) (cit. on p. 8).

[20] Sanjay Garg. *Fundamentals of Aircraft Engine Control*. NESC Academy presentation. 2011. URL: https://nescacademy.nasa.gov/review/downloadfile.php?file=Gargpresentation.pdf&id=102&distr=Public (visited on 03/23/2026) (cit. on p. 8).

[21] Unknown. *Unknown*. Tech. rep. Office of Scientific and Technical Information (OSTI), U.S. Department of Energy. URL: https://www.osti.gov/servlets/purl/1868086 (visited on 03/23/2026) (cit. on pp. 8, 9).

[22] Unknown. «Unknown Title». In: *Unknown Journal* (2022). DOI: 10.1177/09596518221127511. URL: https://journals.sagepub.com/doi/10.1177/09596518221127511 (visited on 03/23/2026) (cit. on p. 8).

[23] Giorgio Guglieri. «Effect of Drive Train and Fuel Control Design on Helicopter Handling Qualities». In: *25th European Rotorcraft Forum*. European Rotorcraft Forum. Rome, Italy, 1999. URL: https://dspace-erf.nlr.nl/bitstreams/a6233499-0f82-40f7-abd0-ee38422a181c/download (visited on 03/23/2026) (cit. on pp. 8, 9).

[24] S. M. J. Ali, Z. Y. Mohammad, and F. Q. Yahya. «Estimation of Model Parameters for Torsional Vibration Analysis of a Turbo-Generator Unit with Reference to Mosul Gas-Turbine Station». In: *Al-Rafidain Engineering Journal* 23.2 () (cit. on p. 9).

[25] SKYbrary Aviation Safety. *Flight Envelope*. EUROCONTROL. 2026. URL: https://skybrary.aero/articles/flight-envelope (visited on 03/23/2026) (cit. on p. 11).

[26] Thomas M. Miller, Wouter C. de Wet, and Bruce W. Patton. *Computational Assessment of Naturally Occurring Neutron and Photon Background Radiation Produced by Extraterrestrial Sources*. NASA Technical Publication NASA/TP–2016-219012. NASA Technical Reports Server (NTRS) document ID 20160009115. Washington, DC, USA: National Aeronautics and Space Administration (NASA), 2016. URL: https://ntrs.nasa.gov/api/citations/20160009115/downloads/20160009115.pdf (cit. on p. 11).

[27] David R. Anderson. *Airplane Performance Envelopes*. Open access chapter, Embry-Riddle Aeronautical University (ERAU). 2021. URL: https://eaglepubs.erau.edu/introductiontoaerospaceflightvehicles/chapter/performance-envelopes/ (visited on 03/24/2026) (cit. on p. 11).

[28] Charles O'Neill. *Standard Atmosphere and Airspeed*. Blog post con diagrammi di flight envelope, KCAS/KTAS/Mach e equazioni di flusso comprimibile. 2014. URL: https://charles-oneill.com/blog/standard-atmosphere-and-airspeed/ (visited on 03/24/2026) (cit. on p. 11).

[29] Jeffrey W. Chapman, Dennis E. Culley, and Joseph W. Connolly. *Transient Optimization of a Gas Turbine Engine*. NASA Technical Memorandum NASA/TM–20220016302. NASA Technical Reports Server (NTRS) document ID 20220016302. Presentato all'AIAA SciTech Forum 2023. Cleveland, OH, USA: National Aeronautics and Space Administration (NASA), 2022. URL: https://ntrs.nasa.gov/api/citations/20220016302/downloads/TransientOptimization_7.pdf (cit. on p. 12).

[30] Patrick Veillette. «Engine Limitations Are Not Mere Suggestions, Part 1». In: *Aviation Week Network* (July 2023). Articolo su limiti operativi motori turbine, overtemp, creep e EGT. URL: https://aviationweek.com/business-aviation/aircraft-propulsion/engine-limitations-are-not-mere-suggestions-part-1 (visited on 03/24/2026) (cit. on p. 12).

[31] Federal Aviation Administration (FAA). *Ratings and Operating Limitations for Turbine Engines (Sections 33.7 and 33.8)*. Tech. rep. AC 33.7-1. Guidance on turbine engine ratings, limits (torque, RPM, EGT, transients), TCDS annotations. Initiated by ANE-111. Washington, DC, USA: U.S. Department of Transportation, Federal Aviation Administration, June 2010. URL: https://www.faa.gov/documentLibrary/media/Advisory_Circular/AC_33_7-1.pdf (cit. on p. 12).

[32] David R. Anderson. *Atmospheric Properties*. Equazioni ISA troposfera, geopotential vs geometric altitude, correzioni umidità, tabelle proprietà. 2021. URL: https://eaglepubs.erau.edu/introductiontoaerospaceflightvehicles/chapter/international-standard-atmosphere-isa/ (visited on 03/24/2026) (cit. on pp. 13, 14).

[33] World Meteorological Organization (WMO). *Aviation - Hazards - Extreme Heat*. Effetti calore estremo su performance aeromobili, density altitude, ISA deviations, scenari hot/high. 2023. URL: https://community.wmo.int/site/knowledge-hub/programmes-and-initiatives/aviation/aviation-hazards-extreme-heat (visited on 03/24/2026) (cit. on p. 14).

[34] ADG Efficiency. *Gas Turbines and Ambient Temperature*. Effetti temperatura ambiente su potenza e efficienza turbine a gas, densità aria, mass flow, regola empirica De Sa & Zubaidy. 2023. URL: https://adgefficiency.com/energy-basics-ambient-temperature-impact-on-gas-turbine-performance/ (visited on 03/24/2026) (cit. on p. 14).

[35] Airport Technology. *The top 10 highest altitude airports in the world*. Articolo descrittivo sugli aeroporti civili a maggiore altitudine (fino a 4,411 m, Daocheng Yading Airport, Cina), con dati su quota, lunghezza pista e traffico passeggeri. 2023. URL: https://www.airport-technology.com/features/the-top-10-highest-altitude-airports-in-the-world/ (visited on 03/24/2026) (cit. on p. 14).

[36] Aircraft Systems Tech. *Turboprop and Turbofan Engines Starting Procedures*. Descrizione delle procedure di avviamento per motori turboprop e turbofan, incluse sequenze di start, limitazioni ITT/EGT, strumenti e condizioni di abort start. Aug. 2020. URL: https://www.aircraftsystemstech.com/2020/08/turboprop-turbofan-engines-and-starting.html (visited on 03/24/2026) (cit. on p. 19).

[37] Bernie D. MacIsaac and Roy Langton. *Gas Turbine Propulsion Systems*. John Wiley & Sons, Ltd, 2011 (cit. on pp. 19, 20, 25, 26, 32).

[38] Emilio Tanzi. «Modellazione di turbine a gas applicata alla progettazione software-in-loop di sistemi di controllo». Relatore: David Naso, Corso di laurea in Ingegneria Meccanica. Tesi di laurea magistrale. Bari: Università degli Studi di Bari, 2026 (cit. on p. 21).

[39] Aerocor Aerospace. *FADEC*. Aerocor Aerospace. 2026. URL: https://www.aerocor.com/aircraft-media/fadec/ (visited on 03/23/2026) (cit. on pp. 22–24, 33).

[40] Airplane Academy. *Torque, ITT, NP, and NG Explained on Turboprop Engines*. Spiegazione operativa dei parametri motore turboprop (torque, ITT, N_P, N_G) e del loro impiego nelle varie fasi di volo. 2022. URL: https://airplaneacademy.com/torque-itt-np-and-ng-explained-on-turboprop-engines/ (visited on 03/24/2026) (cit. on pp. 22, 23).

[41] PPRuNe Forums. *Turboprop Power Setting*. PPRuNe (Professional Pilots Rumour Network). 2026. URL: https://www.pprune.org/tech-log/339624-turboprop-power-setting.html (visited on 03/23/2026) (cit. on p. 23).

[42] PPRuNe Forums. *Why EPR is Set 60–80 kts*. PPRuNe (Professional Pilots Rumour Network). 2026. URL: https://www.pprune.org/tech-log/59626-why-epr-set-60-80-kts.html (visited on 03/23/2026) (cit. on p. 23).

[43] SKYbrary Aviation Safety. *Aircraft Engine Operation and Malfunction: Basic Familiarization for Flight Crews*. Tech. rep. EUROCONTROL / SKYbrary Aviation Safety, 2026. URL: https://skybrary.aero/sites/default/files/bookshelf/1622.pdf (visited on 03/23/2026) (cit. on p. 23).

[44] Skyclear FLTops. *Performance 1 — Power Limits in the Turboprops*. Skyclear FLTops. 2019. URL: https://skyclearfltops.wordpress.com/2019/08/28/performance-1-power-limits-in-the-turboprops/ (visited on 03/23/2026) (cit. on p. 23).

[45] Aircraft Performance Group. *How is the takeoff flight path segmented?* Accessed: 2026-03-24. 2024. URL: https://flyapg.com/kb/how-is-the-takeoff-flight-path-segmented (visited on 03/24/2026) (cit. on p. 24).

[46] Federal Aviation Administration. *AC 33.63-1: Turbine Engine Vibration*. Tech. rep. 33.63-1. Date: 7/25/07; Initiated by: ANE-110. FAA, July 2007. URL: https://www.faa.gov/documentLibrary/media/Advisory_Circular/AC_33_63-1.pdf (cit. on pp. 25, 26).

[47] «Transient processes in turboprop engine control systems during startup». In: vol. 182. EDP Sciences, 2018, p. 01024. DOI: 10.1051/matecconf/201818201024. URL: https://doi.org/10.1051/matecconf%2F201818201024 (cit. on p. 26).

[48] Jonathan L. Kratz. «Transient Optimization of a Gas Turbine Engine». In: *AIAA SciTech Forum*. Document ID: 20220016302; NASA Glenn Research Center. AIAA. National Harbor, MD, Jan. 2023. URL: https://ntrs.nasa.gov/citations/20220016302 (cit. on pp. 26–28).

[49] Siemens Industry, Inc. «Automotive engine test stand overview: Adding value using SINAMICS drives». In: (Oct. 2015). Whitepaper prepared by Brian McMinn, Consulting Sales Application Engineer. URL: https://assets.new.siemens.com/siemens/assets/api/uuid:a10355ce-9683-4766-a90f-0dbc86626cd3/gmc-test-stands-engine-overview-whitepaper.pdf (cit. on p. 28).

[50] Sanjay Garg. *Aircraft Turbine Engine Control Research at NASA Glenn Research Center*. Tech. rep. NASA/TM-2013-217821. Document ID: 20130013439; E-18277-1. Cleveland, OH: NASA Glenn Research Center, Apr. 2013. URL: https://ntrs.nasa.gov/citations/20130013439 (cit. on p. 30).

[51] Jonathan A. DeCastro, Jonathan S. Litt, and Dean K. Frederick. «A Modular Aero-Propulsion System Simulation of a Large Commercial Aircraft Engine». In: *44th AIAA/ASME/SAE/ASEE Joint Propulsion Conference & Exhibit*. NASA/TM-2008-215303; E-16573; Document ID: 20080043619. AIAA. Hartford, CT, Sept. 2008. DOI: 10.2514/6.2008-4579. URL: https://ntrs.nasa.gov/citations/20080043619 (cit. on p. 30).

[52] European Union Aviation Safety Agency (EASA). *Certification Memorandum: Turbine Engine Relighting In Flight*. Tech. rep. CM-PIFS-010. Issue 01, issued 29 April 2015; Applicability: CS-E 910. EASA, Apr. 2015. URL: https://www.easa.europa.eu/sites/default/files/dfu/%27final%27%20CM-PIFS-010%20Issue_01_Turbine%20Engine%20Relighting%20In%20Flight_PUBL.pdf (cit. on p. 32).

[53] Kelly Schwan. «Windmilling Airstarts». In: *King Air Magazine* (Aug. 2013). Republished from August 2013 issue. URL: https://kingairmagazine.com/article/windmilling-airstarts/ (cit. on p. 32).

[54] Airbus. *Engine Relight After an All-Engine Flameout*. Articolo operativo su procedura rilascio motori post-flameout totale. 2023. URL: https://safetyfirst.airbus.com/engine-relight-after-an-all-engine-flameout/?airbus-iframe=true&airbus-post=2053 (visited on 03/24/2026) (cit. on p. 32).

[55] NASA Glenn Research Center. *Inlets*. https://www.grc.nasa.gov/www/k-12/airplane/inlet.html. Beginner's guide to aeronautics. NASA, 2024. (Visited on 03/24/2026) (cit. on p. 32).

[56] Philip P. Walsh and Paul Fletcher. *Gas Turbine Performance*. 2nd. Oxford, UK: Blackwell Publishing, 2004. ISBN: 0-632-06434-X. URL: www.blackwellpublishing.com (cit. on p. 33).

[57] Dave Holmes. *Windmilling Airstarts*. Republished from August 2013 issue. Aug. 2013. URL: https://kingairmagazine.com/article/windmilling-airstarts/ (visited on 03/24/2026) (cit. on p. 33).

[58] *What does NPSS stand for?* https://www.abbreviations.com/NPSS. 40 definitions listed, top: Numerical Propulsion System Simulation. Abbreviations.com (STANDS4 LLC), 2025. (Visited on 03/24/2026) (cit. on p. 35).

[59] NASA Glenn Research Center. *NPSS Numerical Propulsion System Simulation (LEW-17051-1)*. https://software.nasa.gov/software/LEW-17051-1. Software category: Design and Integration Tools. NASA, 2017. (Visited on 03/24/2026) (cit. on p. 35).